

# Ocean Dynamics

## North Atlantic extratropical and subpolar gyre variability during the last 120 years: a gridded dataset of surface temperature, salinity, and density.

### Part 1: Dataset validation and RMS variability

--Manuscript Draft--

<b>Manuscript Number:</b>	ODYN-D-18-00150R1	
<b>Full Title:</b>	North Atlantic extratropical and subpolar gyre variability during the last 120 years: a gridded dataset of surface temperature, salinity, and density. Part 1: Dataset validation and RMS variability	
<b>Article Type:</b>	Topical Collection - Liege 2018	
<b>Keywords:</b>	Sea surface temperature; sea surface salinity; North Atlantic; decennial variability	
<b>Corresponding Author:</b>	Gilles Reverdin Centre National de la Recherche Scientifique FRANCE	
<b>Corresponding Author Secondary Information:</b>		
<b>Corresponding Author's Institution:</b>	Centre National de la Recherche Scientifique	
<b>Corresponding Author's Secondary Institution:</b>		
<b>First Author:</b>	Gilles Reverdin	
<b>First Author Secondary Information:</b>		
<b>Order of Authors:</b>	Gilles Reverdin	
	Andrew Friedman	
	Léon Chafik	
	Naomy Penny Holliday	
	Tanguy Szekely	
	Hedinn Valdimarson	
	Igor Yashayaev	
<b>Order of Authors Secondary Information:</b>		
<b>Funding Information:</b>	CNRS (xxx)	Dr Gilles Reverdin
<b>Abstract:</b>	<p>We present a binned annual product (BINS) of sea surface temperature (SST), salinity (SSS) and water density observations for 1896–2015 of the subpolar North Atlantic between 40°N and 70°N, mostly excluding the shelf areas. The product, which resolves space scales on the order of 200 to 500 km, reproduces most of the pluri-annual variability in different time series covering at least the last three decades or of the along-track ship monitoring. Comparisons with other SSS and SST gridded products available since 1950 suggest that BINS captures the large decadal to multidecadal variability. Comparison with the HadSST3 SST product since 1896 also indicates that the decadal and multidecadal variability is usually well reproduced, with small differences in long-term trends or in areas with marginal data coverage in either of the two products. Outside of the Labrador Sea and Greenland margins, pluri-annual variability is rather similar in different seasons. Variability at periods longer than 15 years is a large part of the total pluri-annual variability, both for SST and SSS, except possibly in the south-western part of the domain. Variability in SST and SSS increases towards the west, with the contribution of salinity variability to density dominating that of temperature in the western Atlantic, except close to the Gulf Stream and North Atlantic Current in the southwest area. Weaker variability and larger relative temperature contributions to density changes are found in the eastern part of the gyre</p>	

	and south of Iceland.
<b>Additional Information:</b>	
<b>Question</b>	<b>Response</b>
Is this manuscript (or major parts of it) currently submitted to another journal or has it been submitted before and then either been rejected or withdrawn?	NO



[Click here to view linked References](#)

1

2  
3  
4  
5  
6  
7  
8  
9  
10  
11  
12  
13  
14  
15  
16  
17  
18  
19  
20  
21  
22  
23  
24  
25  
26  
27  
28  
29  
30  
31  
32  
33  
34  
35  
36  
37  
38  
39  
40  
41  
42  
43  
44  
45  
46  
47  
48  
49  
50  
51  
52  
53  
54  
55  
56  
57  
58  
59  
60  
61  
62  
63  
64  
65

2 North Atlantic extratropical and subpolar gyre variability during the last 120 years:  
3 a gridded dataset of surface temperature, salinity, and density.

4 Part 1: Dataset validation and RMS variability

6 G. Reverdin<sup>1</sup>, A. R. Friedman<sup>2</sup>, L. Chafik<sup>3</sup>, N. P. Holliday<sup>4</sup>, T. Szekely<sup>5</sup>, H. Valdimarson<sup>6</sup>, I.  
7 Yashayev<sup>7</sup>

9 <sup>1</sup> Sorbonne-Université, CNRS/IRD/MNHN (LOCEAN), Paris, France

10 <sup>2</sup> School of Geosciences, University of Edinburgh, UK. ORCID ID [https://orcid.org/0000-](https://orcid.org/0000-0001-6994-2037)  
11 0001-6994-2037

12 <sup>3</sup> Department of Meteorology and Bolin Centre for Climate Research, Stockholm University,  
13 Stockholm, Sweden. ORCID ID <https://orcid.org/0000-0002-5538-545X>

14 <sup>4</sup> National Oceanography Centre, Southampton, UK

15 <sup>5</sup> IUEM, Brest, France

16 <sup>6</sup> Marine and Freshwater Research Institute, Reykjavik, Iceland

17 <sup>7</sup> Bedford Institute of Oceanography, Fisheries and Oceans Canada, Dartmouth, NS, Canada

20 Corresponding author: G. Reverdin, Laboratoire d'Océanographie et de climatologie par  
21 expérimentation et analyse numérique, Institut Pierre Simon Laplace, Sorbonne-Université,  
22 case 100, 4 pl. Jussieu, 75252 Paris Cedex 05, France ([gilles.reverdin@locean-ipsl.upmc.fr](mailto:gilles.reverdin@locean-ipsl.upmc.fr) ;  
23 tel : 33-1-44272342 fax : 33-1-44273805 ; [orcid.org/0000-0002-5583-8236](https://orcid.org/0000-0002-5583-8236))

26 Abstract

1 27 We present a binned annual product (BINS) of sea surface temperature (SST), salinity (SSS)  
2 28 and water density observations for 1896–2015 of the subpolar North Atlantic between 40°N  
3 29 and 70°N, mostly excluding the shelf areas. The product, which resolves space scales on the  
4 30 order of 200 to 500 km, reproduces most of the pluri-annual variability in different time series  
5 31 covering at least the last three decades or of the along-track ship monitoring. Comparisons  
6 32 with other SSS and SST gridded products available since 1950 suggest that BINS captures the  
7 33 large decadal to multidecadal variability. Comparison with the HadSST3 SST product since  
8 34 1896 also indicates that the decadal and multidecadal variability is usually well reproduced,  
9 35 with small differences in long-term trends or in areas with marginal data coverage in either of  
10 36 the two products. Outside of the Labrador Sea and Greenland margins, pluri-annual variability  
11 37 is rather similar in different seasons. Variability at periods longer than 15 years is a large part  
12 38 of the total pluri-annual variability, both for SST and SSS, except possibly in the south-  
13 39 western part of the domain. Variability in SST and SSS increases towards the west, with the  
14 40 contribution of salinity variability to density dominating that of temperature in the western  
15 41 Atlantic, except close to the Gulf Stream and North Atlantic Current in the southwest area.  
16 42 Weaker variability and larger relative temperature contributions to density changes are found  
17 43 in the eastern part of the gyre and south of Iceland.

18 44  
19 45 Keywords: sea surface temperature, sea surface salinity, North Atlantic, decennial variability  
20 46  
21  
22  
23  
24  
25  
26  
27  
28  
29  
30  
31  
32  
33  
34  
35  
36  
37  
38  
39  
40  
41  
42  
43  
44  
45  
46  
47  
48  
49  
50  
51  
52  
53  
54  
55  
56  
57  
58  
59  
60  
61  
62  
63  
64  
65

47

1 48

2 49

## **1. Introduction**

3 50

4 51

5 52

6 53

7 54

8 55

9 56

10 57

11 58

12 59

13 60

14 61

15 62

16 63

17 64

18 65

19 66

20 67

21 68

22 69

23 70

24 71

25 72

26 73

27 74

28 75

29 76

30 77

31 78

32 79

33 80

The North Atlantic subpolar gyre (SPG) receives salty surface water from the subtropical North Atlantic as well as fresh water originating from the Arctic and the Nordic seas and circulating mostly on and along the shelves. It is a formation site of deep and intermediate waters and thereby a major contributor to the lower limb of the Atlantic meridional overturning circulation (AMOC) (Rhein et al. 2011). There is wintertime densification of the surface Labrador and Irminger Seas resulting in intermittent deep convection reaching and exceeding 2400 m in the mid-1990s and 2000 m in recent years (Yashayaev and Loder 2017). Deep dense overflows from the Nordic Seas and the associated mixing with and entrainment of local waters also add important hydrographic connections between the regions and the surface and deep layers. In both instances, one expects that changes in surface density will modulate these vertical exchanges and the properties of the deep and intermediate waters formed, and thus the AMOC. Many model studies (at various spatial resolution) also suggest an influence of surface salinity changes in this region on changes in the AMOC (Frankignoul et al. 2009; Rahmstorf et al. 2015, Böning et al. 2016). Whereas the connection between these surface changes and AMOC is still subject to discussion (Lozier 2012; Williams et al. 2015; Buckley and Marshall 2016), the relation between changes of surface density and upper or intermediate water formation is rather well established (Yashayaev and Loder 2016 2017; Piron et al. 2017). Seawater density is a function of temperature and salinity, with the relative influence of salinity increasing when temperature decreases. Thus, investigating surface density variability and attempting to establish its past patterns of change requires a concurrent analysis of temperature and salinity fields.

Hydrographic data have been used to analyze salinity and temperature with a low spatial resolution over the North Atlantic and neighboring seas, but only on decadal or longer time scales since the mid-1960s and in more restricted areas since 1950 (Polyakov et al. 2005; Skliris et al. 2014; Holliday et al. 2015; Yashayaev 2007; Yashayaev and Loder 2016 2017). These data also rarely provide direct indications of winter surface density field (the local indications can be found in Yashayaev and Loder (2016 2017), but not broad-scale) that is the variable key to the connection between the surface ocean and the ocean interior. In the last twenty years, the advent of profiling floats (Lavender et al. 2000; Roemmich et al. 2009;

81 Riser et al. 2016) has allowed year-round three-dimensional monitoring of large-scale upper  
82 and intermediate ocean variability (Tesdal et al. 2018), but these measurements do not yet  
83 help to resolve the decadal to multidecadal frequencies. Multidecadal time series with at least  
84 annual or seasonal resolution have also been produced at a few sites: Rockall Trough  
85 (Holliday et al., 2015), the Faroe-Shetland Channel (Hughes et al., 2012), south of Iceland  
86 (Icelandic hydrographic surveys), in the center of the Labrador Sea (Yashayaev and Loder  
87 2016 2017), or at station Mike and hydrographic sections in the Norwegian Sea (Yashayaev  
88 and Seidov 2015). Otherwise, mapped monthly fields of T and S have been constructed by  
89 different objective mapping methods based on the EN4 (Good et al. 2013), CORA (Cabanes  
90 et al. 2013) and Ishii et al. (2006) datasets that could have some coverage in a large part of  
91 this domain for the last 65 years. Monthly mapped sea surface temperature (SST) fields have  
92 also been produced with sufficient coverage into large parts of the SPG since the 1890s using  
93 mostly ship log data with a shift in the last two decades to drifter SST data. Carefully  
94 estimated bias correction has been applied to subsets of these data, such as done in Hadley  
95 Centre SST (HadSST3; Kennedy et al. 2011a and 2011b). However, these binned SST  
96 datasets present gaps in some northern regions, in particular before 1922.

97  
98 Long-term box averages in the SPG with near-annual resolution were presented in Reverdin  
99 (2010) and Friedman et al. (2017). Reverdin (2010) described a record of SST and SSS in the  
100 northeastern part of the SPG from 1895–2009. There, co-variability of temperature (T) and  
101 salinity (S) was found on decadal or multidecadal time scales in different seasons, with a  
102 slight dominance of temperature on density variability (partially compensated by the salinity  
103 contribution). Friedman et al. (2017) examined pluri-annual (1-2-1 smoothed over successive  
104 years) salinity time series in larger boxes over the Atlantic from 20°S–70°N (the temperature  
105 reports associated with the salinity data were not examined). The largest salinity root mean  
106 square (RMS) variability was found in the northern tropics, from 5°–20°N. In the subpolar  
107 North Atlantic, RMS variability was shown to decrease to the northeast from the Labrador  
108 Sea to the Nordic seas (Friedman et al. 2017, Fig. 1), though the large grid box size did not  
109 permit finer examination of the spatial structure.

110  
111 Building on the box averaging in these previous two studies, we present a higher-resolution  
112 binned product of temperature and salinity since 1896 in the subpolar North Atlantic and  
113 southern Nordic seas and draw first conclusions obtained with the dataset. Focusing on the  
114 region north of 40°N allows us to describe co-located SSS and SST at higher spatial scales

115 (less than 500km) than presented previously, without having large periods with data gaps  
116 (except during or just after WWI and WWII in some sub-regions).

117  
118 In this paper we present and validate the binned product at pluri-annual time scales, and also  
119 discuss its RMS variability. A second part of this study (in preparation) examines the decadal  
120 and multidecadal variability, and relationship with North Atlantic climate variations. The  
121 dataset sources and construction are described in Section 2. In Section 3 we validate the  
122 dataset and compare it with other products. In Section 4, we examine the spatial distribution  
123 of temporal variability of SSS, SST, and surface density, followed by summary and  
124 discussion in Section 5.

## 2. Data and methods

### 2.1. Dataset construction

125 The main data sources are described in Reverdin et al. (1994), Reverdin (2010), and Friedman  
126 et al. (2017). A significant part of the temperature and salinity (reported as practical salinity)  
127 data was collected on merchant and other selected vessels (including the weather ships), in  
128 particular before the mid-1970s north of 50°N, and before WWII and since 1977 south of  
129 50°N. This is also the case since 1993, mostly along two ship tracks between southern  
130 Newfoundland and Reykjavik and between the North Sea and Greenland (Reverdin et al.  
131 2018), as well as near France and between the English Channel and eastern North America.  
132 For the first two tracks, intake temperature was measured part of the time, XBTs were  
133 dropped and water samples collected, which allows for identification / estimation of possible  
134 temperature and salinity biases in the records from thermosalinographs (TSG) (Alory et al.  
135 2015; Reverdin et al. 2018). The identification of the temperature biases is less certain for the  
136 other vessels since 1993, but water samples were also collected to correct salinity biases in  
137 TSG records. This is complemented by near-surface hydrographic data during cruises, and  
138 since 1996, by measurements from drifters, and upper level data (often near 5-8m depth) from  
139 Argo floats (Roemmich et al. 2009; Riser et al. 2016), as well as from earlier PALACE floats  
140 (Lavender et al. 2000; Davis et al. 2001).

141 The depth of sampling and the methods of collection and analysis have changed in time, as  
142 well as data accuracy, and thus some subsets of the data require correction of identified  
143 biases, both for temperature and salinity, as commented in the earlier papers. Bias correction

149 follows Reverdin et al. (1994) for ship data before the 1990s (based on comparison with  
150 surface data from Nansen casts). There is nonetheless the possibility of seasonal stratification  
151 between the data collected below the surface (for example, from TSG data, Argo floats and  
152 CTD/Nansen casts) and the surface data (for example from drifters, or in earlier times from  
153 bucket sampling). In particular, the change in depth of sampling in time can result in artificial  
154 time variability, due to near-surface stratification. In this region and for the data considered,  
155 this effect/bias is expected to be usually small, in particular between 55°N and 65°N due to  
156 the rarity of low wind conditions, and away from shelves with surface freshwater sources  
157 (melting sea ice or icebergs, outflows from fjords, rivers).

158  
159 We construct annual time series of deviations from the seasonal cycle in boxes for four  
160 different seasons, using a similar methodology as in Friedman et al. (2017) and applied from  
161 1896–2015 for both T and S, over smaller spatial bins. This new box-product will be referred  
162 to as BINS. The boundaries of the 34 boxes were redesigned to better fit with oceanic fronts  
163 and main currents than in Friedman et al. (2017). One box in the central Labrador Sea  
164 corresponds to what is used by Yashayaev and Loder (2016) for creating a combined  
165 Labrador Sea time series, and box boundaries in the eastern subpolar North Atlantic are  
166 chosen as in Holliday et al. (2015). Except for one box off southwest Greenland and one box  
167 on the southern part of the Grand Banks, the boxes do not overlap with the shelves and with  
168 areas of large seasonal sea ice cover. In the northeastern SPG, the resulting boxes provide a  
169 slightly lower spatial resolution than what was used in Reverdin (2010), but for which the  
170 different time series were rather well correlated. To give an idea of the resolution achieved,  
171 the SSS and SST late-winter climatologies are mapped onto the BINS grid boxes (**Fig. 1**),  
172 which shows that the main characteristics of spatial variability are retained by this choice of  
173 grid.

174  
175 The construction of box time series and their error estimates is described in Friedman et al  
176 (2017). Here, the main steps are summarized, with specifics and additions related to BINS  
177 further described. The SSS and SST climatologies were constructed on a 1°×1° grid with little  
178 spatial smoothing and gap-filling, with an adjustment to the mean and up to three sinusoidal  
179 harmonics of the year, when data was sufficient. Deviations from this climatology of  
180 individual data are estimated (T being in °C and S reported in the practical salinity scale 1978  
181 (PSS-78; Fofonoff 1985; UNESCO 1981). For T, outliers were removed using a spatially  
182 variable threshold, based on the local standard deviation. [S outliers were removed similarly,



183 with less influence on the variability]. We compared this to a fixed 3°C error threshold, which  
184 yielded generally similar results albeit with smaller interannual excursions. Larger differences  
185 were found in the central Labrador Sea in the 1920s, a period with extremely low data  
186 coverage. In each box, these individual deviations are then combined for the individual  
187 seasons and years, by median-averaging the individual deviations. The seasonal anomalies are  
188 1-2-1 smoothed over successive years (not applied at the start and end years) and then  
189 averaged annually from December–November, inversely weighted by error. [The annual  
190 period was incorrectly stated as March–February in Friedman et al. (2017)]. Before being  
191 combined, the seasonal anomalies were adjusted to a common baseline over the 40-year  
192 period from 1956–1995, which was chosen due to data coverage.

193  
194 The fall season (September–November) is not included in the central Labrador and southwest  
195 Labrador boxes due to the noisy and poorly correlated S time series in the fall in these two  
196 regions. In the Norwegian Sea, central Labrador, southwest Labrador, and West Greenland,  
197 the winter season (December–February) data are not included before 1947 due to insufficient  
198 coverage.

199  
200 The total number of years with data is shown in **Fig. 2a**. Coverage is below 100 years in the  
201 North Irminger Sea and central Labrador Sea grid boxes; all other grid boxes have more than  
202 100 years of coverage. The periods of missing data occur mainly during WWI and WWII, and  
203 around 1900 (**Fig. 2b**). Multi-year data gaps are linearly interpolated, and attributed an error,  
204 equal to the standard deviation of the whole time series (which is probably an overestimate).  
205 A few missing end years (mostly 1896) in some boxes were filled by extending the first non-  
206 missing value. As in Friedman et al. (2017), regional average error terms are constructed by  
207 RMS averaging the error terms of their constituent individual boxes (which assumes that the  
208 errors are uncorrelated in different boxes). The BINS SSS regional average fields are  
209 compared with those of Friedman et al. (2017) in Appendix A for the common period 1896-  
210 2013, showing differences most commonly within the  $\pm 2$  standard error ranges.

211  
212 Figs. **2c–2d** present an estimate of the average pluri-annual grid box error as the mean  
213 error term divided by the error term during the year when there was no coverage and the error  
214 is maximum (1943, except in the West Greenland box, when it is 1917). This is thus an  
215 indication of the ratio of noise relative to signal. This shows for S, the smallest relative errors  
216 are in the central SPG. For temperature, the largest relative errors are in the western part of

217 the domain, where intra-annual variability and eddy variability are largest and not adequately  
218 sampled in this data set. The normalized area-averaged error for SSS and SST is shown in  
219 **Fig. 2e** and mirrors data coverage, with a larger value in the last year (2015) because error is  
220 not reduced in that year by the filtering.

221  
222 Density is computed from the annual binned SST and SSS values using EOS80 (UNESCO,  
223 1981), and referring the annual anomalies to the March average T and S values. Because SST  
224 is lower in winter and density becomes less sensitive to temperature variations when  
225 temperature decreases, this choice will slightly decrease the dependency of density on SST  
226 compared to using an annual average reference. What motivated this choice was that we  
227 wanted to have an estimate typical of winter conditions. Density errors are calculated from the  
228 errors in pluri-annual SSS and SST, assuming that they are uncorrelated.

## 229 230 **2.2 Seasonal dependency of the pluri-annual variability**

231 The combination of the four seasonal time series to create an annual time series in each bin  
232 implicitly assumes that the four seasons portray comparable signals/patterns of pluri-annual  
233 variability. This is particularly important if one season is missing, as is the case for the winter  
234 season in some boxes for the first part of the records. To get a sense of how well this holds for  
235 individual seasons, we combine the time series of individual bins into seven main multi-box  
236 regions (**Fig. 3a**): the central Labrador Sea / West Greenland Shelf (3 grid boxes), the  
237 southern Nordic seas (3 grid boxes), the north-east part of the SPG (5 grid boxes), the central  
238 SPG (6 grid boxes), a large central area of the intergyre gyre south of 50°N (8 boxes), an  
239 eastern Atlantic region (two boxes), and four boxes in the southwestern region around the  
240 Grand Banks. The regions are chosen for similar source data and coherent variability signals  
241 (except for the last one). For example, the two Norwegian Sea grid boxes contain mostly  
242 Norwegian and Swedish surface data before WWII, and afterwards much hydrographic data.  
243 The central Labrador Sea / West Greenland region contains hydrographic data from the Ice  
244 Patrol and other cruises in the southwest, and a mix of hydrographic data and merchant ship  
245 data until 1960 in the shelf box close to Greenland. South of 50°N, many different countries  
246 contributed to the surface data before WWII, and the French data sources are a large  
247 contribution since the mid-1970s. Three grid boxes are not included in any of these regions  
248 due to low seasonal correlations in S and more varied data sources: the southwest Labrador  
249 Sea, south Greenland/ southwest Irminger Sea, and the western area north of the Gulf Stream.

251 The seasonal correlations are summarized in **Table 3**. For the central SPG and north-east SG  
252 regions (**Fig. 3b-c**, rows 1 and 2), the time series are most complete in all seasons. There, the  
253 different seasons present rather similar variability, both for T and S, although for T, the  
254 summer (June-August season) deviates at times from the other seasons and presents more  
255 variance in the central SPG. Furthermore, after 1960, S anomalies in Sep-Nov in central SPG  
256 tend to be below the ones in the other seasons, and the opposite before. This might either be  
257 the sign of a real long-term seasonal change, or the effect of changes in the dataset around  
258 1960 (transition in this region from bucket collection to other means of collecting water, for  
259 example).

260  
261 In the southern Nordic seas (**Fig. 3b-c**, bottom row), the different seasons also present rather  
262 similar variability, at least since 1950. Before that, this remains largely true for SSS, albeit  
263 with more variability in summer. For SST, this also holds before WWI, however between  
264 1920 and 1940, the different seasons present non-coherent variability. We suspect that this  
265 might be caused by inhomogeneities in the dataset, either spatially, with a southward shift of  
266 the sampling in late autumn to early spring in this period, or due to lower data quality and  
267 larger random as well as systematic errors affecting the results and lowering correlations, such  
268 as the documented use of engine room or intake temperature data from Norwegian vessels.  
269 This is for this reason and the limited winter sampling coverage that we chose not to  
270 incorporate the winter season in the annual averages before 1947 in the two Norwegian Sea  
271 boxes.

272  
273 In the central Labrador Sea / West Greenland Shelf region (**Fig. 3b-c**, row 3), on the other  
274 hand, while there is some similarity between the different seasons in SST (less so for the  
275 summer season), there is much less coherence in SSS, even during the last 50 years of more  
276 regular sampling. Notice in particular the large differences between the spring and autumn  
277 seasons, which originate from the two boxes in central Labrador Sea and along west  
278 Greenland. These differences (and the much larger RMS variability in autumn) justify the  
279 choice of not including the autumn season when combining the different seasons to create the  
280 BINS time series in this region. In the Grand Banks region, however, we have less correlation  
281 with winter season but with similar variance (**Table 3**), so that we chose to retain the winter  
282 season. Elsewhere, and the statistics associated with the comparison between the seasonal  
283 time series (**Table 3**) justify the choice to have retained all seasons in order to reduce the  
284 sampling uncertainty in the BINS pluri-annual time series.

285

1  
2 286

### **3. Dataset validation**

3 287  
4

In order to validate the BINS SST and SSS time series, we compare it first to local compilations of high-quality hydrographic data. We also compare the binned time series to different gridded time series to better characterize the properties of BINS. This includes comparison to gridded analyzed T-S products from hydrographical data from 1950-2015, and with the HADSST3 gridded SST product from 1896-2015. In addition, Appendices A and B show comparisons with Friedman et al (2017) and Reverdin et al. (2018), which are based on different binning (in time and space) of similar data sources.

5 288  
6

7 289  
8

9 290  
10

11 291  
12

13 292  
14

15 293  
16 294

17  
18 295

#### **3.1 BINS and hydrographic time series**

19  
20 296

There are a few published compiled hydrographic time series that are available in the SPG, either from repeated seasonal cruises or a compilation of data from different origins: the Rockall Trough time series since 1975 (Holliday et al. 2015); South Icelandic stations (Sevlogsbanki 5 (Sb5) and Stokksnes 5 (St5)) since the 1970s; and the central Labrador Sea since 1941 (Yashayaev and Loder, 2009 2016). Notice also the time series in the Nordic Seas summarized by (Yashayaev and Seidov 2015). The sites of the Rockall Trough and central Labrador time series fit rather well within some BINS grid boxes, and the South Icelandic time series are just to the north of one BINS grid box (**Fig. 4a**). The results based on hydrographic time series often comprise vertical averages, excluding near-surface (5 to 10 m thick) layer, which is often determined by specifics of performing oceanographic stations and technological limitations. This averaging depth range was not optimized, but in Rockall Trough and near Iceland, it fits with the expected local maximum winter mixed layer. The time series are then averaged over annual means (after removal of an annual cycle), and smoothed with a 1-2-1 filter over successful years, similar to BINS.

21 297  
22

23 298  
24

25 299  
26

27 300  
28

29 301  
30

31 302  
32

33 303  
34

35 304  
36

37 305  
38

39 306  
40

41 307  
42

43 308  
44

45 309  
46

47 310  
48

The comparisons of these upper ocean time series with BINS are presented in **Fig. 4b** (with statistics in **Table 4**). At each site BINS is correlated with the vertically integrated time series, although the surface time series tend to have larger amplitudes. In the Labrador Sea, we compared different ranges, with the best correlation for the comparison to 20-50 m, which is within the mixed layer at least 6 months of the year and closely follows variations in seasonal discharge of freshwater and its interannual variations. There is still a correlation when considering the averages over the 20-200 m layer, which is within the winter mixed layer most years. The thicker layer time series however present less extreme amplitudes than the

49 312  
50

51 313  
52

53 314  
54

55 315  
56

57 316  
58

59 317  
60

61 318  
62

63  
64  
65

319 shallower ones. In the Rockall Trough, we also plot the surface time series based only on  
320 winter data, which is also correlated with the vertically integrated time series. The largest  
321 difference is found for South Iceland, with a low BINS S in the late 1980s that is not found in  
322 the hydrographic time series. However, there is also a difference in latitude between the BINS  
323 box and the site further north of the hydrographic time series.

324  
325 Overall, we find that BINS surface time series are significantly correlated at 0-lag with upper  
326 ocean time series from hydrography, both for T and S (correlation coefficients are in the range  
327 0.73 to 0.88 for the different time series of salinity or temperature), and exhibit very  
328 comparable RMS variability, as described in **Table 4a**. The analysis of lag correlation  
329 (summarized in **Table 4b**) indicates that the annually averaged BINS T and S precede by one  
330 year the vertically integrated upper ocean analysis both at the Rockall and Southern Iceland  
331 sites (for SST, the one-year lag correlation coefficients are respectively 0.80 and 0.89; and for  
332 SSS, respectively 0.77 and 0.88), as expected from winter ventilation of the upper ocean and  
333 time series analysis of the 20 to 40-year long weather-ship time series in the SPG (Reverdin et  
334 al., 1997). Interestingly, this is not the case for the Norwegian Sea time series.

### 3.2. BINS and gridded objective analyses

337 We compare the BINS time series with other gridded products of hydrographic data at their  
338 near-surface level that we average over the bins of the BINS analysis and filter in time to  
339 correspond to the same time resolution (1-2-1 running average over successive years  
340 December to November). This includes the  $1^\circ \times 1^\circ$  EN4, version 4.2.1 (Good et al. 2013) fields  
341 from 1950-2015, as well as the 1950-2012  $1^\circ \times 1^\circ$  product of Ishii et al. (2006), version 6.12  
342 (referred to as ISHII). We also compared BINS to the CORA5.0 fields (Cabanès et al. 2013)  
343 that have been extended to 1950, but that exclude Nansen cast data, and thus cannot be used  
344 for the analysis of salinity before 1980, and have much coarser spatial sampling in  
345 temperature than EN4 or ISHII. On the other hand, when sampling is sufficient (mostly, in the  
346 northeastern part), results with CORA are comparable to the ones of ISHII, and will not be  
347 discussed further.

348  
349 Because of the differences in sampling and mapping, the comparison in individual boxes with  
350 BINS often presents a large scatter. We will thus average the time series over the same  
351 domains as for the seasonal time series (**Fig. 3a**). [One difference is that the central SPG and  
352 north-east SPG are combined into one SPG region]. Except in the Labrador Sea or near the

353 Grand Banks, the time series of the three products (**Fig. 5**) are well correlated (**Table 5**).  
1 354 Correlation coefficients are larger for SST than for SSS, and for SSS, are usually larger  
2 355 between ISHII and BINS than between EN4 and BINS. In the Labrador Sea (row 2), there are  
3 356 differences both for SST and for SSS. For SSS, the large positive peak in BINS originate from  
4 357 a data gap in one of the three bins that are averaged in the regional time series. On the other  
5 358 hand, the altogether weaker SST-signal in ISHII in this box, something also found, but to a  
6 359 lesser domain in the other regions might result from the objective mapping method used or  
7 360 from more strident tests on outliers (Ishii and Kimoto, 2009). We also notice in the southern  
8 361 Labrador Sea for the last 20 years smaller positive SSS (and SST) anomalies in BINS than in  
9 362 the other two products, possibly a result of the thermosalinograph (TSG) data incorporated in  
10 363 BINS and not in the other products (Reverdin et al. 2018). On the other hand, near the Grand  
11 364 Banks during the last 20 years, T is higher in BINS than in the other products. Elsewhere, the  
12 365 major variability is portrayed with similar amplitude and roughly at the same time in the  
13 366 different products. For example in the SPG or southern Nordic seas, the salinity time series  
14 367 portray the events sometimes described as great salinity anomalies (Belkin et al. 1998), the  
15 368 largest one in the central SPG happening in the early 1970s and referred to as the Great  
16 369 Salinity Anomaly (Dickson et al. 1988). The figures also suggest larger differences between  
17 370 the different products in the 1990s, in particular in the intergyre region.

371  
372 The high overall agreement might result from a share of common hydrographic data  
373 incorporated in the different products. However, there is also a large portion of specific data  
374 that are not in all the products (T from mechanical or expandable bathythermographs are used  
375 in EN4 and ISHII, but not in BINS, and different sets of surface data are in BINS, but not  
376 used in EN4 and ISHII). There are also large methodological differences between the  
377 different products, both in data selection and validation and in mapping techniques and how  
378 seasonal anomalies are grouped or not. These comparisons, as well as the comparisons  
379 presented in 3.1, thus reinforce our assessment of usually small sampling errors for the BINS  
380 product during that period, and that the product captures the major events of pluri-annual  
381 variability at the grid box scale since 1950.

### 382 383 **3.3 BINS and HadSST3**

384 For long-term surface temperature, we make use of comparisons with the HadSST3 monthly  
385 product (Kennedy et al. 2011a and 2011b). Data in BINS and HadSST3 originate from  
386 different data streams. Although some data are certainly incorporated in both products, the

387 overlap is probably rather minimal, as discussed in Reverdin et al. (1994). In particular, the  
388 data before 1920 north of 58°N in BINS originate mostly from Danish and Norwegian  
389 sources which are not incorporated in HadSST3. In the last two decades, data from TSGs on  
390 merchant vessels or from profiling floats are a large contribution to BINS but are not included  
391 in HadSST3, whereas the drifter SST data used in HadSST3 are mostly not in BINS. Even in  
392 the post-WWII to mid-1970s period, when ocean weather ships contribute both to HadSST3  
393 and BINS, temperature data in the two products often originate from different sensors. BINS  
394 and HadSST3 also account for biases and uncertainties differently. We note that HadSST3  
395 does not apply smoothing or interpolation between neighboring grid cells, facilitating more  
396 direct regional comparisons.

397  
398 We examine the monthly HadSST3 anomalies, version 3.1.1.0 (median realization). We area-  
399 average the HadSST3 grid boxes into similar sub-regions similar to those shown in **Fig. 3a**.  
400 The southwest Labrador Sea BINS grid box is also examined, which closely corresponds to  
401 one HadSST3 grid box. Generally however, the large 5°×5° HadSST3 grid boxes do not align  
402 directly with BINS grid boxes; the specific grid boxes are shown in **Fig. C1**. We average the  
403 HadSST3 anomalies into 3-month seasons (skipping over missing values). The seasonal  
404 anomalies are 1-2-1 smoothed (excluding endpoints) over successive years, and the seasonal  
405 anomalies are averaged into Dec–Nov annual means (again skipping over missing values).  
406 The winter season is not included in the southern Nordic, central Labrador, or southwest  
407 Labrador annual means before 1947 to match the BINS coverage. Likewise, the fall season is  
408 excluded from the central Labrador and southwest Labrador sub-regions. In general, we find  
409 that the BINS data are more seasonally coherent at low frequencies before WWII (not  
410 shown).

411  
412 The HadSST3 and BINS regional time series are compared in **Fig. 6**, with the respective  
413 1896-2015 and 1950-2015 correlations listed in **Table 6**. Overall, the products are very highly  
414 correlated since 1950. In the first half of the record, the largest differences between the  
415 products are generally found during periods of data gaps and linear interpolation near the end  
416 of WWI and WWII, when BINS error estimates are also large. Among regions, the agreement  
417 is less good in the southern Nordic seas (**Fig. 6b**) before the 1940s; we also find that the  
418 HadSST3 seasons are also much less correlated before the 1940s (not shown). To some  
419 extent, the early differences come from the most poorly sampled northwestern part of this  
420 region, but also from Danish and Norwegian data incorporated in this product and not in

421 HadSST3. Furthermore, in the 1930s, the differences might also originate from Norwegian  
422 data interpreted in BINS as recorded continuously on a water line inside the ship, and thus  
423 attributed a large positive bias. The central Labrador Sea / West Greenland shelf (**Fig. 6a**)  
424 also shows less agreement before 1930. The products correspond very well after the 1930s,  
425 although HadSST3 has less of a cooling in the 1980s. The two SPG regions are both very  
426 strongly correlated over the length of the record (**Fig. 6c,d**). The Southwest Labrador Sea grid  
427 box (**Fig. 6e**) generally corresponds well after the gap periods in the early 1900s. In the  
428 regions further south (**Fig. 6f,g,h**), the two time series usually show a good agreement, and  
429 are most of the time compatible with the BINS error estimate. The largest differences are near  
430 the Grand Banks (**Fig. 6g**) before 1920, maybe as a result of different seasonal coverage; and  
431 in the intergyre region (**Fig. 6f**) in the early 1950s. This is the only place where the error  
432 estimate does not explain the difference between the curves, maybe because data in BINS for  
433 some of these boxes were only available in the summer season for a few years in the early  
434 1950s.

#### 4. Characteristics of T, S and surface density RMS variability

437 In this section, we examine the linear trends and the RMS variability of the linearly detrended  
438 pluri-annual time series. The 1896–2015 BINS least-squares linear trends are shown in **Fig.**  
439 **7a–7c**. We construct error estimates for the linear trends by block resampling using the time  
440 series error estimates (resampled every 2 years to account for the 1-2-1 filter). The SSS trend  
441 (**Fig. 7a**) shows a negative trend throughout most of the domain, except for the southwest and  
442 part of the eastern boundary; the pattern is consistent with the 1896–2013 trend shown in  
443 Friedman et al. (2017). The SST trend (**Fig. 7b**) shows strong warming in the Gulf Stream,  
444 and to a lesser extent along the eastern margin. There is cooling in West Greenland / Central  
445 Labrador, and near 52-55°N/30°W. However, error bars due to higher frequency variability or  
446 sampling are often large. Both the increase in T and the decrease in S contribute to an overall  
447 decrease in surface density (**Fig. 7c**).

449 The 1896–2015 HadSST3 trend is shown in (**Fig. 7d**). The trends are calculated for grid  
450 boxes with 5 or less years with missing data. [Note that specific seasons are not removed from  
451 the spatial grid boxes as for the HadSST3 indices discussed above]. Error terms for HadSST3  
452 are computed by multiplying the white-noise standard error of the slope by a factor of  $\sqrt{2}$   
453 on account of the 1-2-1 filter. Like BINS, the HadSST3 trend shows significant warming in  
454 the Gulf Stream extension, and also along the eastern margin. HadSST3 also shows a region



455 of cooling in the central SPG from 50-60°N, referred to as the ‘warming hole’ (Drijfhout et  
1 456 al., 2012), which is not well reproduced in BINS. Checking this particular difference suggests  
2 457 that data in the pre-1917 period originated mostly from one group of data from the ICES  
3 458 archive, often reported at set longitudes, and for which we applied an overall correction of -  
4 459 0.2°C on temperature, but with little comparison data to define it (Reverdin et al. 1994).  
5 460 Notice however that nonetheless, for the area average of the central SPG (**Fig. 6c**), the  
6 461 difference between BINS and HADSST3 is not significant for that period.  
7 462

14 463 The detrended RMS standard deviation of the pluri-annual T and S time series (**Figs. 8a** and  
15 464 **8b**) correspond to the expectation that large-scale temperature RMS standard deviation  
16 465 diminishes from west to east; whereas the salinity RMS values are largest in the west, then  
17 466 near 50°N with a decrease from west to east and from the southern to the northern SPG. This  
18 467 pattern is indicative on one hand of larger air-sea and hydrographical/heat forcings in the  
19 468 western SPG, and on the other hand of the presence during some winters of a rather shallow  
20 469 mixed layer in the western SPG (even in the Labrador Sea, where deep convection also often  
21 470 takes place (Yashayaev and Loder 2016)). In mid-ocean near 45-50°N, there might also be a  
22 471 contribution of displacements of hydrographical fronts.  
23 472

32 473 Surface density standard deviation (**Fig. 8c**) diminishes both from west to east and south to  
33 474 north. The relative contributions of T and S to detrended density variability are shown in **Fig.**  
34 475 **8d**. The contributions of SST and SSS to surface density variability are opposite in most  
35 476 places (as there is a positive correlation between SST and SSS variability on intra-annual to  
36 477 centennial time scale in a large part of this domain, so the effects of these variables on density  
37 478 variability tend to compensate each other). This also might explain a pattern of density rms  
38 479 variability which presents weaker zonal gradients in the west than what is found in SST or  
39 480 SSS.  
40 481

49 482 Interestingly, in the westernmost part of the domain, except near the Gulf Stream, the salinity  
50 483 contribution to density variability dominates over the temperature contribution (**Fig. 8d**),  
51 484 whereas in the eastern and northern parts of the SPG, temperature dominates. Thus in the first  
52 485 region, density tends to be positively correlated to SSS and SST, whereas in the other region it  
53 486 is negatively correlated with SSS and SST. In general, the SSS contribution is slightly larger  
54 487 for the non-detrended data (not shown), due to its relatively larger centennial trends in this  
55 488 part of the ocean (discussed in part 2 of this study).  
56 489  
57 490  
58 491  
59 492  
60 493  
61 494  
62 495  
63 496  
64 497  
65 498

489

1 490 Next, we show the total RMS variability contained at multidecadal frequencies. We low-pass  
2 491 filter the time series using a spectral filter with half power at a period close to 15 years. **Fig. 9**  
3 492 shows the percentage of the detrended pluri-annual variance explained by the low-pass  
4 493 filtered time series. The low-pass filtered variance percentage of SSS (**Fig. 9a**) and SST (**Fig.**  
5 494 **9b**) are less correlated spatially than overall RMS variability. For S, what striking is the lower  
6 495 percentages in the western part (as low as 40%) than in the eastern part of the domain (larger  
7 496 than 60%), whereas for T, it is mostly the northern part which has a larger percentage of  
8 497 variance in the multidecadal frequencies, with percentage of detrended variance reaching up  
9 498 to 80%. The low percentages of multidecadal variability for SSS in the northwest is  
10 499 consistent with the penetration in the ocean interior of short-lived freshwater pulses  
11 500 originating from the western shelves and the rim of the Labrador Sea (examples of recent  
12 501 short-term SSS variability in this region are presented in Tesdal et al. (2018)).

13 502  
14 503 The low-pass filtered time series explain comparatively less density variance, particularly in  
15 504 the western SPG region (**Fig. 9c**, values usually less than 50%), which suggests coordinated  
16 505 SSS and SST variations at lower frequencies with thus partial compensation on their  
17 506 contribution to density changes. Indeed, the low-pass filtered correlation of SSS and SST  
18 507 (**Fig. 8d**) is positive in most grid boxes, with large magnitudes in the central SPG, around  
19 508 Greenland and in the south-west north of the Gulf Stream as well as around the Grand Banks.  
20 509 Notice however, less significant correlation in other areas of the western, southern, and  
21 510 eastern parts of the domain close to Europe. The relationship between SSS and SST variations  
22 511 will be examined further in part 2 of this study.

23 512

## 24 513 **5. Discussion and Conclusions**

25 514 We have constructed a spatially averaged binned product BINS of pluri-annual T, S, and  
26 515 surface density for 1896-2015 north of 40°N, similar to what was done for S in Friedman et  
27 516 al. (2017), but at a higher spatial resolution. We deliberately excluded the shelf regions  
28 517 (except for one box along southwestern Greenland and one box on the southern Grand  
29 518 Banks), which have different dynamics, variability and sampling issues (Reverdin et al.  
30 519 2018). We have shown that in recent decades, the BINS pluri-annual variability of SST and  
31 520 SSS is coherent with published time series of upper ocean heat and salinity based on high  
32 521 quality hydrographic data. It provides also rather similar results to an analysis of SST and SSS

33 522

34 523

35 524

36 525

37 526

38 527

39 528

40 529

522 variability along two ship tracks since 1993, based on the same in situ data set for its main  
1 523 part (Reverdin et al. 2018).  
2  
3 524  
4  
5 525 Furthermore, BINS compares well with two gridded products of hydrographic data (EN4  
6  
7 526 from 1950-2015 and ISHII from 1950-2012), which use different data selection and mapping  
8  
9 527 methods. This suggests that in this region, the processing and spatial averaging of the  
10  
11 528 individual data in the spatial bins done in BINS is usually sufficient to portray the pluri-  
12  
13 529 annual variability of SST on the grid box scale, at least since 1950, and that during this  
14  
15 530 period, the data set used does not contain large biases compared to these other data sets. On  
16  
17 531 pluri-annual time scales, BINS SST also fits largely with what is portrayed in HadSST3,  
18  
19 532 except in the pre-WWII period for the Labrador Sea and the Norwegian Sea. Insufficient  
20  
21 533 coverage or erroneous data, either in HadSST3 or BINS, might be causing these  
22  
23 534 discrepancies. Thus, more care should be taken when interpreting variability in BINS before  
24  
25 535 1950.  
26  
27 536  
28  
29 537 The product combines time series of pluri-annual variability in different seasons. This was  
30  
31 538 required to reduce sampling errors to a reasonable level (in particular pre-1950), but this  
32  
33 539 might also mask or alias important differences between the seasons. For example in the  
34  
35 540 northern part of the subtropical gyre (thus, south of the region we investigate) a strong  
36  
37 541 seasonal modulation in the recent trends towards increasing SSS has been documented,  
38  
39 542 associated to important seasonal changes of the hydrological cycle (Yu et al. 2017). In the  
40  
41 543 Labrador Sea, too, on an interannual time scale, large summer-time anomalies of SSS have  
42  
43 544 been documented in the recent decade (2008 and 2012) that don't have a clear counterpart in  
44  
45 545 other seasons (Tesdal et al. 2018). Such events, and also the seasonality of atmospheric  
46  
47 546 forcing, seasonal thermal stratification and mixing, could induce large pluri-annual  
48  
49 547 differences between the anomalies in different seasons. Indeed, **Fig. 3** suggests that the  
50  
51 548 differences between seasons are large in the central Labrador Sea, but for the other open-  
52  
53 549 ocean regions, different seasons present more similar decadal and longer frequencies.  
54  
55 550 Possibly, insufficient accuracy of the binned time series and the change in collection and  
56  
57 551 measurement techniques could preclude further investigation of the seasonality of the decadal  
58  
59 552 or longer variability with this dataset. For example, in boxes of the southern SPG, we noticed  
60  
61 553 SSS differences in the autumn around 1960 that could be a data artifact. Differences with  
62  
63 554 HadSST3 taking place around 2000 could also be data-related (either in HadSST3 with  
64  
65 555 drifting buoy data becoming more numerous, or in BINS with the Argo data afterwards).

556 Nonetheless, a more homogeneous 25-year dataset in the central SPG resolving seasonal  
1 557 variability along well sampled ship lines (Reverdin et al. 2018) also pointed out a similarity in  
2  
3 558 pluri-annual variability for the different seasons, although interannual RMS variability tended  
4  
5 559 to be larger there too in early summer for SST.  
6

7 560  
8  
9 561 This aside, the seasonal inhomogeneity in data coverage, with less sampling in winter in  
10  
11 562 particular before 1955, should have little impact on the reconstructed pluri-annual time series.  
12  
13 563 We however warn that this might not be a wise substitute for the seasonal time series, in  
14  
15 564 particular for studies of winter conditions the central Labrador Sea or water mass formation,  
16  
17 565 but then obviously the available binned data present more gaps, and the original seasonal time  
18  
19 566 series have larger error bars.  
20

21 567  
22 568 Density is a non-linear function of temperature and salinity, with the character of non-  
23  
24 569 linearity increasing at low T. We deliberately emphasized winter characteristics when  
25  
26 570 estimating density from temperature and salinity time series, but use the BINS time series  
27  
28 571 which combine SST and SSS anomalies in the four (or three) different seasons. We noticed  
29  
30 572 that in some regions pluri-annual variability has smaller amplitude in winter (Table 3  
31  
32 573 summarizing **Fig. 3**), thus this choice might result in an overestimation of winter-time pluri-  
33  
34 574 annual density variability. It would be also misleading to use these density pluri-annual time  
35  
36 575 series as a proxy for water density in other seasons.  
37

38 576  
39 577 We do not have a direct comparison of SSS BINS time series prior to the 1950s. We base our  
40  
41 578 evaluation that they provide reasonable estimates for this early period mostly on comparisons  
42  
43 579 of the SST BINS time series with HadSST3 binned data. However, before 1950 in the Nordic  
44  
45 580 Seas and Labrador Sea, the binned data have larger uncertainties and winter seasons are  
46  
47 581 poorly (or not at all) sampled. Thus, clearly our estimates for SSS are also less certain in these  
48  
49 582 regions prior to 1950. A possibility for further validation would be to compare with  
50  
51 583 independent proxy-based estimates of surface variability. Few such proxy time series have  
52  
53 584 been derived in this region resolving the multidecadal variability in SST and even less in  
54  
55 585 SSS, and their uncertainties are probably too large for such a validation (Hall et al.  
56  
57 586 (2010), for a site in the Iceland Basin (Gardar drift); Richter et al. (2009), for a site in the  
58  
59 587 northern Rockall Trough area (Feni drift); Moffa-Sanchez et al. (2017) and references  
60  
61 588 therein as well as Thornalley et al. (2018), for a site in the southeastern Labrador Sea).  
62  
63 589  
64  
65

590 BINS has sufficient spatial resolution to resolve large-scale patterns of RMS standard  
1 591 deviation of the variability in SST, SSS and density (this was done after removing linear  
2 592 trends). RMS variability in SSS and to a lesser degree in SST increases towards the west, with  
3 593 the contribution to density of SSS variability dominating that of SST in the west, whereas in  
4 594 the eastern and northern parts of the SPG, temperature typically dominates the variability. The  
5 595 portion of variability in multidecadal frequencies (here with a cut-off at 15 years) could be  
6 596 ascertained. It is found both for SST and SSS to be a very large part of pluri-annual  
7 597 variability, with lesser relative contribution in the west for SSS and in the southern part for  
8 598 SST. For density, it is less prominent, except in the northeastern part of the SPG, where SST  
9 599 variability contribution dominates and is very much at multidecadal frequencies (also see  
10 600 Holliday et al. 2015). The higher frequencies are more influenced by the sampling  
11 601 uncertainties, in particular the effect of interpolation and interannual smoothing during data  
12 602 gaps in either specific seasons or all seasons (near WWII, for example). Thus this analysis of  
13 603 the relative importance of multidecadal variability is more dataset-dependent than the RMS  
14 604 variability

15  
16  
17  
18  
19  
20  
21  
22  
23  
24  
25  
26  
27  
28  
29  
30

### 31 607 **Acknowledgements**

32 608 This is a contribution to the French SSS observation service, which is supported by French  
33 609 agencies INSU/CNRS, IRD, CNES and IPEV, as well as from SOERE CTDO2. The Rockall  
34 610 Trough time series were provided with support from the UK Natural Environment Research  
35 611 Council (Extended Ellett Line program, National Capability). The station time series south of  
36 612 Iceland were provided with Icelandic support. The annual oceanographic monitoring of the  
37 613 Labrador Sea was initiated as a Canadian contribution to the World Ocean Circulation  
38 614 Experiment in 1990 and is presently conducted as a core component of the Atlantic Zone Off-  
39 615 Shelf Monitoring Program (AZOMP) run by the Bedford Institute of Oceanography of  
40 616 Fisheries and Oceans Canada. The International Argo Program is part of the Global Ocean  
41 617 Observing System (Argo, 2000). Argo data are available from the Coriolis Global Data  
42 618 Center, Institut français de recherche pour l'exploitation de la mer (Ifremer). The HadSST3  
43 619 and EN4 data were provided by the Met Office Hadley Center, and the ISHII data were  
44 620 provided by the NCAR Research Data Archive. A.R.F. was supported by SOERE CTDO2  
45 621 and the ERC funded project TITAN (EC-320691). L.C. acknowledges support from the  
46 622 Swedish National Space Board (SNSB; Dnr 133/17).

47 623  
48  
49  
50  
51  
52  
53  
54  
55  
56  
57  
58  
59  
60  
61  
62  
63  
64  
65

624 **References**

- 1  
2 625 Alory G, Delcroix T, Téchiné P, Diverrès D, Varillon D, Cravatte S, ... Roubaud F (2015)  
3 626 The French contribution to the voluntary observing ships network of sea surface salinity.  
4 627 Deep Sea Res I 105: 1–18. <http://doi.org/10.1016/j.dsr.2015.08.005>  
5 628 Argo (2000) Argo float data and metadata from Global Data Assembly Centre (Argo GDAC).  
6 629 SEANOE. <http://doi.org/10.17882/42182>  
7  
8 630 Belkin I M, Levitus S, Antonov J, Malmberg S.-A (1998) “Great Salinity Anomalies” in the  
9 631 North Atlantic. Prog Oceanogr 41(1): 1–68. [http://doi.org/10.1016/S0079-6611\(98\)00015-](http://doi.org/10.1016/S0079-6611(98)00015-9)  
10 632 9  
11 633 Böning C W, Behrens E, Biastoch A, Getzlaff K, Bamber J L (2016) Emerging Impact of  
12 634 Greenland Meltwater on Deepwater Formation in the North Atlantic Ocean. Nature  
13 635 Geoscience. <https://doi.org/10.1038/ngeo2740>.  
14  
15 636 Buckley M W, Marshall J (2016) Observations, Inferences, and Mechanisms of the Atlantic  
16 637 Meridional Overturning Circulation: A Review. Reviews of Geophysics 54 (1):  
17 638 2015RG000493. <https://doi.org/10.1002/2015RG000493>.  
18  
19 639 Cabanes C, Grouazel A, von Schuckmann K, Hamon M, Turpin V, Coatanoan C, Paris F, et al  
20 640 (2013) The CORA Dataset: Validation and Diagnostics of in-Situ Ocean Temperature and  
21 641 Salinity Measurements. Ocean Sci 9 (1): 1–18. <https://doi.org/10.5194/os-9-1-2013>.  
22 642 Davis R E, Sherman J T, Dufour J (2001) Profiling ALACEs and other advances in  
23 643 autonomous subsurface floats. J Atmos Ocean Tech 18: 982-993.  
24  
25 644 Dickson R R, Meincke J, Malmberg M S-A, Lee A J (1988) The “Great Salinity Anomaly”  
26 645 in the northern North Atlantic 1968 – 1982. Prog Oceanogr 20: 103– 151.  
27 646 Drijfhout S, van Oldenborgh G J, Cimadoribus A (2012) Is a Decline of AMOC Causing the  
28 647 Warming Hole above the North Atlantic in observed and modeled warming patterns? J  
29 648 Clim 25: 8373–79. <https://doi.org/10.1175/JCLI-D-12-00490.1>.  
30  
31 649 Ebisuzaki W (1997) A method to estimate the statistical significance of a correlation when the  
32 650 data are serially correlated. J Clim 10(9): 2147–2153.  
33 651 Fofonoff N P (1985) Physical properties of seawater: A new salinity scale and equation of  
34 652 state for seawater. J Geophys Res 90(C2): 3332–3342.  
35 653 <https://doi.org/10.1029/JC090iC02p03332>.  
36  
37 654 Frankignoul C, Deshayes J, Curry R (2009) The Role of Salinity in the Decadal Variability of  
38 655 the North Atlantic Meridional Overturning Circulation. Climate Dynamics 33(6): 777–93.  
39 656 <https://doi.org/10.1007/s00382-008-0523-2>.  
40  
41 657 Friedman A R, Reverdin G, Khodri M, Gastineau G (2017) A new record of Atlantic sea surface  
42 658 salinity from 1896 to 2013 reveals the signatures of climate variability and long-term trends.  
43 659 Geophys Res Lett 44: 1866–1876. DOI:10.1002/2017GL072582.  
44 660 Good S-A, Martin M J, Rayner N A (2013) EN4: Quality Controlled Ocean Temperature and  
45 661 Salinity Profiles and Monthly Objective Analyses with Uncertainty Estimates. J Geophys  
46 662 Res 118(12): 6704–16. <https://doi.org/10.1002/2013JC009067>.  
47  
48 663 Hall I R, Boessenkool K P, Barker S, McCave I N, Elderfield H (2010) Surface and deep  
49 664 ocean coupling in the subpolar North Atlantic during the last 230 years. Paleoceanogr 25.  
50 665 doi:10.1029/2009PA001886.  
51 666 Holliday N P, Cunningham S A, Johnson C, Gary S F, Griffiths C, Read J F, Sherwin T  
52 667 (2015) Multidecadal variability of potential temperature, salinity, and transport in the  
53 668 eastern subpolar North Atlantic. J Geophys Res 120. doi:10.1002/2015JC010762.  
54  
55 669 Hughes, S. L., Holliday, N. P., Gaillard, F., and the ICES Working Group on Oceanic  
56 670 Hydrography, 2012. Variability in the ICES/NAFO region between 1950 and 2009:  
57 671 observations from the ICES Report on Ocean Climate. – ICES Journal of Marine  
58 672 Science, doi:10.1093/icesjms/fss044.Icelandic hydrographic surveys ...  
59  
60  
61  
62  
63  
64  
65

- 673 Ishii M, Kimoto M, Sakamoto K, Iwasaki S I (2006) Steric sea level changes estimated  
1 674 from historical ocean subsurface temperature and salinity analyses. *J Oceanography*  
2 675 62(2): 155-170.
- 3 676 Kennedy J J, Rayner N A, Smith R O, Parker D E, Saunby M (2011) Reassessing Biases and  
4 677 Other Uncertainties in Sea Surface Temperature Observations Measured in Situ since  
5 678 1850: 1. Measurement and Sampling Uncertainties. *J Geophys Res* 116.  
6 679 doi:201110.1029/2010JD015218.
- 7 680 Kennedy J J, Rayner N A, Smith R O, Saunby M, Parker D E (2011) Reassessing biases and  
8 681 other uncertainties in sea-surface temperature observations since 1850: 2. Biases and  
9 682 homogenisation. *J Geophys Res* 116 D14104. doi:10.1029/2010JD015220
- 10 683 Lavender K L, Davis R E, Owens W B (2000) Mid-depth recirculation observed on the  
11 684 interior Labrador and Irminger seas by direct velocity measurements. *Nature* 607: 66- 69.
- 12 685 Lozier M S (2012) Overturning in the North Atlantic. *Ann Rev of Marine Sci* 4(1): 291–315.  
13 686 <http://doi.org/10.1146/annurev-marine-120710-100740>
- 14 687 Moffa-Sanchez P, Hall I R (2017) North Atlantic variability and its links to European climate  
15 688 over the last 3000 years. *Nature comm.* 8:1726, 555. doi:10.1038/s41467-017-01884-8.
- 16 689 Piron A, Thierry V, Mercier H, Caniaux G (2017) Gyre-scale deep convection in the subpolar  
17 690 North Atlantic Ocean during winter 2014–2015. *Geophys Res Lett* 44: 1439–1447.  
18 691 doi:10.1002/2016GL071895.
- 19 692 Polyakov I V, Bhatt U S, Simmons H L, Walsh D, Walsh J E, Zhang X (2005) Multidecadal  
20 693 Variability of North Atlantic Temperature and Salinity during the Twentieth Century. *J*  
21 694 *Clim* 18(21): 4562–4581. <http://doi.org/10.1175/JCLI3548.1>
- 22 695 Rahmstorf S, Box J E, Feulner G, Mann M E, Robinson A, Rutherford S, Schaffernicht E J  
23 696 (2015) Exceptional twentieth-century slowdown in Atlantic Ocean overturning circulation.  
24 697 *Nature Climate Change* 5(5): 475–480. <http://doi.org/10.1038/nclimate2554>
- 25 698 Reverdin G (2010) North Atlantic Subpolar Gyre Surface Variability (1895–2009). *J Clim*  
26 699 23(17): 4571–4584. <http://doi.org/10.1175/2010JCLI3493.1>
- 30 700 Reverdin G, Cayan D, Dooley H, Ellett D, Levitus S, du Penhoat Y, Dessier A (1994) Surface  
31 701 Salinity of the North-Atlantic - Can We Reconstruct Its Fluctuations Over the Last 100  
32 702 Years. *Prog Oceanogr* 33(4): 303–346. [http://doi.org/10.1016/0079-6611\(94\)90021-3](http://doi.org/10.1016/0079-6611(94)90021-3)
- 33 703 Reverdin G, Cayan D, Kushnir Y (1997) Decadal variability of hydrography in the upper  
34 704 northern North Atlantic 1948-1990. *J Geophys Res* 102: 8505-8531.
- 35 705 Reverdin G, Alory G, Diverres D, Bringas F, Goni G, Heilmann L, Chafik L, Szekely T,  
36 706 Friedman A R (2018) North Atlantic subpolar gyre along predetermined ship tracks since  
37 707 1993: a monthly data set of surface temperature, salinity, and density. *Earth Syst Sci Data*  
38 708 10: 1403-1415. <https://doi.org/10.5194/essd-10-1403-2018>.
- 39 709 Rhein M, Kieke D, Hüttl-Kabus S, Roessler A, Mertens C, Meissner R, Klein B, Böning C W,  
40 710 Yashayaev I (2011) Deep water formation, the subpolar gyre, and the meridional  
41 711 overturning circulation in the subpolar North Atlantic. *Deep Sea Res II* 58: 1819-1832.  
42 712 doi:10.1016/j.dsr2.2010.10.061
- 43 713 Richter T O., Peeters F J C, Weering T C E (2009) Late Holocene (0-2.4 ka BP) surface water  
44 714 temperature and salinity variability, Feni Drift, NE Atlantic Ocean. *Quat Sci Rev* 28:  
45 715 1941-1955.
- 46 716 Riser S C, Freeland H J, Roemmich D, Wijffels S, Troisi A, Belbéoch M, Gilbert D, et al.  
47 717 (2016) Fifteen Years of Ocean Observations with the Global Argo Array. *Nature Climate*  
48 718 *Change* 6 (2): 145–53. <https://doi.org/10.1038/nclimate2872>.
- 49 719 Roemmich, D, Johnson G C, Riser S, Davis R E, Gilson J, Owens W B, Garzoli S L, Schmid  
50 720 C, Ignaszewski M (2009) [The Argo Program: Observing the global ocean with profiling](https://doi.org/10.5670/oceanog.2009.36)  
51 721 [floats](https://doi.org/10.5670/oceanog.2009.36). *Oceanography*. 22:34-43. [10.5670/oceanog.2009.36](https://doi.org/10.5670/oceanog.2009.36)

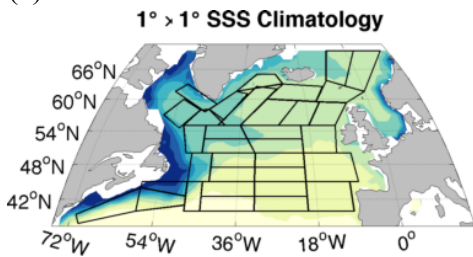
722 Skliris N, Marsh R, Josey S A, Good S A, Liu C, Allan R P (2014) Salinity changes in the  
1 723 World Ocean since 1950 in relation to changing surface freshwater fluxes. *Climate*  
2 724 *Dynamics* 43(3-4): 709–736. <http://doi.org/10.1007/s00382-014-2131-7>  
3 725 Tesdal J, Abernathy R P, Goes J I, Gordon A L, Haine T W (2018) Salinity Trends within  
4 726 the Upper Layers of the Subpolar North Atlantic. *J Clim* 31: 2675–2698.  
5 727 <https://doi.org/10.1175/JCLI-D-17-0532.1>  
6 728 Thornalley D J R, Oppo D W, Ortega P, Robson J I, Brierley C M, Davis R, Hall I R, Moffa-  
7 729 Sanchez P, Rose N L, Spooner P T, Yashayaev I, Keigwin L D (2018) Anomalous weak  
8 730 Labrador Sea convection and Atlantic overturning during the past 150 years. *Nature* 556.  
9 731 <https://doi.org/10.1038/s41586-018-0007-4>.  
10 732 UNESCO (1981) The Practical Salinity Scale 1978 and the International Equation of State of  
11 733 Seawater 1980. UNESCO technical papers in marine science 36: 25pp.  
12 734 Williams R G, Roussenov V, Lozier M S, Smith D (2015) Mechanisms of heat content and  
13 735 thermocline change in the subtropical and subpolar North Atlantic. *J Clim* 28: 9803-9813.  
14 736 doi:10.1175/JCLI-D-15-0097.1.  
15 737 Yashayaev I (2007) Hydrographic changes in the Labrador Sea, 1960-2005. *Prog Oceanogr*  
16 738 73: 242-276. doi:10.1016/j.pocean.2007.04.015.  
17 739 Yashayaev I, Loder J W (2009) Enhanced production of Labrador Sea Water in 2008,  
18 740 *Geophys Res Lett* 36 L01606. doi:10.1029/2008GL036162.  
19 741 Yashayaev I, Loder J W (2016) Recurrent replenishment of Labrador Sea water and  
20 742 associated decadal-scale variability. *J Geophys Res* 121:8095-8114.  
21 743 doi:10.1002/2016JC012046.  
22 744 Yashayaev I, Loder J W (2017) Further intensification of deep convection in the Labrador  
23 745 Sea in 2016. *Geophys Res Lett* 44:1429-1438, doi:/10.1002/2016GL071668.  
24 746 Yashayaev I, Seidov D (2015) The role of the Atlantic water in multidecadal ocean  
25 747 variability in the Nordic and Barents Seas. *Prog Oceanogr* 132: 68-127.  
26 748 Yu L, Jin X Liu H (2017) Poleward Shift in Ventilation of the North Atlantic Subtropical  
27 749 Underwater. *Geophysical Research Letters* 44. doi:  
28 750 <https://doi.org/10.1002/2017GL075772>  
29 751  
30  
31  
32  
33  
34  
35  
36  
37  
38  
39  
40  
41  
42  
43  
44  
45  
46  
47  
48  
49  
50  
51  
52  
53  
54  
55  
56  
57  
58  
59  
60  
61  
62  
63  
64  
65



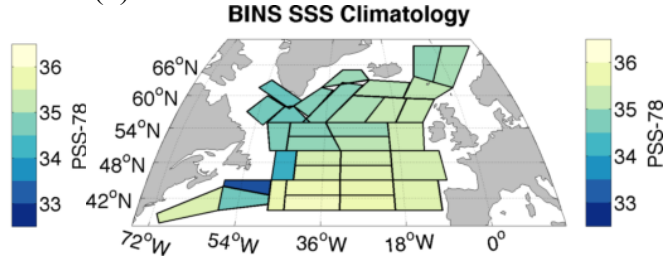
752 **Figures.**

1 753

(a)



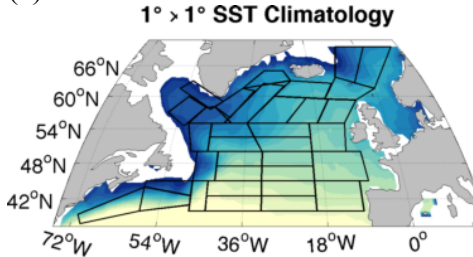
(b)



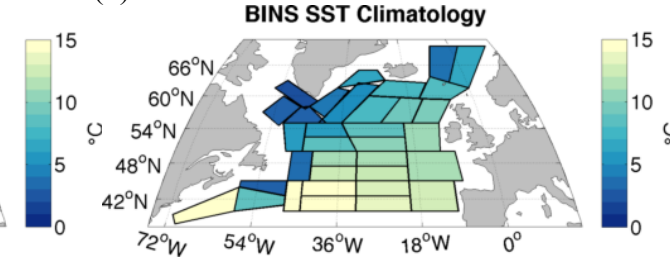
10 754

11 755

(c)



(d)



19 756

20 757

**Figure 1.** Gridded climatologies (approximately 1896–2000). (a) and (c): 1°×1° March climatologies for (a) SSS and (c) SST. (b) and (d): BINS March–May climatologies for (b) SSS and (d) SST.

21 758

22 759

23 760

24 760

25

26

27

28

29

30

31

32

33

34

35

36

37

38

39

40

41

42

43

44

45

46

47

48

49

50

51

52

53

54

55

56

57

58

59

60

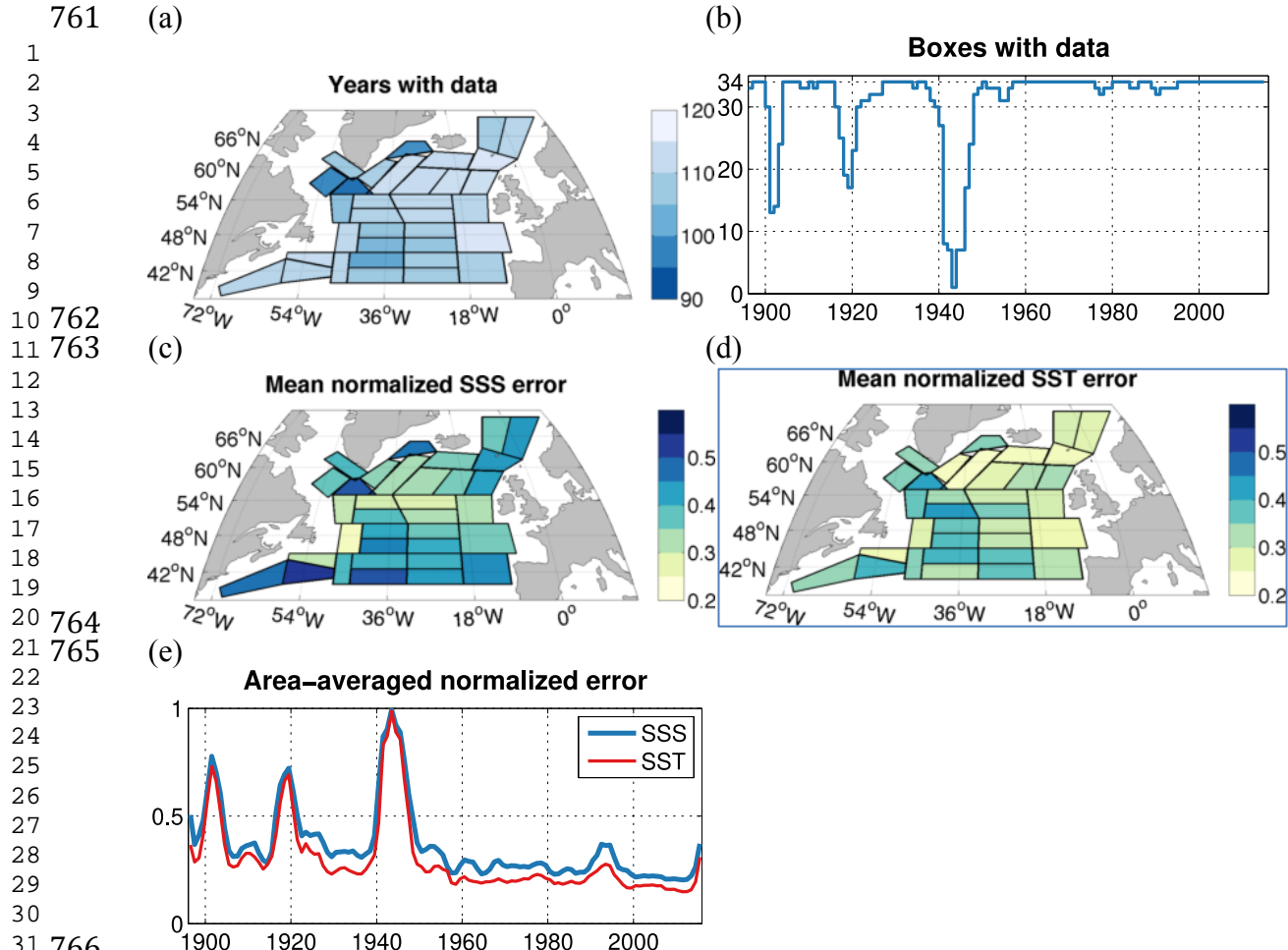
61

62

63

64

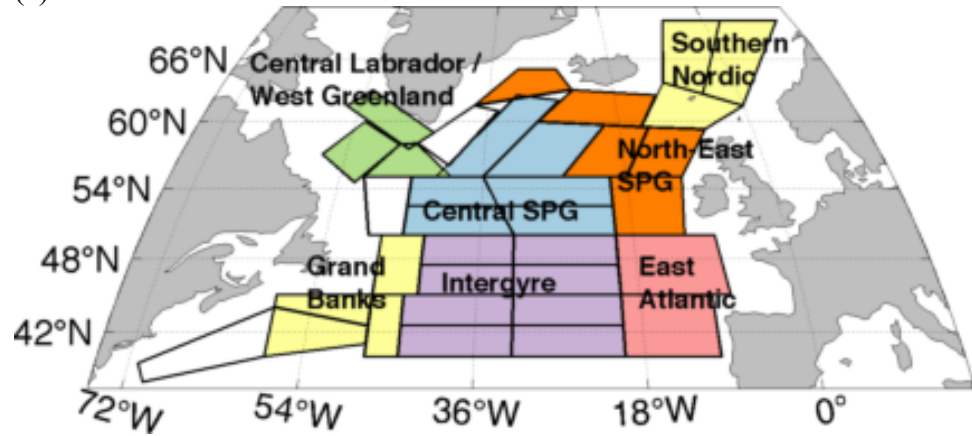
65



**Figure 2.** (a) Outline of BINS boxes, with number of years with data from 1896–2015 (out of a maximum of 120). (b) Time series of total BINS boxes with coverage (out of a maximum 34). The data counts in (a) and (b) are from after applying the 1-2-1 filter. (c) Mean annual SSS grid box error, defined as the mean grid box error divided by its maximum error (usually in 1943). (d) Same as (c), for SST. (e) Area-weighted normalized annual grid box error for SSS and SST.

16  
17  
18  
19  
20  
21  
22  
23  
24  
25  
26  
27  
28  
29  
30  
31  
32  
33  
34  
35  
36  
37  
38  
39  
40  
41  
42  
43  
44  
45  
46  
47  
48  
49  
50  
51  
52  
53  
54  
55  
56  
57  
58  
59  
60  
61  
62  
63  
64  
65

(a)



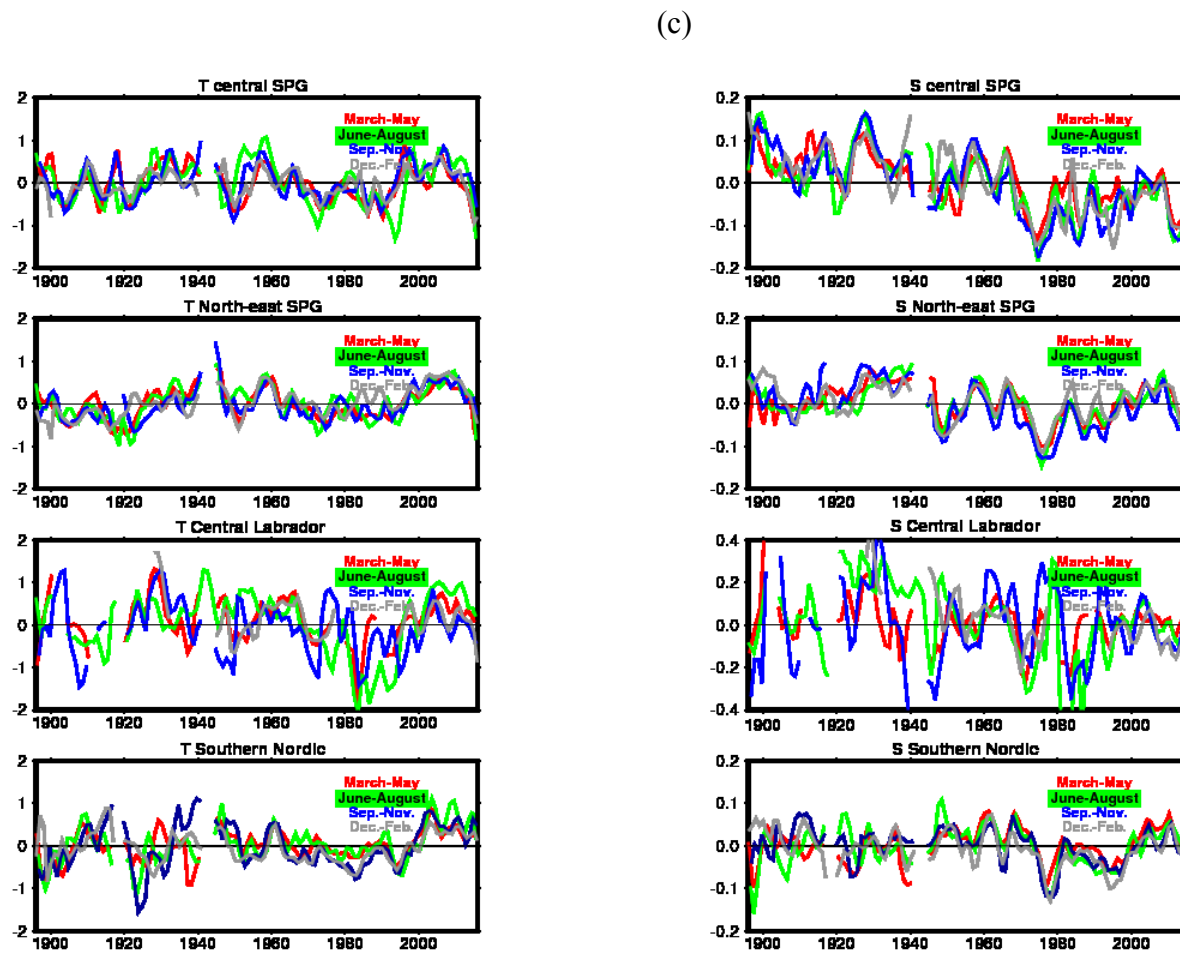


**Figure 3.** (a) Regional domains described in the text. (b-c) Seasonal time series for (b) T ( $^{\circ}\text{C}$ ) and (c) S (PSS-78) averaged over four domains portrayed in (a): central SPG, north-east SPG, central Labrador Sea / West Greenland, and the southern Nordic Seas.

16  
17  
18  
19  
20  
21  
22  
23  
24  
25  
26  
27  
28  
29  
30  
31  
32  
33  
34  
35  
36  
37  
38  
39  
40  
41  
42  
43  
44  
45  
46  
47  
48  
49  
50  
51  
52  
53  
54  
55  
56  
57  
58  
59  
60  
61  
62  
63  
64  
65

**Table 3.** Seasonal RMS and Pearson correlation coefficient. RMS values are in °C for T, and PSS-78 for S (×1000).  
Corresponding regions are shown on Fig. 3a.

<b>Region</b>	<b>Length</b>		<b>12-2</b>	<b>3-5</b>	<b>6-8</b>	<b>9-11</b>		<b>12-2</b>	<b>3-5</b>	<b>6-8</b>	<b>9-11</b>
Central SPG	112-116 yrs	<b>T RMS</b>	0.304	0.407	0.505	0.404	<b>S RMS</b>	73	60	72	79
		<b>T corr.</b>					<b>S corr.</b>				
		<b>12-2</b>		0.58	0.52	0.57	<b>12-2</b>		0.72	0.77	0.78
		<b>3-5</b>			0.55	0.71	<b>3-5</b>			0.79	0.82
		<b>6-8</b>				0.62	<b>6-8</b>				0.86
<b>Region</b>	<b>Length</b>		<b>12-2</b>	<b>3-5</b>	<b>6-8</b>	<b>9-11</b>		<b>12-2</b>	<b>3-5</b>	<b>6-8</b>	<b>9-11</b>
N-E SPG	113-115 yrs	<b>T RMS</b>	0.339	0.338	0.375	0.336	<b>S RMS</b>	42	41	44	55
		<b>T corr.</b>					<b>S corr.</b>				
		<b>12-2</b>		0.65	0.54	0.60	<b>12-2</b>		0.72	0.75	0.73
		<b>3-5</b>			0.76	0.71	<b>3-5</b>			0.81	0.78
		<b>6-8</b>				0.74	<b>6-8</b>				0.80
			<b>12-2</b>	<b>3-5</b>	<b>6-8</b>	<b>9-11</b>		<b>12-2</b>	<b>3-5</b>	<b>6-8</b>	<b>9-11</b>
Southern Nordic		<b>T RMS</b>	0.358	0.351	0.425	0.524	<b>S RMS</b>	41	40	47	41
		<b>T corr.</b>					<b>S corr.</b>				
		<b>12-2</b>		0.31	0.40	0.61	<b>12-2</b>		0.50	0.43	0.66
		<b>3-5</b>			0.69	0.41	<b>3-5</b>			0.66	0.52
		<b>6-8</b>				0.57	<b>6-8</b>				0.61
			<b>12-2</b>	<b>3-5</b>	<b>6-8</b>	<b>9-11</b>		<b>12-2</b>	<b>3-5</b>	<b>6-8</b>	<b>9-11</b>
Central Labrador/ West Greenland*		<b>T RMS</b>	0.47	0.385	0.482	0.602	<b>S RMS</b>	130	95	131	162
		<b>T corr.</b>					<b>S corr.</b>				
		<b>12-2</b>		0.81	0.20	0.60	<b>12-2</b>		0.37	0.50	0.27
		<b>3-5</b>			0.60	0.78	<b>3-5</b>			0.56	0.50
		<b>6-8</b>				0.52	<b>6-8</b>				0.42

16  
17  
18  
19  
20  
21  
22  
23  
24  
25  
26  
27  
28  
29  
30  
31  
32  
33  
34  
35  
36  
37  
38  
39  
40  
41  
42  
43  
44  
45  
46  
47  
48  
49  
50  
51  
52  
53  
54  
55  
56  
57  
58  
59  
60  
61  
62  
63  
64  
65

		<b>12-2</b>	<b>3-5</b>	<b>6-8</b>	<b>9-11</b>		<b>12-2</b>	<b>3-5</b>	<b>6-8</b>	<b>9-11</b>
Grand Banks	<b>T RMS</b>	0.95	0.792	0.890	0.990	<b>S RMS</b>	148	156	132	150
	<b>T corr.</b>					<b>S corr.</b>				
	<b>12-2</b>		0.26	0.33	0.29	<b>12-2</b>		0.09	0.24	0.51
	<b>3-5</b>			0.56	0.21	<b>3-5</b>			0.49	0.33
	<b>6-8</b>				0.44	<b>6-8</b>				0.50
Intergyre	<b>T RMS</b>	0.49	0.42	0.61	0.49	<b>S RMS</b>	87	76	82	100
	<b>T corr.</b>					<b>S corr.</b>				
	<b>12-2</b>		0.56	0.19	0.42	<b>12-2</b>		0.64	0.65	0.73
	<b>3-5</b>			0.44	0.53	<b>3-5</b>			0.51	0.55
	<b>6-8</b>				0.42	<b>6-8</b>				0.59
East Atlantic	<b>T RMS</b>	0.37	0.37	0.41	0.51	<b>S RMS</b>	53	61	55	54
	<b>T corr.</b>					<b>S corr.</b>				
	<b>12-2</b>		0.59	0.41	0.57	<b>12-2</b>		0.40	0.53	0.56
	<b>3-5</b>			0.57	0.52	<b>3-5</b>			0.59	0.34
	<b>6-8</b>				0.38	<b>6-8</b>				0.51

\* small number of common points, and varying number of boxes; thus not reliable, in particular for S.  
Both for Southern Nordic and Central Labrador, very different number of years in winter and other seasons  
(only on the order of 60 years with winter data in some of the boxes included in the average)

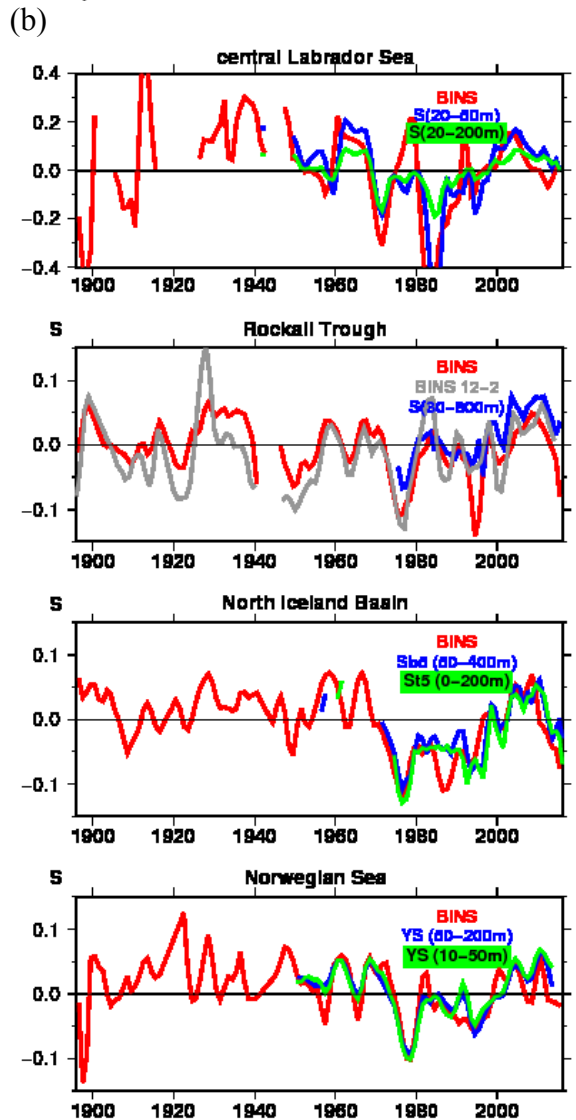
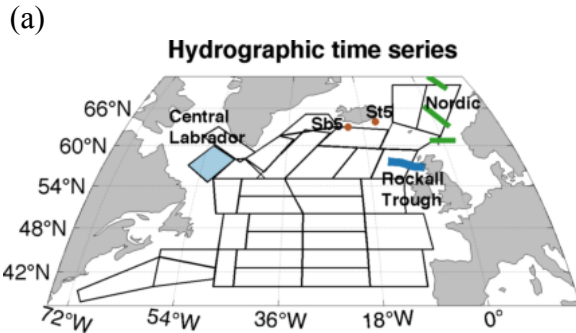


**Figure 4.** (a) Map showing hydrographic time series locations with BINS grid boxes. (b) Comparison for S of BINS (in red) with hydrographic time series low passed 1-2-1 over successive years; Central Labrador Sea (top; green and blue for different layer averages), Rockall Trough (top middle; the green curve is from BINS but for the winter (Dec-Feb.) season; blue is the vertically averaged (30-800m) S time series), Nor Iceland Basin (lower middle; two vertically averaged station time series are presented); and eastern Norwegian Sea (bottom; the blue and green time series is a compilation of the offshore data (median averaged) in 3 Norwegian Sea sections presented in Yashayaev and Seidov (2015), for two different depth ranges).

16  
17  
18  
19  
20  
21  
22  
23  
24  
25  
26  
27  
28  
29  
30  
31  
32  
33  
34  
35  
36  
37  
38  
39  
40  
41  
42  
43  
44  
45  
46  
47  
48  
49  
50  
51  
52  
53  
54  
55  
56  
57  
58  
59  
60  
61  
62  
63  
64  
65

**Table 4a.** Hydrographic sections and BINS: RMS variability for S (PSS-78) and T (°C), and lag-0 correlation coefficient.

<b>Region</b>	<b>Years S</b>	<b>RMS (S)</b>		<b>corr (S)</b>	<b>Years T</b>	<b>RMS (T)</b>		<b>corr (T)</b>
		<b>section</b>	<b>BINS</b>			<b>section</b>	<b>BINS</b>	
S Rockall (30–800m)	37	.040	0.048	0.73	37	0.284	0.350	0.80
S Iceland (50–400m)	47	.050	0.043	0.81	47	0.413	0.391	0.87
Central Labrador (20–50m)	69	.155	0.169	0.76	67	0.715	0.716	0.74
Norwegian Sea (10-50m)	64	.039	0.038	0.82	64	0.31	0.31	0.87

**Table 4b.** Hydrographic section lag correlation with BINS.

<b>Region</b>	<b>Lag</b>	<b>Years (S)</b>	<b>corr. (S)</b>	<b>Years (T)</b>	<b>corr. (T)</b>
South Rockall	-2	35	0.57	35	0.56
(30–800m)	-1	36	0.70	36	0.65
	0	37	0.73	37	0.80
	+1	37	0.77	37	0.80
(BINS leads)	+2	37	0.68	37	0.72

<b>Region</b>	<b>Lag</b>	<b>Years (S)</b>	<b>corr. (S)</b>	<b>Years (T)</b>	<b>corr. (T)</b>
South Iceland	-2	45	0.54	44	0.59
(50–400m)	-1	46	0.68	45	0.74
	0	47	0.81	45	0.87
	+1	47	0.88	45	0.89
(BINS leads)	+2	47	0.83	45	0.81

<b>Region</b>	<b>Lag</b>	<b>Years (S)</b>	<b>corr. (S)</b>	<b>Years (T)</b>	<b>corr. (T)</b>
Eastern Norwegian Sea	-2	64	0.48	64	0.70
(10-50m)	-1	64	0.72	64	0.81
	0	64	0.82	64	0.87
	+1	64	0.74	64	0.83
(BINS leads)	+2	64	0.54	64	0.72



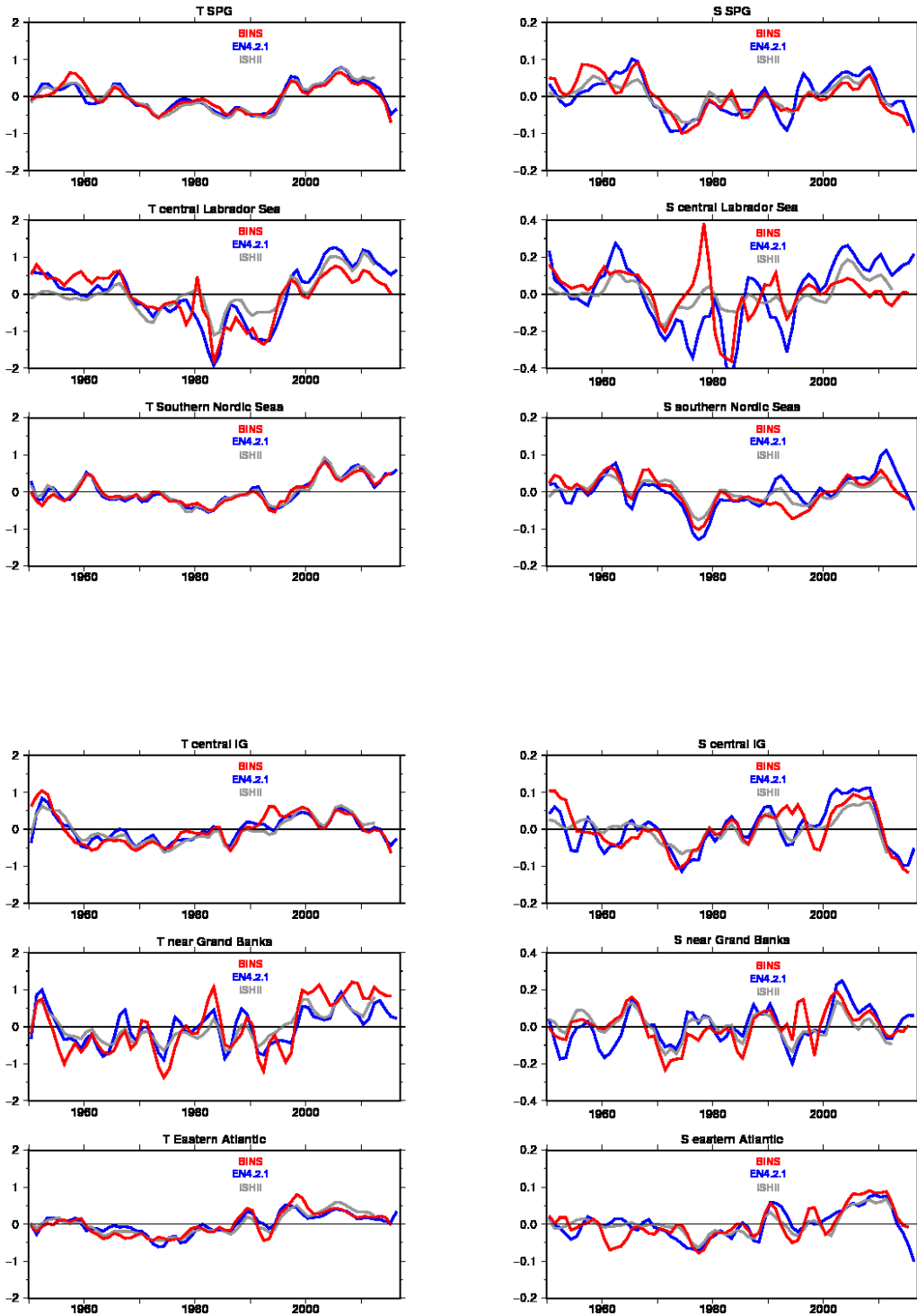


**Figure 5.** Comparison of regional T (left, °C) and S (right, PSS-78) time series from BINS with EN4 (1950-2015) and ISHII (1950-2012) surface products. The regional domains are the ones presented in Fig. 3. Here, the SPG region includes both the central SPG and the north-east SPG (and the south Greenland/southwest Irminger Sea box).

16  
17  
18  
19  
20  
21  
22  
23  
24  
25  
26  
27  
28  
29  
30  
31  
32  
33  
34  
35  
36  
37  
38  
39  
40  
41  
42  
43  
44  
45  
46  
47  
48  
49  
50  
51  
52  
53  
54  
55  
56  
57  
58  
59  
60  
61  
62  
63  
64  
65

**Table 5.** RMS variability and correlation with BINS: (a) EN4, (b) ISHII.

<b>(a) EN4 / BINS</b>		<b>RMS (S)</b>			<b>corr (S)</b>	<b>RMS (T)</b>		<b>corr (T)</b>
		<b>(PSS-78)</b>				<b>°C</b>		
<b>Region</b>	<b>Time period</b>	<b>EN4</b>	<b>BINS</b>			<b>EN4</b>	<b>BINS</b>	
SPG	1950–2015	0.050	0.046	0.78		0.36	0.34	0.93
Central Labrador/ West Greenland	1950–2015	0.173	0.121	0.49		0.76	0.63	0.87
Central Labrador/ West Greenland	excluding 1976–1979	0.169	0.112	0.67		0.78	0.64	0.87
Southern Nordic S	1950–2015	0.045	0.039	0.75		0.34	0.32	0.96
Intergyre	1950–2012	0.057	0.057	0.78		0.33	0.43	0.85
Grand Banks	1950–2012	0.098	0.114	0.40		0.47	0.69	0.42
East Atlantic	1950–2012	0.037	0.042	0.73		0.26	0.32	0.84

<b>(b) ISHII / BINS</b>		<b>RMS (S)</b>			<b>corr (S)</b>	<b>RMS (T)</b>		<b>corr (T)</b>
		<b>(PSS-78)</b>				<b>°C</b>		
<b>Region</b>	<b>Time period</b>	<b>ISHII</b>	<b>BINS</b>			<b>ISHII</b>	<b>BINS</b>	
SPG	1950–2012	0.034	0.045	0.90		0.38	0.34	0.95
Central Labrador/ West Greenland	1950–2012	0.075	0.124	0.55		0.50	0.64	0.74
Central Labrador/ West Greenland	excluding 1976-79	0.077	0.115	0.61		0.52	0.65	0.75
Southern Nordic	1950–2012	0.028	0.040	0.91		0.35	0.32	0.9
Intergyre	1950–2012	0.034	0.045	0.71		0.34	0.34	0.62
Grand Banks	1950–2012	0.068	0.124	0.45		0.41	0.65	0.42
East Atlantic	1950–2012	0.030	0.040	0.73		0.28	0.32	0.65

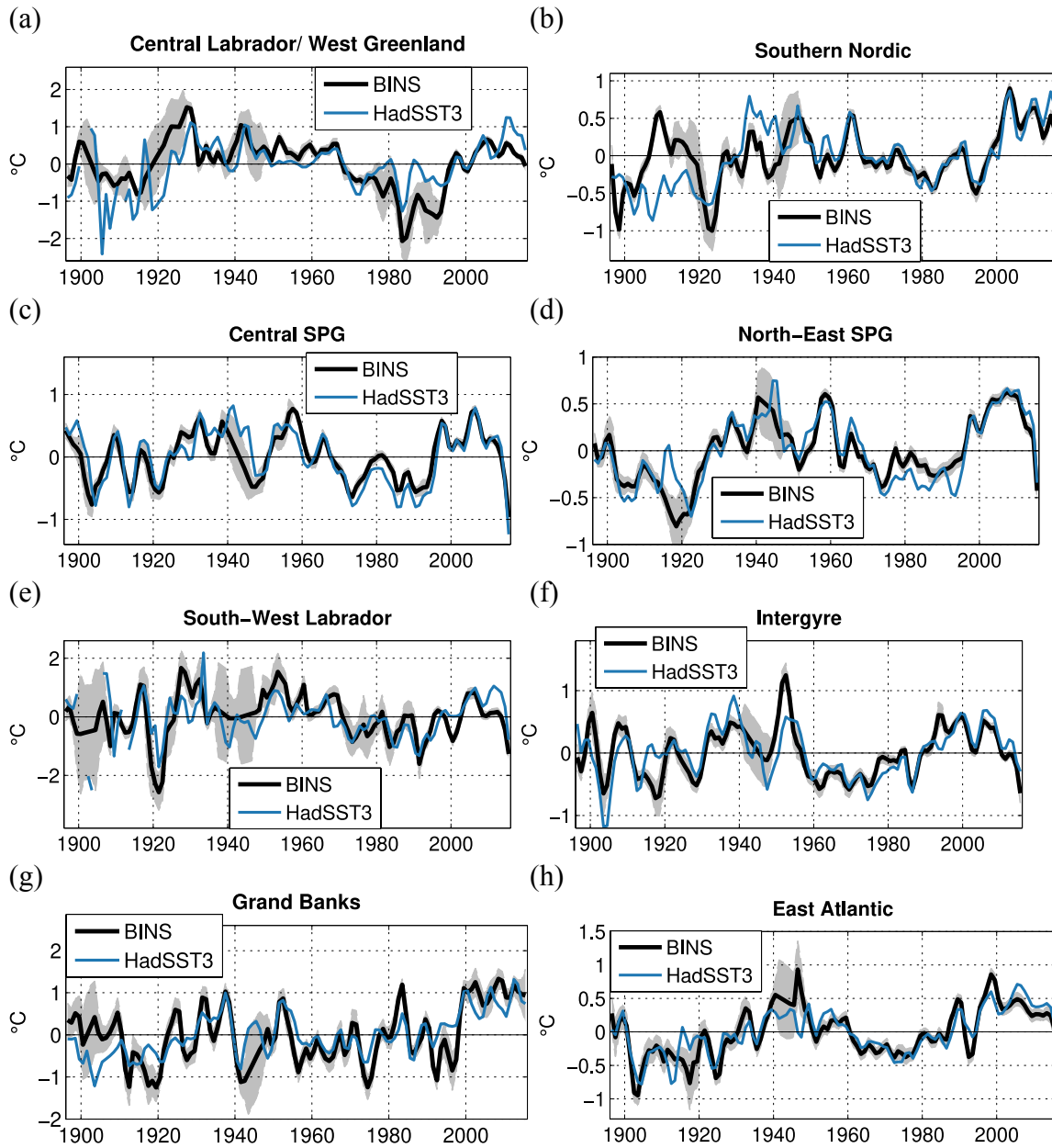


**Figure 6.** Area-averaged BINS and HadSST3 SST anomalies: (a) central Labrador / West Greenland, (b) southern Nordic, (c) central SPG, (d) north-east SPG, (e) south-west Labrador, (f) intergyre, (g) Grand Banks / Labrador Current, (h) east Atlantic. Shading indicates  $\pm 2$  BINS error terms. The corresponding regions are shown in **Fig. C1**.

**Table 6.** HadSST3 correlation with BINS SST

<b>Region</b>	<b>Time period</b>	<b>corr</b>	<b>Time period</b>	<b>corr</b>
Central SPG	1896–2015	0.84	1950–2015	0.95
N-E SPG	1896–2015	0.87	1950–2015	0.93
Central Labrador/ West Greenland	except 1900–01, 1910	0.57	1950–2015	0.72
SW Labrador	except 1900–01, 1904–1905, 1912	0.56	1950–2015	0.71
Southern Nordic	1896–2015	0.65	1950–2015	0.93
Intergyre	1896–2015	0.74	1950–2015	0.84
Grand Banks	1896–2015	0.67	1950–2015	0.82
East Atlantic	1896–2015	0.82	1950–2015	0.89

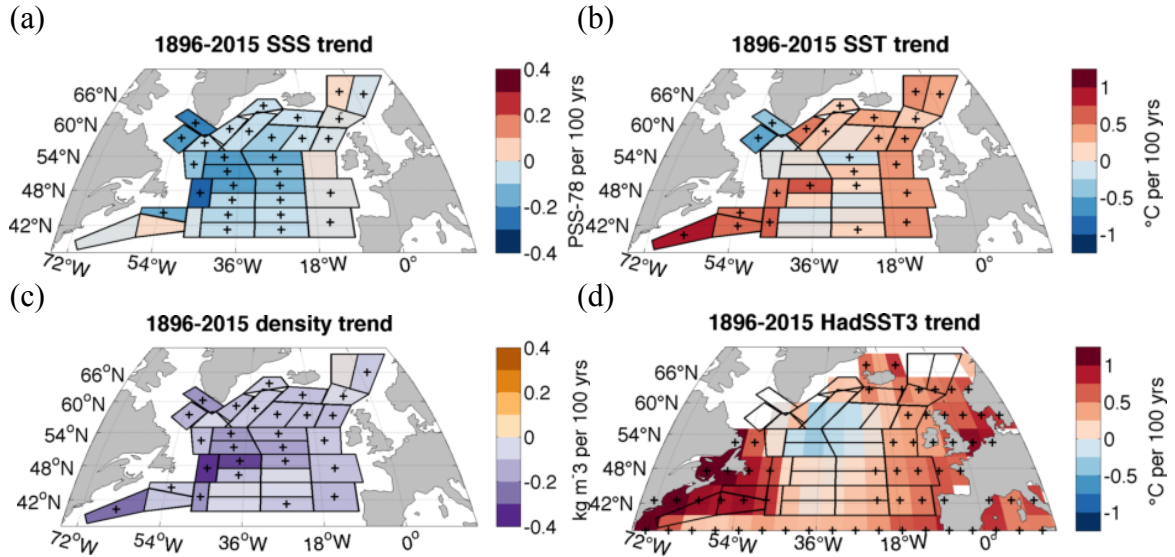


**Figure 7.** Trend over 1896–2015 (a) SSS; (b), SST; and (c) density; per 100 years. Pluses indicate where the slope magnitude is larger than twice the estimated error. (d) HadSST3 trend, per 100 years.

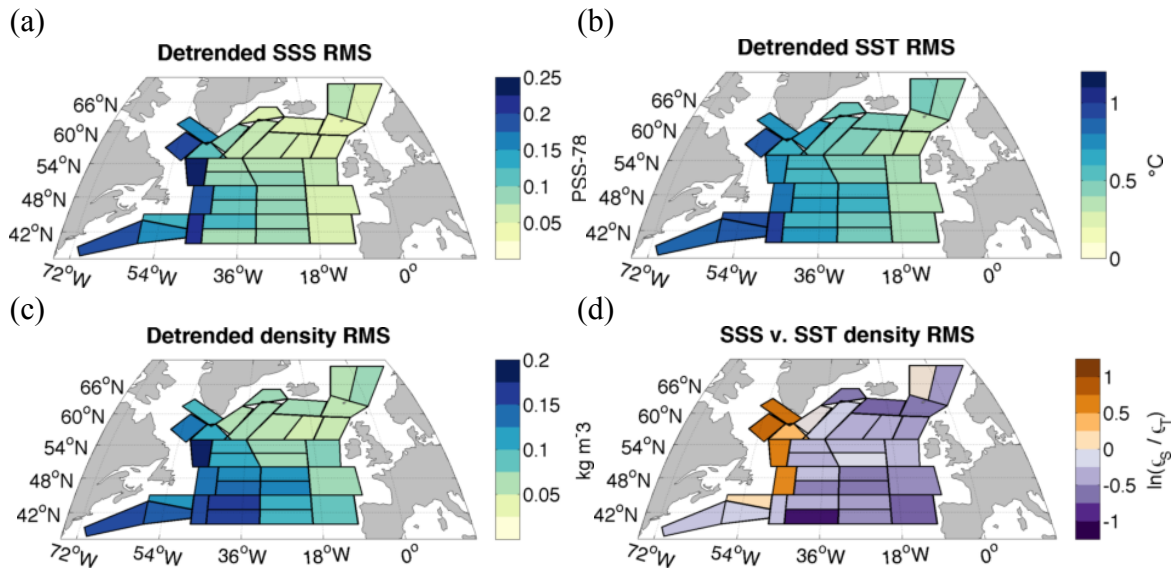


**Figure 8.** Detrended pluri-annual (1-2-1 filtered) RMS variability for (a) SSS, (b) SST, and (c) density ( $\rho$ ). (d) Ratio of the contributions of detrended SSS and SST to density RMS variability (plotted as a logarithm).

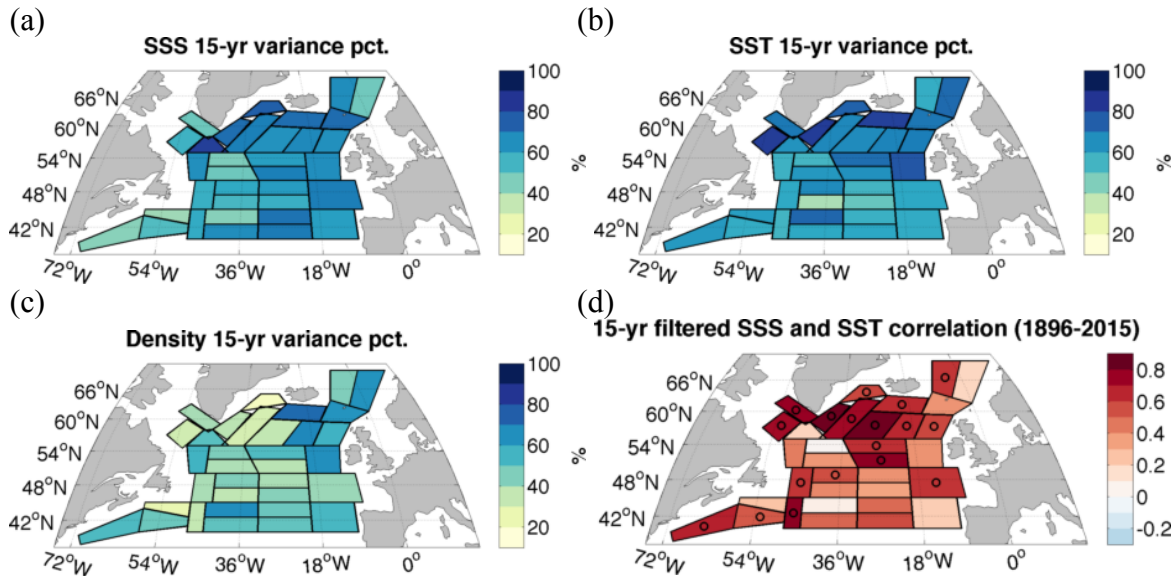


**Figure 9.** Percentage of detrended pluri-annual (1-2-1) variance explained by the 15-year low-pass filtered time series for (a) SSS, (b) SST, and (c) density. (d) Detrended correlation coefficient between the low-pass filtered SSS and SST. Circles indicate where the correlation is significant at  $p < 0.05$ , estimated with a random-phase bootstrap test to account for serial autocorrelation (Ebisuzaki, 1997).

## Appendix A. Comparison with Friedman et al. (2017)

The BINS boxes mainly use the same underlying SSS data as the large boxes north of 40°N in Friedman et al. (2017). The datasets cover a similar area (**Fig. A1a**), though as mentioned previously, the BINS boxes more carefully avoid shelf regions (except for southwest Greenland and the southern part of the Grand Banks). Most of the source data used in the two analyses are the same. Additionally, BINS also incorporates two small datasets from the 1900s and 1910s, plus a few recent transects (and 2014–2015). There are more gaps in the 19 BINS time series than in Friedman et al. (2017): in particular in 1918–1921, and during and just after WWII; these gaps are linearly interpolated in the smaller boxes. Also, when sampling is poor, but varying geographically within the larger boxes, it is possible that some spatial variability is aliased in the temporal variability in the larger boxes.

**Fig. A1b** compares the NATL index from Friedman et al. (2017), area-averaged SSS from 45°–62°N, with SSS averaged over a similar area in BINS. [NATL from Friedman et al. (2017) is only plotted through 2012, as 2013 was subject to endpoint smoothing]. The two products are very highly correlated ( $r=0.94$ , 1896–2012), and compatible considering the differences in area and error estimates. Greater differences are found for smaller regions in the first half of the record, particularly during the gap years mentioned above (not shown)

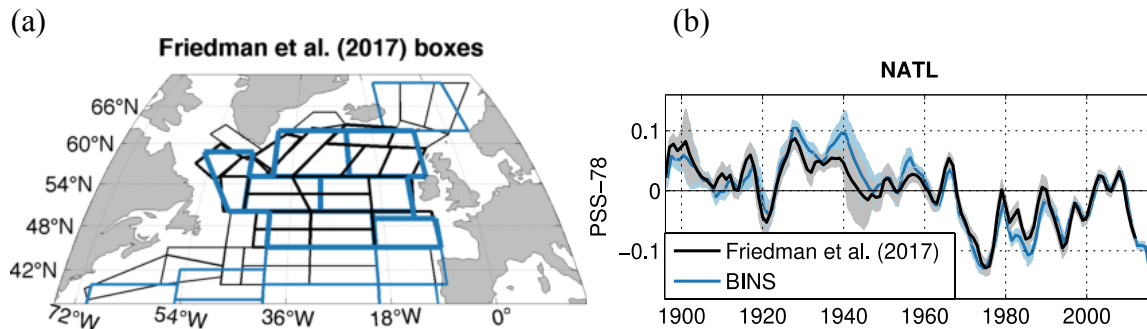


**Figure A1.** (a) Grid boxes from Friedman et al. (2017) (blue) and BINS (black). Thick lines indicate the NATL region. (c) Comparison of NATL index from Friedman et al. (2017) and BINS grid boxes. Anomalies are from 1896–2012; shading indicates  $\pm 2$  error terms.

## Appendix B. Comparison with Reverdin et al. (2018)

1  
2 As a check on the BINS time series, we compare the boxes with time series constructed with  
3 mostly similar data, monthly binned along two ship routes since mid-1993, intersecting near  
4 59.5°N/32°W: AX02 between Iceland and southern Newfoundland and AX01 between the  
5 North Sea and southern Greenland, mostly along 59.5°N (Reverdin et al. 2018), shown in **Fig.**  
6  
7 **B1a**. Time series along AX02 start in July 1993 with few gaps, whereas for AX01 some large  
8 data gaps were filled until late 1997. These time series, referred to as B-AX01 and B-AX02,  
9 provide increased spatial resolution at seasonal time scales, and portray very coherent  
10 variability where they intersect.  
11  
12  
13  
14  
15  
16

17  
18 We illustrate the comparison of pluri-annual variability of T and S between B-AX01 and  
19 BINS for overlapping boxes in the common period 1993-2015 (**Fig. B1b**). For S, the  
20 corresponding filtered RMS variability is larger in B-AX01 than in BINS by up to 20%, but  
21 with very high correlation coefficients (all larger than 0.95). The smaller RMS amplitudes of  
22 salinity in BINS probably result from the larger box sizes and the resulting spatial averaging.  
23 RMS variability is more similar for T, but with a slightly smaller correlation in the Iceland  
24 Basin (0.80) where gaps in 1993-1997 were the most common in B-AX01. Altogether, the  
25 comparisons for the two ship tracks suggest that the method used for BINS in the box  
26 averaging to produce pluri-annual variability yields correct results when data coverage is  
27 sufficient.  
28  
29  
30  
31  
32  
33  
34  
35  
36  
37  
38  
39  
40  
41  
42  
43  
44  
45  
46  
47  
48  
49  
50  
51  
52  
53  
54  
55  
56  
57  
58  
59  
60  
61  
62  
63  
64  
65



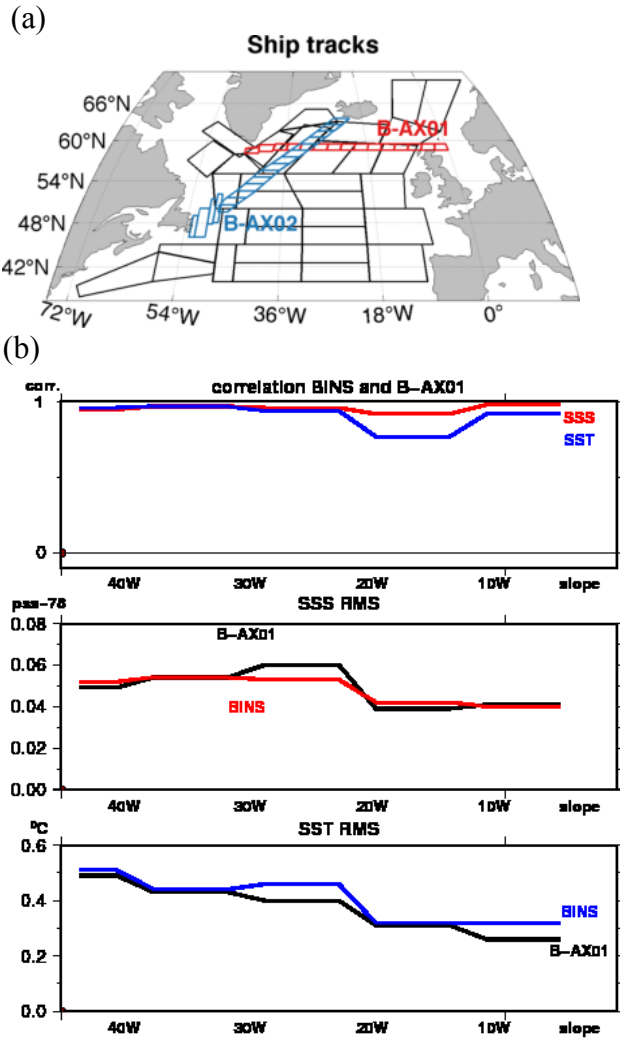


**Figure B1.** (a) AX01 (red) and AX02 (blue), from (Reverdin et al. 2018). (b) Comparison of B-AX01 with BINS, 1993–2015. The monthly time series of B-AX01 have been yearly-averaged (Dec-Nov), low-pass (1-2-1) filtered over successive years, and then averaged over the bins in BINS: correlation coefficient (top) for T (blue) and S (red), and RMS (middle for S and bottom for T) (B-AX01 in black, BINS in blue (T) and red (S)).

## Appendix C: Locations of BINS and HadSST3 grid boxes.

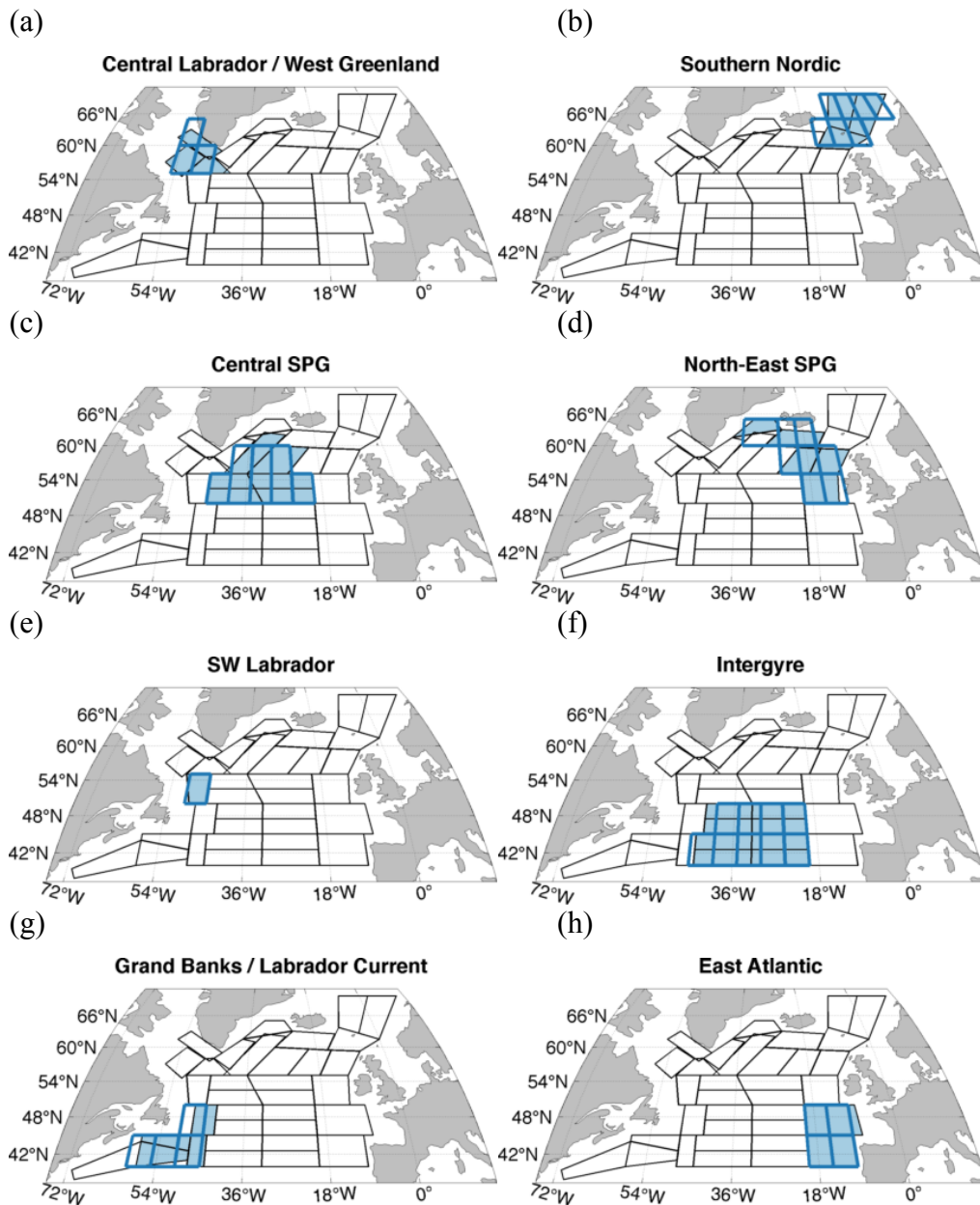


**Figure C1.** Locations of BINS and HadSST3 grid box regions used in the Section 3.3. Thick blue lines show the 5°×5° HadSST3 grid boxes; shading shows the corresponding BINS grid boxes: (a) central Labrador / West Greenland, (b) southern Nordic, (c) central SPG, (d) north-east SPG, (e) south-west Labrador, (f) intergyre, (g) Grand Banks / Labrador Current, (h) east Atlantic.



[Click here to view linked References](#)

1  
2  
3  
4  
5  
6  
7 1  
8  
9 2  
10 3  
11 4  
12 5  
13 6  
14 7  
15 8  
16 9  
17 10  
18 11  
19 12  
20 13  
21 14  
22 15  
23 16  
24 17  
25 18  
26 19  
27 20  
28 21  
29 22  
30 23  
31 24  
32 25  
33 26  
34 27  
35 28  
36 29  
37 30  
38 31  
39 32  
40 33  
41 34  
42 35  
43 36  
44 37  
45 38  
46 39  
47 40  
48 41  
49 42  
50 43  
51 44  
52 45  
53 46  
54 47  
55 48  
56 49  
57 50  
58 51  
59 52  
60 53  
61 54  
62 55  
63 56  
64 57  
65 58

North Atlantic extratropical and subpolar gyre variability during the last 120 years:  
a gridded dataset of surface temperature, salinity, and density.

Part 1: Dataset validation and RMS variability

G. Reverdin<sup>1</sup>, A. R. Friedman<sup>2</sup>, L. Chafik<sup>3</sup>, N. P. Holliday<sup>4</sup>, T. Szekely<sup>5</sup>, H. Valdimarsson<sup>6</sup>, I.  
Yashayaev<sup>7</sup>

<sup>1</sup> Sorbonne-Université, CNRS/IRD/MNHN (LOCEAN), Paris, France. ORCID ID  
<https://orcid.org/0000-0002-5583-8236>

<sup>2</sup> School of Geosciences, University of Edinburgh, UK. ORCID ID <https://orcid.org/0000-0001-6994-2037>

<sup>3</sup> Department of Meteorology and Bolin Centre for Climate Research, Stockholm University,  
Stockholm, Sweden. ORCID ID <https://orcid.org/0000-0002-5538-545X>

<sup>4</sup> National Oceanography Centre, Southampton, UK. ORCID ID <https://orcid.org/0000-0002-9733-8002>

<sup>5</sup> IUEM, Brest, France

<sup>6</sup> Marine and Freshwater Research Institute, Reykjavik, Iceland

<sup>7</sup> Bedford Institute of Oceanography, Fisheries and Oceans Canada, Dartmouth, NS, Canada

Corresponding author: G. Reverdin, Laboratoire d'Océanographie et de climatologie par  
expérimentation et analyse numérique, Institut Pierre Simon Laplace, Sorbonne-Université,  
case 100, 4 pl. Jussieu, 75252 Paris Cedex 05, France ([gilles.reverdin@locean-ipsl.upmc.fr](mailto:gilles.reverdin@locean-ipsl.upmc.fr) ;  
tel : 33-1-44272342 fax : 33-1-44273805 ; [orcid.org/0000-0002-5583-8236](https://orcid.org/0000-0002-5583-8236))

1  
2  
3  
4  
5  
6  
7  
8  
9  
10  
11  
12  
13  
14  
15  
16  
17  
18  
19  
20  
21  
22  
23  
24  
25  
26  
27  
28  
29  
30  
31  
32  
33  
34  
35  
36  
37  
38  
39  
40  
41  
42  
43  
44  
45  
46  
47  
48  
49  
50  
51  
52  
53  
54  
55  
56  
57  
58  
59  
60  
61  
62  
63  
64  
65

Abstract

We present a binned annual product (BINS) of sea surface temperature (SST), sea surface salinity (SSS) and sea surface density (SSD) observations for 1896–2015 of the subpolar North Atlantic between 40°N and 70°N, mostly excluding the shelf areas. The product of bin averages over spatial scales on the order of 200 to 500 km, reproduces most of the interannual variability in different time series covering at least the last three decades or of the along-track ship monitoring. Comparisons with other SSS and SST gridded products available since 1950 suggest that BINS captures the large decadal to multidecadal variability. Comparison with the HadSST3 SST product since 1896 also indicates that the decadal and multidecadal variability is usually well reproduced, with small differences in long-term trends or in areas with marginal data coverage in either of the two products. Outside of the Labrador Sea and Greenland margins, interannual variability is rather similar in different seasons. Variability at periods longer than 15 years is a large part of the total interannual variability, both for SST and SSS, except possibly in the south-western part of the domain. Variability in SST and SSS increases towards the west, with the contribution of salinity variability to density dominating that of temperature in the western Atlantic, except close to the Gulf Stream and North Atlantic Current in the southwest area. Weaker variability and larger relative temperature contributions to density changes are found in the eastern part of the gyre and south of Iceland.

Keywords: sea surface temperature, sea surface salinity, surface density, North Atlantic, decadal variability

1  
2  
3  
4  
5  
6  
750  
8  
951  
1052  
**1. Introduction**

1153 The North Atlantic subpolar gyre (SPG) receives salty surface water from the  
1254 subtropical North Atlantic as well as fresh water originating from the Arctic and the Nordic  
13 seas and circulating mostly on and along the shelves. It is a formation site of deep and  
1455 intermediate waters and thereby a major contributor to the lower limb of the Atlantic  
1556 meridional overturning circulation (AMOC) (Rhein et al. 2011). There is wintertime  
1657 densification of the surface Labrador and Irminger Seas resulting in intermittent deep  
17 convection reaching and exceeding 2400 m in the mid-1990s and 2000 m in recent years  
1858 (Yashayaev and Loder 2017). Deep dense overflows from the Nordic Seas and the associated  
1959 mixing with and entrainment of local waters also add important hydrographic connections  
20 between the regions and the surface and deep layers. In both instances, one expects that  
2160 changes in surface density will modulate these vertical exchanges and the properties of the  
2261 deep and intermediate waters formed, and thus the AMOC. Many model studies (at various  
2362 spatial resolution) also suggest an influence of surface salinity changes in this region on  
24 changes in the AMOC (Frankignoul et al. 2009; Rahmstorf et al. 2015, Böning et al. 2016).  
2563 Whereas the connection between these surface changes and AMOC is still subject to  
2664 discussion (Lozier 2012; Williams et al. 2015; Buckley and Marshall 2016), the relation  
2765 between changes of surface density and upper or intermediate water formation is rather well  
28 established (Yashayaev and Loder 2016 2017; Piron et al. 2017). Seawater density is a  
2971 function of temperature and salinity, with the relative influence of salinity increasing when  
3072 temperature decreases. Thus, investigating surface density variability and attempting to  
3173 establish its past patterns of change requires a concurrent analysis of temperature and salinity  
3274 fields.

3375  
3476 Hydrographic data in the North Atlantic and neighboring seas have been used to analyze  
35 salinity and temperature on decadal time scales with a low spatial resolution , but only since  
3677 the mid-1960s and in more restricted areas since 1950 (Polyakov et al. 2005; Skliris et al.  
3778 2014; Holliday et al. 2015; Yashayaev 2007; Yashayaev and Loder 2016 2017). These data  
3879 also rarely provide direct indications of winter surface density field (regional estimates can be  
3980 found in Yashayaev and Loder (2016 2017)) that is the variable key to the connection  
4081 between the surface ocean and the ocean interior. In the last twenty years, the advent of  
4182 profiling floats (Lavender et al. 2000; Roemmich et al. 2009; Riser et al. 2016) has allowed  
4283

1  
2  
3  
4  
5  
6  
784 year-round three-dimensional monitoring of large-scale upper and intermediate ocean  
8  
985 variability (Tesdal et al. 2018), but these measurements do not yet help to resolve the decadal  
1086 to multidecadal frequencies. Multidecadal time series with at least annual or seasonal  
1187 resolution have also been produced at a few sites: Rockall Trough (Holliday et al., 2015), the  
12  
1388 Faroe-Shetland Channel (Hughes et al., 2012), south of Iceland (Icelandic hydrographic  
1489 surveys), in the center of the Labrador Sea (Yashayaev and Loder 2016 2017), or at station  
15  
1690 Mike and hydrographic sections in the Norwegian Sea (Yashayaev and Seidov 2015).  
1791 Otherwise, mapped monthly fields of T and S have been constructed by different objective  
1892 mapping methods based on the EN4 (Good et al. 2013), CORA (Cabanes et al. 2013) and  
19  
2093 Ishii et al. (2006) datasets that could have some coverage in a large part of this domain for the  
2194 last 65 years. Monthly mapped sea surface temperature (SST) fields have also been produced  
2295 with sufficient coverage into large parts of the SPG since the 1890s using mostly ship log data  
23  
2496 with a shift in the last two decades to drifter SST data. Carefully estimated bias correction has  
2597 been applied to subsets of these data, such as done in Hadley Centre SST (HadSST3;  
26  
2698 Kennedy et al. 2011a and 2011b). However, these binned SST datasets present gaps in some  
27  
2899 northern regions, in particular before 1922.

29  
30  
3101 Long-term box averages in the SPG with near-annual resolution were presented in Reverdin  
3202 (2010) and Friedman et al. (2017). Reverdin (2010) described a record of SST and SSS in the  
3303 northeastern part of the SPG from 1895–2009. There, co-variability of temperature (T) and  
34  
3504 salinity (S) was found on decadal or multidecadal time scales in different seasons, with a  
3605 slight dominance of temperature on density variability (partially compensated by the salinity  
37  
38106 contribution). Friedman et al. (2017) examined interannual (1-2-1 smoothed over successive  
3907 years) salinity time series in larger boxes over the Atlantic from 20°S–70°N (the temperature  
4008 reports associated with the salinity data were not examined). The largest salinity root mean  
41  
42109 square (RMS) variability was found in the northern tropics, from 5°–20°N. In the subpolar  
4310 North Atlantic, RMS variability was shown to decrease to the northeast from the Labrador  
44  
44111 Sea to the Nordic seas (Friedman et al. 2017, Fig. 1), though the large grid box size did not  
45  
4612 permit finer examination of the spatial structure.

4713  
48  
49114 Using similar box averaging as in these previous two studies, we present a higher-resolution  
5015 binned product of temperature and salinity since 1896 in the subpolar North Atlantic and  
5116 southern Nordic seas and draw first conclusions obtained with the dataset. Focusing on the  
52  
5317 region north of 40°N allows us to describe co-located SSS and SST at higher spatial scales

1  
2  
3  
4  
5  
6  
7 118 (less than 500km) than presented previously, without having large periods with data gaps  
8  
9 119 (except during or just after WWI and WWII in some sub-regions).

10 120  
11 121 In this paper we present and validate the binned product at interannual time scales, and also  
12 122 discuss its RMS variability. A second part of this study (in preparation) examines the decadal  
13 123 and multidecadal variability, and relationship with North Atlantic climate variations. The  
14 124 dataset sources and construction are described in Section 2. In Section 3 we validate the  
15 125 dataset and compare it with other products. In Section 4, we examine the spatial distribution  
16 126 of temporal variability of SSS, SST, and surface density, followed by summary and  
17 127 discussion in Section 5.

## 2. Data and methods

### 2.1. Dataset construction

21 128  
22 129  
23  
24 130  
25 131  
26 132 The main data sources are described in Reverdin et al. (1994), Reverdin (2010), and Friedman  
27 133 et al. (2017). A significant part of the temperature and salinity (reported as practical salinity)  
28 134 data was collected on merchant and other selected vessels (including the weather ships), in  
29 135 particular before the mid-1970s north of 50°N, and before WWII and since 1977 south of  
30 136 50°N. This is also the case since 1993, mostly along two ship tracks between southern  
31 137 Newfoundland and Reykjavik and between the North Sea and Greenland (Reverdin et al.  
32 138 2018), as well as near France and between the English Channel and eastern North America.  
33 139 For the first two tracks, intake temperature was measured part of the time, XBTs were  
34 140 dropped and water samples collected, which allows for identification / estimation of possible  
35 141 temperature and salinity biases in the records from thermosalinographs (TSG) (Alory et al.  
36 142 2015; Reverdin et al. 2018). The identification of the temperature biases is less certain for the  
37 143 other vessels since 1993, but water samples were also collected to correct salinity biases in  
38 144 TSG records. This is complemented by near-surface hydrographic data during cruises, and  
39 145 since 1996, by measurements from drifters, and upper level data (often near 5-8m depth) from  
40 146 Argo floats (Roemmich et al. 2009; Riser et al. 2016), as well as from earlier PALACE floats  
41 147 (Lavender et al. 2000; Davis et al. 2001).

42 148  
43 149 The depth of sampling and the methods of collection and analysis have changed in time, as  
44 150 well as data accuracy, and thus some subsets of the data require correction of identified  
45 151 biases, both for temperature and salinity, as commented in the earlier papers. Bias correction

1  
2  
3  
4  
5  
6  
7  
8  
9  
10  
11  
12  
13  
14  
15  
16  
17  
18  
19  
20  
21  
22  
23  
24  
25  
26  
27  
28  
29  
30  
31  
32  
33  
34  
35  
36  
37  
38  
39  
40  
41  
42  
43  
44  
45  
46  
47  
48  
49  
50  
51  
52  
53  
54  
55  
56  
57  
58  
59  
60  
61  
62  
63  
64  
65

follows Reverdin et al. (1994) for ship data before the 1990s (based on comparison with surface data from Nansen casts). There is nonetheless the possibility of seasonal stratification between the data collected below the surface (for example, from TSG data, Argo floats and CTD/Nansen casts) and the surface data (for example from drifters, or in earlier times from bucket sampling). In particular, the change in depth of sampling in time can result in artificial time variability, due to near-surface stratification. In other parts of the world, this has been documented due to surface heating and evaporation or precipitation (Boutin et al., 2016). In regions of sustained wind conditions, and away from shelves with surface freshwater sources (melting sea ice or icebergs, outflows from fjords, river plumes), we expect stratification on the order of or less than 0.01 in practical salinity and 0.1°C in temperature. Sustained wind conditions are commonly melt in all seasons near 55-65°N, and probably a little less so in particular in spring/summer further south and north.

We construct annual time series of deviations from the seasonal cycle in boxes for four different seasons, using a similar methodology as in Friedman et al. (2017) and applied from 1896–2015 for both T and S, over smaller spatial bins. This new box-product will be referred to as BINS. The boundaries of the 34 boxes were redesigned to better fit with oceanic fronts and main currents than in Friedman et al. (2017). One box in the central Labrador Sea corresponds to what is used by Yashayaev and Loder (2016) for creating a combined Labrador Sea time series, and box boundaries in the eastern subpolar North Atlantic are chosen as in Holliday et al. (2015). Except for one box off southwest Greenland and one box on the southern part of the Grand Banks, the boxes do not overlap with the shelves and with areas of large seasonal sea ice cover. In the northeastern SPG, the resulting boxes provide a slightly lower spatial resolution than what was used in Reverdin (2010), but for which the different time series were rather well correlated. To give an idea of the resolution achieved, the SSS and SST late-winter climatologies are mapped onto the BINS grid boxes (**Fig. 1**), which shows that the main characteristics of spatial variability are retained by this choice of grid.

The construction of box time series and their error estimates is described in Friedman et al (2017). Here, the main steps are summarized, with specifics and additions related to BINS further described. The SSS and SST climatologies were constructed on a 1°×1° grid with little spatial smoothing and gap-filling, with an adjustment to the mean and up to three sinusoidal harmonics of the year, when data was sufficient. Deviations from this climatology of



1  
2  
3  
4  
5  
6  
7 186 individual data are estimated (T being in °C and S reported in the practical salinity scale 1978  
8  
9 187 (PSS-78; Fofonoff 1985; UNESCO 1981). For T, outliers were removed using a spatially  
10 188 variable threshold (between 3°C and 6°C), inspired by the local standard deviation. We  
11 189 compared this to a fixed 3°C error threshold, which yielded generally similar results albeit  
12  
13 190 with smaller interannual excursions. Largest differences were found in the central Labrador  
14 191 Sea in the 1920s, a period with extremely low data coverage. S outliers were removed  
15  
16 192 similarly, with less influence on the variability. In each box, these individual deviations are  
17 193 then combined for the individual seasons and years, by median-averaging the individual  
18 194 deviations. The seasonal anomalies are 1-2-1 smoothed over successive years (not applied at  
19  
20 195 the start and end years) and then averaged annually from December–November, inversely  
21 196 weighted by error. [The annual period was incorrectly stated as March–February in Friedman  
22 197 et al. (2017)]. Before being combined, the seasonal anomalies were adjusted to a common  
23  
24 198 baseline over the 40-year period from 1956–1995, which was chosen due to data coverage.  
25 199  
26 200 The fall season (September–November) is not included in most areas north of 45°N in the  
27  
28 201 western Atlantic, including in the central Labrador and southwest Labrador boxes due to  
29 202 poorly correlated T or S time series in the fall with the other seasons in these regions. In the  
30  
31 203 Norwegian Sea, central Labrador, southwest Labrador, and West Greenland, the winter  
32 204 season (December–February) data are not included before 1947 due to insufficient coverage.  
33 205  
34  
35 206 The total number of years with data is shown in **Fig. 2a**. Coverage is below 100 years in the  
36 207 North Irminger Sea and central Labrador Sea grid boxes; all other grid boxes have more than  
37  
38 208 100 years of coverage. The periods of missing data occur mainly during WWI and WWII, and  
39 209 around 1900 (**Fig. 2b**). Multi-year data gaps are linearly interpolated, and attributed an error,  
40 210 equal to the standard deviation of the whole time series (which is probably an overestimate).  
41  
42 211 A few missing end years (mostly 1896) in some boxes were filled by extending the first non-  
43 212 missing value. As in Friedman et al. (2017), regional average error terms are constructed by  
44 213 RMS averaging the error terms of their constituent individual boxes (which assumes that the  
45  
46 214 errors are uncorrelated in different boxes). The BINS SSS regional average fields are  
47 215 compared with those of Friedman et al. (2017) in Appendix A for the common period 1896-  
48  
49 216 2013, showing differences most commonly within the  $\pm 2$  standard error ranges.

50 217  
51 218 Figs. **2c–2d** present an estimate of the average interannual grid box error as the mean  
52  
53 219 error term divided by the error term during the year when there was no coverage and the error

1  
2  
3  
4  
5  
6  
7  
8  
9  
10  
11  
12  
13  
14  
15  
16  
17  
18  
19  
20  
21  
22  
23  
24  
25  
26  
27  
28  
29  
30  
31  
32  
33  
34  
35  
36  
37  
38  
39  
40  
41  
42  
43  
44  
45  
46  
47  
48  
49  
50  
51  
52  
53  
54  
55  
56  
57  
58  
59  
60  
61  
62  
63  
64  
65

is maximum (1943, except in the West Greenland box, when it is 1917). This is thus an indication of the ratio of noise relative to signal. This shows for S, the smallest relative errors are in the central SPG. For temperature, the largest relative errors are in the western part of the domain, where intra-annual variability and eddy variability are largest and not adequately sampled in this data set. The normalized area-averaged error for SSS and SST is shown in **Fig. 2e** and mirrors data coverage, with a larger value in the last year (2015) because error is not reduced in that year by the filtering.

Density is computed from the annual binned SST and SSS values using EOS80 (UNESCO, 1981), and referring the annual anomalies to the March average T and S values. Because SST is lower in winter and density becomes less sensitive to temperature variations when temperature decreases, this choice slightly decreases the dependency of density on SST compared to using an annual average reference. What motivated this choice was that we wanted to have an estimate typical of winter conditions. Density errors are calculated from the errors in interannual SSS and SST, assuming that they are uncorrelated.

### 2.2 Seasonal dependency of the interannual variability

The combination of the four seasonal time series to create an annual time series in each bin implicitly assumes that the four seasons portray comparable signals/patterns of interannual variability. This is particularly important if one season is missing, as is the case for the winter season in some boxes for the first part of the records. To get a sense of how well this holds for individual seasons, we combine the time series of individual bins into seven main multi-box regions (**Fig. 3a**): the central Labrador Sea / West Greenland Shelf (3 grid boxes), the southern Nordic seas (3 grid boxes), the north-east part of the SPG (5 grid boxes), the central SPG (6 grid boxes), a large central area of the intergyre gyre south of 50°N (8 boxes), an eastern Atlantic region (two boxes), and four boxes in the southwestern region around the Grand Banks. The regions are chosen for similar source data and coherent variability signals (except for the last one). For example, the two Norwegian Sea grid boxes contain mostly Norwegian and Swedish surface data before WWII, and afterwards much hydrographic data. The central Labrador Sea / West Greenland region contains hydrographic data from the Ice Patrol and other cruises in the southwest, and a mix of hydrographic data and merchant ship data until 1960 in the shelf box close to Greenland. South of 50°N, many different countries contributed to the surface data before WWII, and the French data sources are a large contribution since the mid-1970s. Three grid boxes are not included in any of these regions

1  
2  
3  
4  
5  
6  
7 54 due to low seasonal correlations in S and more varied data sources: the southwest Labrador  
8  
9 55 Sea, south Greenland/ southwest Irminger Sea, and the western area north of the Gulf Stream.

10 56  
11 57 The seasonal correlations are summarized in **Table 3**. For the central SPG and north-east SG  
12  
13 58 regions (**Fig. 3b-c**, rows 1 and 2), the time series are most complete in all seasons. There, the  
14 59 different seasons present rather similar variability, both for T and S, although for T, the  
15  
16 60 summer (June-August season) deviates at times from the other seasons and presents more  
17 61 variance in the central SPG. Furthermore, after 1960, S anomalies in Sep-Nov in central SPG  
18 62 tend to be below the ones in the other seasons, and the opposite before. This might either be  
19  
20 63 the sign of a real long-term seasonal change, or the effect of changes in the dataset around  
21 64 1960 (transition in this region from bucket collection to other means of collecting water, for  
22 65 example).

23  
24 66  
25 67 In the southern Nordic seas (**Fig. 3b-c**, bottom row), the different seasons also present rather  
26  
27 68 similar variability, at least since 1950. Before that, this remains largely true for SSS, albeit  
28 69 with more variability in summer. For SST, this also holds before WWI, however between  
29 70 1920 and 1940, the different seasons present non-coherent variability. We suspect that this  
30  
31 71 might be caused by inhomogeneities in the dataset, either spatially, with a southward shift of  
32 72 the sampling in late autumn to early spring in this period, or due to lower data quality and  
33 73 larger random as well as systematic errors affecting the results and lowering correlations, such  
34  
35 74 as the documented use of engine room or intake temperature data from Norwegian vessels.  
36 75 For this reason and the limited winter sampling coverage, we chose not to incorporate the  
37  
38 76 winter season in the annual averages before 1947 in the two Norwegian Sea boxes.

39 77  
40 78 In the central Labrador Sea / West Greenland Shelf region (**Fig. 3b-c**, row 3), on the other  
41  
42 79 hand, while there is some similarity between the different seasons in SST (less so for the  
43 80 summer season), there is much less coherence in SSS, even during the last 50 years of more  
44 81 regular sampling. Notice in particular the large differences between the spring and autumn  
45  
46 82 seasons, which originate from the two boxes in central Labrador Sea and along west  
47 83 Greenland. These differences (and the much larger RMS variability in autumn) justify the  
48  
49 84 choice of not including the autumn season when combining the different seasons to create the  
50 85 BINS time series in this region. In the Grand Banks region, however, we have less correlation  
51 86 with winter season but with similar variance (**Table 3**), so that we chose to retain the winter  
52  
53 87 season. Elsewhere, the statistics associated with the comparison between the seasonal time

54  
55  
56  
57  
58  
59  
60  
61  
62  
63  
64  
65

1  
2  
3  
4  
5  
6  
788 series (**Table 3**) justify the choice to have retained all seasons in order to reduce the sampling  
8  
989 uncertainty in the BINS interannual time series.

### 1090 **2.3 Other products**

11291 In the next section, we validate BINS with some of the few published compiled hydrographic  
12292 time series that are available in the SPG, either from repeated seasonal cruises or a  
1493 compilation of data from different origins: the Rockall Trough time series since 1975  
15294 (Holliday et al. 2015); South Icelandic stations (Sevlogsbanki 5 (Sb5) and Stokksnes 5 (St5))  
16295 since the 1970s; and the central Labrador Sea since 1941 (Yashayaev and Loder, 2009 2016).  
1896 Notice also the time series in the Norwegian Sea summarized by (Yashayaev and Seidov  
19297 2015). We will also compare BINS to gridded datasets. These include the  $1^{\circ} \times 1^{\circ}$  EN4, version  
2298 4.2.1 (Good et al. 2013) fields from 1950-2015, as well as the 1950-2012  $1^{\circ} \times 1^{\circ}$  product of  
2299 Ishii et al. (2006), version 6.12 (referred to as ISHII). We also compared BINS to the  
23400 CORA5.0 fields (Cabanes et al. 2013) that have been extended to 1950, but that exclude  
2501 Nansen cast data, and thus cannot be used for the analysis of salinity before 1980, and have  
26302 much coarser spatial sampling in temperature than EN4 or ISHII. On the other hand, when  
27303 sampling is sufficient (mostly, in the northeastern part), results with CORA are comparable to  
29304 those of ISHII, and will not be discussed further. For long-term surface temperature, we also  
30305 compare BINS with the HadSST3 monthly product (Kennedy et al. 2011a and 2011b).  
3206

### 3307 **3. Dataset validation**

34308 In order to validate the BINS SST and SSS time series, we compare it first to local  
37309 compilations of high-quality hydrographic data. We also compare the binned time series to  
38310 different gridded time series to better characterize the properties of BINS. In addition,  
39311 Appendices A and B show comparisons with Friedman et al (2017) and Reverdin et al.  
40312 (2018), which are based on different binning (in time and space) of similar data sources.  
41313  
42314

#### 4315 **3.1 BINS and hydrographic time series**

44316 The sites of the different time series are presented in Fig. 4a. The Rockall Trough and central  
47317 Labrador time series fit rather well within some BINS grid boxes, and the South Icelandic  
48318 time series are just to the north of one BINS grid box. The results based on hydrographic time  
49319 series often comprise vertical averages, excluding the near-surface (5 to 10 m thick) layer,  
51320 which is often determined by specifics of performing oceanographic stations and  
52321

Mis en forme : Police :Non Gras

1  
2  
3  
4  
5  
6  
7  
8  
9  
10  
11  
12  
13  
14  
15  
16  
17  
18  
19  
20  
21  
22  
23  
24  
25  
26  
27  
28  
29  
30  
31  
32  
33  
34  
35  
36  
37  
38  
39  
40  
41  
42  
43  
44  
45  
46  
47  
48  
49  
50  
51  
52  
53  
54  
55  
56  
57  
58  
59  
60  
61  
62  
63  
64  
65

technological limitations. This averaging depth range was not optimized, but in Rockall Trough and near Iceland, it fits with the expected local maximum winter mixed layer. The time series are then averaged over annual means (after removal of an annual cycle), and smoothed with a 1-2-1 filter over successful years, similar to BINS.

The comparisons of these upper ocean time series with BINS are presented in **Fig. 4b** (with statistics in **Table 4**). At each site BINS is correlated with the vertically integrated time series, although the surface time series tend to have larger amplitudes. In the Labrador Sea, we compared different ranges, with the best correlation for the comparison to 20-50 m, which is within the mixed layer at least 6 months of the year and closely follows variations in seasonal discharge of freshwater and its interannual variations. There is still a correlation when considering the averages over the 20-200 m layer, which is within the winter mixed layer most years. The thicker layer time series however present less extreme amplitudes than the shallower ones. In the Rockall Trough, we also plot the surface time series based only on winter data, which is also correlated with the vertically integrated time series. The largest difference is found for South Iceland, with a low BINS S in the late 1980s that is not found in the hydrographic time series. However, there is also a difference in latitude between the BINS box and the site further north of the hydrographic time series.

Overall, we find that BINS surface time series are significantly correlated at 0-lag with upper ocean time series from hydrography, both for T and S (correlation coefficients are in the range 0.73 to 0.88 for the different time series of salinity or temperature), and exhibit very comparable RMS variability, as described in **Table 4a**. The analysis of lag correlation (summarized in **Table 4b**) indicates that the annually averaged BINS T and S precede by one year the vertically integrated upper ocean analysis both at the Rockall and Southern Iceland sites (for SST, the one-year lag correlation coefficients are respectively 0.80 and 0.89; and for SSS, respectively 0.77 and 0.88), as expected from winter ventilation of the upper ocean and time series analysis of the 20 to 40-year long weather-ship time series in the SPG (Reverdin et al., 1997). Interestingly, this is not the case for the Norwegian Sea time series.

### 3.2. BINS and gridded objective analyses

We compare the BINS time series with other gridded products of hydrographic data at their near-surface level that we average over the bins of the BINS analysis and filter in time to

1  
2  
3  
4  
5  
6  
7  
8  
9  
10  
11  
12  
13  
14  
15  
16  
17  
18  
19  
20  
21  
22  
23  
24  
25  
26  
27  
28  
29  
30  
31  
32  
33  
34  
35  
36  
37  
38  
39  
40  
41  
42  
43  
44  
45  
46  
47  
48  
49  
50  
51  
52  
53  
54  
55  
56  
57  
58  
59  
60  
61  
62  
63  
64  
65

correspond to the same time resolution (1-2-1 running average over successive years  
December to November).

Because of the differences in sampling and mapping, the comparison in individual boxes with  
BINS often presents a large scatter. We will thus average the time series over the same  
domains as for the seasonal time series (**Fig. 3a**). [One difference is that the central SPG and  
north-east SPG are combined into one SPG region]. Except in the Labrador Sea or near the  
Grand Banks, the time series of the three products (**Fig. 5**) are well correlated (**Table 5**).  
Correlation coefficients are larger for SST than for SSS, and for SSS, are usually larger  
between ISHII and BINS than between EN4 and BINS. In the Labrador Sea (row 2), there are  
differences both for SST and for SSS. For SSS, the large positive peak in BINS originates  
from a data gap in one of the three bins that are averaged in the regional time series. On the  
other hand, the altogether weaker SST-signal in ISHII in this box, something also found, but  
to a lesser domain in the other regions might result from the objective mapping method used  
or from more strident tests on outliers (Ishii and Kimoto, 2009). We also notice in the  
southern Labrador Sea for the last 20 years smaller positive SSS (and SST) anomalies in  
BINS than in the other two products, possibly a result of the thermosalinograph (TSG) data  
incorporated in BINS and not in the other products (Reverdin et al. 2018). On the other hand,  
near the Grand Banks during the last 20 years, T is higher in BINS than in the other products.  
Elsewhere, the major variability is portrayed with similar amplitude and roughly at the same  
time in the different products. For example in the SPG or southern Nordic seas, the salinity  
time series portray the events sometimes described as great salinity anomalies (Belkin et al.  
1998), the largest one in the central SPG happening in the early 1970s and referred to as the  
Great Salinity Anomaly (Dickson et al. 1988). The figures also suggest larger differences  
between the different products in the 1990s, in particular in the intergyre region.

The high overall agreement might result from a share of common hydrographic data  
incorporated in the different products. However, there is also a large portion of specific data  
that are not in all the products (T from mechanical or expandable bathythermographs are used  
in EN4 and ISHII, but not in BINS, and different sets of surface data are in BINS, but not  
used in EN4 and ISHII). There are also large methodological differences between the  
different products, both in data selection and validation and in mapping techniques and how  
seasonal anomalies are grouped or not. These comparisons, as well as the comparisons  
presented in 3.1, thus reinforce our assessment of usually small sampling errors for the BINS

1  
2  
3  
4  
5  
6  
7  
8  
9  
10  
11  
12  
13  
14  
15  
16  
17  
18  
19  
20  
21  
22  
23  
24  
25  
26  
27  
28  
29  
30  
31  
32  
33  
34  
35  
36  
37  
38  
39  
40  
41  
42  
43  
44  
45  
46  
47  
48  
49  
50  
51  
52  
53  
54  
55  
56  
57  
58  
59  
60  
61  
62  
63  
64  
65

product during that period, and that the product captures the major events of interannual variability at the grid box scale since 1950.

### 3.3 BINS and HadSST3

SST data in BINS and HadSST3 originate from different data streams. Although some data are certainly incorporated in both products, the overlap is probably rather minimal, as discussed in Reverdin et al. (1994). In particular, the data before 1920 north of 58°N in BINS originate mostly from Danish and Norwegian sources which are not incorporated in HadSST3. In the last two decades, data from TSGs on merchant vessels or from profiling floats are a large contribution to BINS but are not included in HadSST3, whereas the drifter SST data used in HadSST3 are mostly not in BINS. Even in the post-WWII to mid-1970s period, when ocean weather ships contribute both to HadSST3 and BINS, temperature data in the two products often originate from different sensors. BINS and HadSST3 also account for biases and uncertainties differently. HadSST3 does not apply smoothing or interpolation between neighboring grid cells, facilitating more direct regional comparisons.

We examine the monthly HadSST3 anomalies, version 3.1.1.0 (median realization). We average the HadSST3 grid boxes into similar sub-regions similar to those shown in **Fig. 3a**. The southwest Labrador Sea BINS grid box is also examined, which closely corresponds to one HadSST3 grid box. Generally however, the large 5°×5° HadSST3 grid boxes do not align directly with BINS grid boxes; the specific grid boxes are shown in **Fig. C1**. We average the HadSST3 anomalies into 3-month seasons (skipping over missing values). The seasonal anomalies are 1-2-1 smoothed (excluding endpoints) over successive years, and the seasonal anomalies are averaged into Dec–Nov annual means (again skipping over missing values). The winter season is not included in the southern Nordic, central Labrador, or southwest Labrador annual means before 1947 to match the BINS coverage. Likewise, the fall season is excluded from the central Labrador and southwest Labrador sub-regions. In general, we find that the BINS data are more seasonally coherent at low frequencies before WWII (not shown).

The HadSST3 and BINS regional time series are compared in **Fig. 6**, with the respective 1896-2015 and 1950-2015 correlations listed in **Table 6**. Overall, the products are very highly correlated since 1950. In the first half of the record, the largest differences between the products are generally found during periods of data gaps and linear interpolation near the end

1  
2  
3  
4  
5  
6  
7 of WWI and WWII, when BINS error estimates are also large. Among regions, the agreement  
8  
9 is less good in the southern Nordic seas (**Fig. 6b**) before the 1940s; we also find that the  
10 HadSST3 SST in different seasons are also much less correlated there before the 1940s (not  
11 shown). To some extent, the early differences come from the most poorly sampled  
12 northwestern part of this region, but also from Danish and Norwegian data incorporated in  
13 this product and not in HadSST3. Furthermore, in the 1930s, the differences might also  
14 originate from Norwegian data interpreted in BINS as recorded continuously on a water line  
15 inside the ship, and thus attributed a large positive bias. The central Labrador Sea / West  
16 Greenland shelf (**Fig. 6a**) also shows less agreement before 1930. The products correspond  
17 very well after the 1930s, although HadSST3 has less of a cooling in the 1980s. The two SPG  
18 regions are both very strongly correlated over the length of the record (**Fig. 6c,d**). The  
19 Southwest Labrador Sea grid box (**Fig. 6e**) generally corresponds well after the gap periods in  
20 the early 1900s. In the regions further south (**Fig. 6f,g,h**), the two time series usually show a  
21 good agreement, and are most of the time compatible with the BINS error estimate. The  
22 largest differences are near the Grand Banks (**Fig. 6g**) before 1920, maybe as a result of  
23 different seasonal coverage, but also in the 1990s, when BINS tends to present lower values.  
24 Large differences are also found in the intergyre region (**Fig. 6f**) in the early 1950s. This is  
25 the only place where the error estimate does not explain the difference between the curves,  
26 maybe because, for a few years in the early 1950s, data in BINS for some of these boxes were  
27 only available in the summer season, and thus are less representative of annual averages.

#### 4. Characteristics of T, S and surface density RMS variability

28 In this section, we examine the linear trends and the RMS variability of the linearly detrended  
29 interannual time series. The 1896–2015 BINS least-squares linear trends are shown in **Fig.**  
30 **7a–7c**. We construct error estimates for the linear trends by block resampling using the time  
31 series error estimates (resampled every 2 years to account for the 1-2-1 filter). The SSS trend  
32 (**Fig. 7a**) shows a negative trend throughout most of the domain, except for the southwest and  
33 part of the eastern boundary; the pattern is consistent with the 1896–2013 trend shown in  
34 Friedman et al. (2017). The SST trend (**Fig. 7b**) shows strong warming in the Gulf Stream,  
35 and to a lesser extent along the eastern margin. There is cooling in West Greenland / Central  
36 Labrador, and near 52-55°N/30°W. However, error bars due to higher frequency variability or  
37 sampling are often large. Both the increase in T and the decrease in S contribute to an overall  
38 decrease in surface density (**Fig. 7c**).



1  
2  
3  
4  
5  
6  
7  
8  
9  
10  
11  
12  
13  
14  
15  
16  
17  
18  
19  
20  
21  
22  
23  
24  
25  
26  
27  
28  
29  
30  
31  
32  
33  
34  
35  
36  
37  
38  
39  
40  
41  
42  
43  
44  
45  
46  
47  
48  
49  
50  
51  
52  
53  
54  
55  
56  
57  
58  
59  
60  
61  
62  
63  
64  
65

The 1896–2015 HadSST3 trend is shown in **(Fig. 7d)**. The trends are calculated for grid boxes with 5 or fewer years with missing data. [Note that specific seasons are not removed from the spatial grid boxes as for the HadSST3 indices discussed above]. Error terms for HadSST3 are computed by multiplying the white-noise standard error of the slope by a factor of  $\sqrt{2}$  on account of the 1-2-1 filter. Like BINS, the HadSST3 trend shows significant warming in the Gulf Stream extension, and also along the eastern margin. HadSST3 also shows a region of cooling in the central SPG from 50-60°N, referred to as the ‘warming hole’ (Drijfhout et al., 2012), which is not well reproduced in BINS. Checking this particular difference suggests that data in the pre-1917 period originated mostly from one group of data from the ICES archive, often reported at set longitudes, and for which we applied an overall correction of  $-0.2^{\circ}\text{C}$  on temperature, but with little comparison data to define it (Reverdin et al. 1994). Notice however that nonetheless, for the area average of the central SPG **(Fig. 6c)**, the difference between BINS and HADSST3 is not significant for that period.

The detrended RMS standard deviation of the interannual T and S time series **(Figs. 8a and 8b)** correspond to the expectation that large-scale temperature RMS standard deviation diminishes from west to east; whereas the salinity RMS values are largest in the west, then near 50°N with a decrease from west to east and from the southern to the northern SPG. This pattern is indicative on one hand of larger air-sea and hydrographical/heat forcings in the western SPG, and on the other hand of the presence during some winters of a rather shallow mixed layer in the western SPG (even in the Labrador Sea, where deep convection also often takes place (Yashayaev and Loder 2016)). In mid-ocean near 45-50°N, there might also be a contribution of displacements of hydrographical fronts.

Surface density standard deviation **(Fig. 8c)** diminishes both from west to east and south to north. The relative contributions of T and S to detrended density variability are shown in **Fig. 8d**. The contributions of SST and SSS to surface density variability are opposite in most places (the effects of these variables on density variability tend to compensate each other, as there is a positive correlation between SST and SSS variability on intra-annual to centennial time scale in a large part of this domain). This also might explain a pattern of density rms variability which presents weaker zonal gradients in the west than what is found in SST or SSS.

1  
2  
3  
4  
5  
6  
7 90 Interestingly, in the westernmost part of the domain, except near the Gulf Stream, the salinity  
8  
9 91 contribution to density variability dominates over the temperature contribution (**Fig. 8d**),  
10 92 whereas in the eastern and northern parts of the SPG, temperature dominates. Thus in the first  
11 93 region, density tends to be positively correlated with SSS and SST, whereas in the other  
12 94 region it is negatively correlated with SSS and SST. In the northern part, this was not  
13 94 expected, as temperature is lower than further south, which would contribute to diminish the  
14 95 contribution of temperature variations to density variations. However, this is counteracted by  
15 96 a lower ratio of SSS over SST variability in the northern regions. In general, the SSS  
16 96 contribution is slightly larger for the non-detrended data (not shown), due to its relatively  
17 97 larger centennial trends in this part of the ocean (discussed in part 2 of this study).  
18 98  
19 99  
20 99

21 100  
22 101 Next, we show the total RMS variability contained at multidecadal frequencies. We low-pass  
23 102 filter the time series using a spectral filter with half power at a period close to 15 years. **Fig. 9**  
24 102 shows the percentage of the detrended interannual variance explained by the low-pass filtered  
25 103 time series. The low-pass filtered variance percentage of SSS (**Fig. 9a**) and SST (**Fig. 9b**) are  
26 104 less correlated spatially than overall RMS variability. For S, what striking is the lower  
27 105 percentages in the western part (as low as 40%) than in the eastern part of the domain (larger  
28 106 than 60%), whereas for T, it is mostly the northern part which has a larger percentage of  
29 107 variance in the multidecadal frequencies, with percentage of detrended variance reaching up  
30 108 to 80%. The low percentages of multidecadal variability for SSS in the northwest is  
31 109 consistent with the penetration in the ocean interior of short-lived freshwater pulses  
32 110 originating from the western shelves and the rim of the Labrador Sea (examples of recent  
33 111 short-term SSS variability in this region are presented in Tesdal et al. (2018)).  
34 112  
35 113

36 114 The low-pass filtered time series explain comparatively less density variance, particularly in  
37 115 the western SPG region (**Fig. 9c**, values usually less than 50%), which suggests coordinated  
38 116 SSS and SST variations at lower frequencies with thus partial compensation on their  
39 117 contribution to density changes. Indeed, the low-pass filtered correlation of SSS and SST  
40 118 (**Fig. 9d**) is positive in most grid boxes, with large magnitudes in the central SPG, around  
41 119 Greenland and in the south-west north of the Gulf Stream as well as around the Grand Banks.  
42 120 Notice however, less significant correlation in other areas of the western, southern, and  
43 121 eastern parts of the domain close to Europe. The relationship between SSS and SST variations  
44 122 will be examined further in part 2 of this study.  
45 123  
46 123  
47 123  
48 123  
49 123  
50 123  
51 123  
52 123  
53 123  
54 123  
55 123  
56 123  
57 123  
58 123  
59 123  
60 123  
61 123  
62 123  
63 123  
64 123  
65 123

## 5. Discussion and Conclusions

We have constructed a spatially averaged binned product BINS of interannual T, S, and surface density for 1896-2015 north of 40°N, similar to what was done for S in Friedman et al. (2017), but at a higher spatial resolution. We deliberately excluded the shelf regions (except for one box along southwestern Greenland and one box on the southern Grand Banks), which have different dynamics, variability and sampling issues (Reverdin et al. 2018). We have shown that in recent decades, the BINS interannual variability of SST and SSS is coherent with published time series of upper ocean heat and salinity based on high quality hydrographic data. It provides also rather similar results to an analysis of SST and SSS variability along two ship tracks since 1993, based on the same in situ data set for its main part (Reverdin et al. 2018).

Furthermore, BINS compares well with two gridded products of hydrographic data (EN4 from 1950-2015 and ISHII from 1950-2012), which use different data selection and mapping methods. This suggests that in this region, the processing and spatial averaging of the individual data in the spatial bins done in BINS is usually sufficient to portray the interannual variability of SST on the grid box scale, at least since 1950, and that during this period, the data set used does not contain large biases compared to these other data sets. On interannual time scales, BINS SST also fits largely with what is portrayed in HadSST3, except in the pre-WWII period for the Labrador Sea and the Norwegian Sea. Insufficient coverage or erroneous data, either in HadSST3 or BINS, might be causing these discrepancies. Thus, more care should be taken when interpreting variability in BINS before 1950.

The product combines time series of interannual variability in different seasons. This was required to reduce sampling errors to a reasonable level (in particular pre-1950), but this might also mask or alias important differences between the seasons. For example in the northern part of the subtropical gyre (thus, south of the region we investigate) a strong seasonal modulation in the recent trends towards increasing SSS has been documented, associated to important seasonal changes of the hydrological cycle (Yu et al. 2017). In the Labrador Sea, too, on an interannual time scale, large summer-time anomalies of SSS have been documented in the recent decade (2008 and 2012) that don't have a clear counterpart in other seasons (Tesdal et al. 2018). Such events, and also the seasonality of atmospheric forcing, seasonal thermal stratification and mixing, could induce large interannual differences between the anomalies in different seasons. Indeed, **Fig. 3** suggests that the differences

1  
2  
3  
4  
5  
6  
7 58 between seasons are large in the central Labrador Sea, but for the other open-ocean regions,  
8  
9 59 different seasons present more similar decadal and longer frequencies. Possibly, the  
10 60 insufficient accuracy of binned time series and the change in collection and measurement  
11 61 techniques could preclude further investigation of the seasonality of the decadal or longer  
12 62 variability with this dataset. For example, in boxes of the southern SPG, we noticed SSS  
13 63 differences in the autumn around 1960 that could be a data artifact. Differences with  
14 64 HadSST3 taking place around 2000 could also be data-related (either in HadSST3 with  
15 65 drifting buoy data becoming more numerous, or in BINS with the Argo data afterwards).  
16  
17 66 Nonetheless, a more homogeneous 25-year dataset in the central SPG resolving seasonal  
18 67 variability along well sampled ship lines (Reverdin et al. 2018) also pointed out a similarity in  
19 68 interannual variability for the different seasons, although interannual RMS variability tended  
20 69 to be larger there too in early summer for SST.  
21  
22  
23

24 70  
25 71 This aside, the seasonal inhomogeneity in data coverage, with less sampling in winter in  
26 72 particular before 1955, should have little impact on the reconstructed interannual time series.  
27  
28 73 We however warn that this might not be a wise substitute for the seasonal time series, in  
29 74 particular for studies of winter conditions the central Labrador Sea or water mass formation,  
30  
31 75 but then obviously the available binned data present more gaps, and the original seasonal time  
32 76 series have larger error bars.

33 77  
34 78 Density is a non-linear function of temperature and salinity, with the character of non-  
35 79 linearity increasing at low T. We deliberately emphasized winter characteristics when  
36 80 estimating density from temperature and salinity time series, but use the BINS time series  
37 81 which combine SST and SSS anomalies in the four (or three) different seasons. We noticed  
38 82 that in some regions interannual variability has smaller amplitude in winter (Table 3  
39 83 summarizing **Fig. 3**), thus this choice might result in an overestimation of winter-time  
40 84 interannual density variability. It would be also misleading to use these density interannual  
41 85 time series as a proxy for water density in other seasons.  
42  
43  
44  
45

46 86  
47 87 We do not have a direct comparison of SSS BINS time series prior to the 1950s. We estimate  
48 88 that they provide reasonable estimates for this early period mostly based on comparisons of  
49 89 the SST BINS time series with HadSST3 binned data. However, before 1950 in the Nordic  
50 90 Seas and Labrador Sea, the binned data have larger uncertainties and winter seasons are  
51 91 poorly (or not at all) sampled. Thus, clearly our estimates for SSS are also less certain in these  
52  
53

54  
55  
56  
57  
58  
59  
60  
61  
62  
63  
64  
65

1  
2  
3  
4  
5  
6  
7 92 regions prior to 1950. A possibility for further validation would be to compare with  
8  
9 93 independent proxy-based estimates of surface variability. Few such proxy time series have  
10 94 been derived in this region resolving the multidecadal variability in SST and even less in  
11 95 SSS, and their uncertainties are probably too large for such a validation (Hall et al.  
12  
13 96 (2010), for a site in the Iceland Basin (Gardar drift); Richter et al. (2009), for a site in the  
14 97 northern Rockall Trough area (Feni drift); Moffa-Sanchez et al. (2017) and references  
15  
16 98 therein as well as Thornalley et al. (2018), for a site in the southeastern Labrador Sea).

17 99  
18 00 BINS has sufficient spatial resolution to resolve large-scale patterns of RMS standard  
19  
20 01 deviation of the variability in SST, SSS and density (this was done after removing linear  
21 02 trends). RMS variability in SSS and to a lesser degree in SST increases towards the west, with  
22  
23 03 the contribution to density of SSS variability dominating that of SST in the west, whereas in  
24 04 the eastern and northern parts of the SPG, temperature typically dominates the variability. The  
25 05 portion of variability in multidecadal frequencies (here with a cut-off at 15 years) could be  
26  
27 06 ascertained. It is found both for SST and SSS to be a very large part of interannual variability,  
28 07 with lesser relative contribution in the west for SSS and in the southern part for SST. For  
29  
30 08 density, it is less prominent, except in the northeastern part of the SPG, where SST variability  
31 09 contribution dominates and is very much at multidecadal frequencies (also see Holliday et al.  
32 10 2015). The higher frequencies are more influenced by the sampling uncertainties, in particular  
33  
34 11 the effect of interpolation and interannual smoothing during data gaps in either specific  
35 12 seasons or all seasons (near WWII, for example). Thus this analysis of the relative importance  
36 13 of multidecadal variability is more dataset-dependent than the RMS variability

#### 37 38 14 39 15 40 16 **Acknowledgements**

41  
42 17 This is a contribution to the French SSS observation service, which is supported by French  
43 18 agencies INSU/CNRS, IRD, CNES and IPEV, as well as from SOERE CTDO2. The Rockall  
44 19 Trough time series were provided with support from the UK Natural Environment Research  
45  
46 20 Council (Extended Ellett Line program, National Capability). The station time series south of  
47 21 Iceland were provided with Icelandic support. The annual oceanographic monitoring of the  
48  
49 22 Labrador Sea was initiated as a Canadian contribution to the World Ocean Circulation  
50 23 Experiment in 1990 and is presently conducted as a core component of the Atlantic Zone Off-  
51 24 Shelf Monitoring Program (AZOMP) run by the Bedford Institute of Oceanography of  
52  
53 25 Fisheries and Oceans Canada. The International Argo Program is part of the Global Ocean

1  
2  
3  
4  
5  
6  
726 Observing System (Argo, 2000). Argo data are available from the Coriolis Global Data  
8  
927 Center, Institut français de recherche pour l'exploitation de la mer (Ifremer). The HadSST3  
1028 and EN4 data were provided by the Met Office Hadley Center, and the ISHII data were  
11  
1229 provided by the NCAR Research Data Archive. A.R.F. was supported by SOERE CTDO2  
13  
1430 and the ERC funded project TITAN (EC-320691). L.C. acknowledges support from the  
15  
1631 Swedish National Space Board (SNSB; Dnr 133/17). [Comments by two reviewers and by](#)  
17  
1832 [Semyon Grodsky were appreciated.](#)  
19

### 2034 References

- 2135 Alory G, Delcroix T, Téchiné P, Diverres D, Varillon D, Cravatte S, ... Roubaud F (2015)  
2236 The French contribution to the voluntary observing ships network of sea surface salinity.  
2337 Deep Sea Res I 105: 1–18. <http://doi.org/10.1016/j.dsr.2015.08.005>  
2438 Argo (2000) Argo float data and metadata from Global Data Assembly Centre (Argo GDAC).  
2539 SEANOE. <http://doi.org/10.17882/42182>  
2640 Belkin I M, Levitus S, Antonov J, Malmberg S.-A (1998) “Great Salinity Anomalies” in the  
2741 North Atlantic. Prog Oceanogr 41(1): 1–68. [http://doi.org/10.1016/S0079-6611\(98\)00015-9](http://doi.org/10.1016/S0079-6611(98)00015-9)  
2842  
2943 Böning C W, Behrens E, Biastoch A, Getzlaff K, Bamber J L (2016) Emerging Impact of  
3044 Greenland Meltwater on Deepwater Formation in the North Atlantic Ocean. Nature  
3145 Geoscience. <https://doi.org/10.1038/ngeo2740>.  
3246 Boutin J, Chao T, Asher W, Delcroix T, Drucker R, Drushka K, Kolodziejczyk N, Lee T,  
3347 Reul N, Reverdin G, Schanze J, Soloviev A, Yu L, Anderson J, Brucker L, Dinnat E,  
3448 Santos-Garcia A, Jones W, Maes C, Meissner T, Tang W, Vinogradova N, Ward B (2016)  
3549 Satellite and In Situ Salinity : Understanding Near-Surface Stratification and Sub-footprint  
3650 Variability. Bull. Amer. Meteor. Soc., 97, 1391–1407, doi: 10.1175/BAMS-D-15-  
3751 00032.1.  
3852 Buckley M W, Marshall J (2016) Observations, Inferences, and Mechanisms of the Atlantic  
3953 Meridional Overturning Circulation: A Review. Reviews of Geophysics 54 (1):  
4054 2015RG000493. <https://doi.org/10.1002/2015RG000493>.  
4155 Cabanes C, Grouazel A, von Schuckmann K, Hamon M, Turpin V, Coatanoan C, Paris F, et al  
4256 (2013) The CORA Dataset: Validation and Diagnostics of in-Situ Ocean Temperature and  
4357 Salinity Measurements. Ocean Sci 9 (1): 1–18. <https://doi.org/10.5194/os-9-1-2013>.  
4458 Davis R E, Sherman J T, Dufour J (2001) Profiling ALACEs and other advances in  
4559 autonomous subsurface floats. J Atmos Ocean Tech 18: 982-993.  
4660 Dickson R R, Meincke J, Malmberg M S-A, Lee A J (1988) The “Great Salinity Anomaly”  
4761 in the northern North Atlantic 1968 – 1982. Prog Oceanogr 20: 103– 151.  
4862 Drijfhout S, van Oldenborgh G J, Cimadoribus A (2012) Is a Decline of AMOC Causing the  
4963 Warming Hole above the North Atlantic in observed and modeled warming patterns?” J  
5064 Clim 25: 8373–79. <https://doi.org/10.1175/JCLI-D-12-00490.1>.  
5165 Ebisuzaki W (1997) A method to estimate the statistical significance of a correlation when the  
5266 data are serially correlated. J Clim 10(9): 2147–2153.  
5367 Fofonoff N P (1985) Physical properties of seawater: A new salinity scale and equation of  
5468 state for seawater. J Geophys Res 90(C2): 3332–3342.  
5569 <https://doi.org/10.1029/JC090iC02p03332>.

1  
2  
3  
4  
5  
6  
7  
8  
9  
10  
11  
12  
13  
14  
15  
16  
17  
18  
19  
20  
21  
22  
23  
24  
25  
26  
27  
28  
29  
30  
31  
32  
33  
34  
35  
36  
37  
38  
39  
40  
41  
42  
43  
44  
45  
46  
47  
48  
49  
50  
51  
52  
53  
54  
55  
56  
57  
58  
59  
60  
61  
62  
63  
64  
65

Frankignoul C, Deshayes J, Curry R (2009) The Role of Salinity in the Decadal Variability of the North Atlantic Meridional Overturning Circulation. *Climate Dynamics* 33(6): 777–93. <https://doi.org/10.1007/s00382-008-0523-2>.

Friedman A R, Reverdin G, Khodri M, Gastineau G (2017) A new record of Atlantic sea surface salinity from 1896 to 2013 reveals the signatures of climate variability and long-term trends. *Geophys Res Lett* 44: 1866–1876. DOI:10.1002/2017GL072582.

Good S-A, Martin M J, Rayner N A (2013) EN4: Quality Controlled Ocean Temperature and Salinity Profiles and Monthly Objective Analyses with Uncertainty Estimates. *J Geophys Res* 118(12): 6704–16. <https://doi.org/10.1002/2013JC009067>.

Hall I R, Boessenkool K P, Barker S, McCave I N, Elderfield H (2010) Surface and deep ocean coupling in the subpolar North Atlantic during the last 230 years. *Paleoceanogr* 25. doi:10.1029/2009PA001886.

Holliday N P, Cunningham S A, Johnson C, Gary S F, Griffiths C, Read J F, Sherwin T (2015) Multidecadal variability of potential temperature, salinity, and transport in the eastern subpolar North Atlantic. *J Geophys Res* 120. doi:10.1002/2015JC010762.

Hughes, S. L., Holliday, N. P., Gaillard, F., and the ICES Working Group on Oceanic Hydrography, 2012. Variability in the ICES/NAFO region between 1950 and 2009: observations from the ICES Report on Ocean Climate. – ICES Journal of Marine Science, doi:10.1093/icesjms/fss044.Icelandic hydrographic surveys ...

Ishii M, Kimoto M, Sakamoto K, Iwasaki S I (2006) Steric sea level changes estimated from historical ocean subsurface temperature and salinity analyses. *J Oceanography* 62(2): 155-170.

Kennedy J J, Rayner N A, Smith R O, Parker D E, Saunby M (2011) Reassessing Biases and Other Uncertainties in Sea Surface Temperature Observations Measured in Situ since 1850: 1. Measurement and Sampling Uncertainties. *J Geophys Res* 116. doi:201110.1029/2010JD015218.

Kennedy J J, Rayner N A, Smith R O, Saunby M, Parker D E (2011) Reassessing biases and other uncertainties in sea-surface temperature observations since 1850: 2. Biases and homogenisation. *J Geophys Res* 116 D14104. doi:10.1029/2010JD015220

Lavender K L, Davis R E, Owens W B (2000) Mid-depth recirculation observed on the interior Labrador and Irminger seas by direct velocity measurements. *Nature* 607: 66- 69.

Lozier M S (2012) Overturning in the North Atlantic. *Ann Rev of Marine Sci* 4(1): 291–315. <http://doi.org/10.1146/annurev-marine-120710-100740>

Moffa-Sanchez P, Hall I R (2017) North Atlantic variability and its links to European climate over the last 3000 years. *Nature comm.* 8:1726, 555. doi:10.1038/s41467-017-01884-8.

Piron A, Thierry V, Mercier H, Caniaux G (2017) Gyre-scale deep convection in the subpolar North Atlantic Ocean during winter 2014–2015. *Geophys Res Lett* 44: 1439–1447. doi:10.1002/2016GL071895.

Polyakov I V, Bhatt U S, Simmons H L, Walsh D, Walsh J E, Zhang X (2005) Multidecadal Variability of North Atlantic Temperature and Salinity during the Twentieth Century. *J Clim* 18(21): 4562–4581. <http://doi.org/10.1175/JCLI3548.1>

Rahmstorf S, Box J E, Feulner G, Mann M E, Robinson A, Rutherford S, Schaffernicht E J (2015) Exceptional twentieth-century slowdown in Atlantic Ocean overturning circulation. *Nature Climate Change* 5(5): 475–480. <http://doi.org/10.1038/nclimate2554>

Reverdin G (2010) North Atlantic Subpolar Gyre Surface Variability (1895–2009). *J Clim* 23(17): 4571–4584. <http://doi.org/10.1175/2010JCLI3493.1>

Reverdin G, Cayan D, Dooley H, Ellett D, Levitus S, du Penhoat Y, Dessier A (1994) Surface Salinity of the North-Atlantic - Can We Reconstruct Its Fluctuations Over the Last 100 Years. *Prog Oceanogr* 33(4): 303–346. [http://doi.org/10.1016/0079-6611\(94\)90021-3](http://doi.org/10.1016/0079-6611(94)90021-3)

1  
2  
3  
4  
5  
6  
7  
8  
9  
10  
11  
12  
13  
14  
15  
16  
17  
18  
19  
20  
21  
22  
23  
24  
25  
26  
27  
28  
29  
30  
31  
32  
33  
34  
35  
36  
37  
38  
39  
40  
41  
42  
43  
44  
45  
46  
47  
48  
49  
50  
51  
52  
53  
54  
55  
56  
57  
58  
59  
60  
61  
62  
63  
64  
65

Reverdin G, Cayan D, Kushnir Y (1997) Decadal variability of hydrography in the upper northern North Atlantic 1948-1990. *J Geophys Res* 102: 8505-8531.

Reverdin G, Alory G, Diverres D, Bringas F, Goni G, Heilmann L, Chafik L, Szekely T, Friedman A R (2018) North Atlantic subpolar gyre along predetermined ship tracks since 1993: a monthly data set of surface temperature, salinity, and density. *Earth Syst Sci Data* 10: 1403-1415. <https://doi.org/10.5194/essd-10-1403-2018>.

Rhein M, Kieke D, Hüttl-Kabus S, Roessler A, Mertens C, Meissner R, Klein B, Böning C W, Yashayaev I (2011) Deep water formation, the subpolar gyre, and the meridional overturning circulation in the subpolar North Atlantic. *Deep Sea Res II* 58: 1819-1832. doi:10.1016/j.dsr2.2010.10.061

Richter T O., Peeters F J C, Weering T C E (2009) Late Holocene (0-2.4 ka BP) surface water temperature and salinity variability, Feni Drift, NE Atlantic Ocean. *Quat Sci Rev* 28: 1941-1955.

Riser S C, Freeland H J, Roemmich D, Wijffels S, Troisi A, Belbéoch M, Gilbert D, et al. (2016) Fifteen Years of Ocean Observations with the Global Argo Array. *Nature Climate Change* 6 (2): 145–53. <https://doi.org/10.1038/nclimate2872>.

Roemmich, D, Johnson G C, Riser S, Davis R E, Gilson J, Owens W B, Garzoli S L, Schmid C, Ignaszewski M (2009) [The Argo Program: Observing the global ocean with profiling floats](https://doi.org/10.5670/oceanog.2009.36). *Oceanography*. 22:34-43. [10.5670/oceanog.2009.36](https://doi.org/10.5670/oceanog.2009.36)

Skliris N, Marsh R, Josey S A, Good S A, Liu C, Allan R P (2014) Salinity changes in the World Ocean since 1950 in relation to changing surface freshwater fluxes. *Climate Dynamics* 43(3-4): 709–736. <http://doi.org/10.1007/s00382-014-2131-7>

Tesdal J, Abernathey R P, Goes J I, Gordon A L, Haine T W (2018) Salinity Trends within the Upper Layers of the Subpolar North Atlantic. *J Clim* 31: 2675–2698. <https://doi.org/10.1175/JCLI-D-17-0532.1>

Thornalley D J R, Oppo D W, Ortega P, Robson J I, Brierley C M, Davis R, Hall I R, Moffa-Sanchez P, Rose N L, Spooner P T, Yashayaev I, Keigwin L D (2018) Anomalously weak Labrador Sea convection and Atlantic overturning during the past 150 years. *Nature* 556. <https://doi.org/10.1038/s41586-018-0007-4>.

UNESCO (1981) The Practical Salinity Scale 1978 and the International Equation of State of Seawater 1980. UNESCO technical papers in marine science 36: 25pp.

Williams R G, Roussenov V, Lozier M S, Smith D (2015) Mechanisms of heat content and thermocline change in the subtropical and subpolar North Atlantic. *J Clim* 28: 9803-9813. doi:10.1175/JCLI-D-15-0097.1.

Yashayaev I (2007) Hydrographic changes in the Labrador Sea, 1960-2005. *Prog Oceanogr* 73: 242-276. doi:10.1016/j.pocean.2007.04.015.

Yashayaev I, Loder J W (2009) Enhanced production of Labrador Sea Water in 2008, *Geophys Res Lett* 36 L01606. doi:10.1029/2008GL036162.

Yashayaev I, Loder J W (2016) Recurrent replenishment of Labrador Sea water and associated decadal-scale variability. *J Geophys Res* 121:8095-8114. doi:10.1002/2016JC012046.

Yashayaev I, Loder J W (2017) Further intensification of deep convection in the Labrador Sea in 2016. *Geophys Res Lett* 44:1429-1438, doi:/10.1002/2016GL071668.

Yashayaev I, Seidov D (2015) The role of the Atlantic water in multidecadal ocean variability in the Nordic and Barents Seas. *Prog Oceanogr* 132: 68-127.

Yu L, Jin X Liu H (2017) Poleward Shift in Ventilation of the North Atlantic Subtropical Underwater. *Geophysical Research Letters* 44. doi: <https://doi.org/10.1002/2017GL075772>



1  
2  
3  
4  
5  
6  
7  
8  
9  
10  
11  
12  
13  
14  
15  
16  
17  
18  
19  
20  
21  
22  
23  
24  
25  
26  
27  
28  
29  
30  
31  
32  
33  
34  
35  
36  
37  
38  
39  
40  
41  
42  
43  
44  
45  
46  
47  
48  
49  
50  
51  
52  
53  
54  
55  
56  
57  
58  
59  
60  
61  
62  
63  
64  
65

**Figures.**

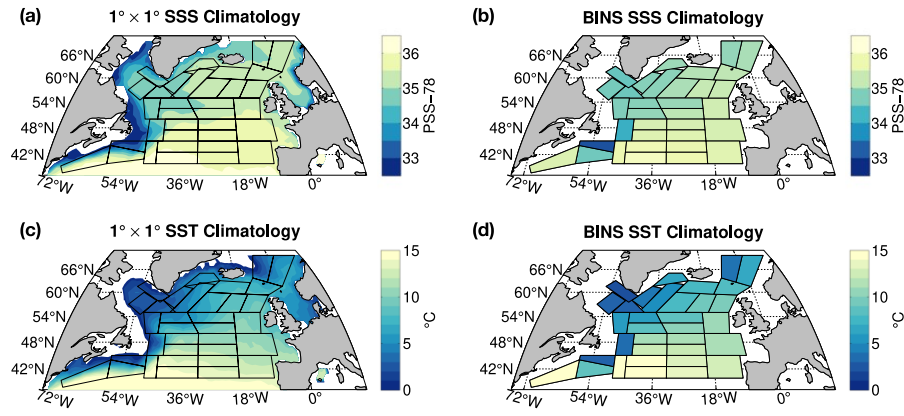


**Figure 1.** Gridded climatologies ( ) for 1896-2000. (a) and (c): 1°×1° March climatologies for (a) SSS and (c) SST. (b) and (d): BINS March–May climatologies for (b) SSS and (d) SST.

1  
2  
3  
4  
5  
6  
7  
8  
9  
10  
11  
12  
13  
14  
15  
16  
17  
18  
19  
20  
21  
22  
23  
24  
25  
26  
27  
28  
29  
30  
31  
32  
33  
34  
35  
36  
37  
38  
39  
40  
41  
42  
43  
44  
45  
46  
47  
48  
49  
50  
51  
52  
53  
54  
55  
56  
57  
58  
59  
60  
61  
62  
63  
64  
65

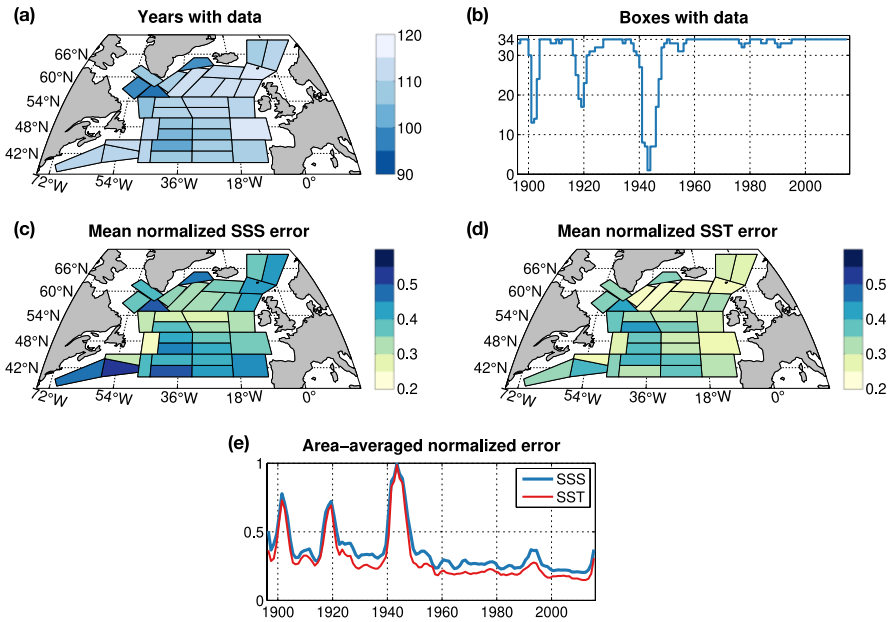


**Figure 2.** (a) Outline of BINS boxes, with number of years with data from 1896–2015 (out of a maximum of 120). (b) Time series of total BINS boxes with coverage (out of a maximum 34). The data counts in (a) and (b) are from after applying the 1-2-1 filter. (c) Mean annual SSS grid box error, defined as the mean grid box error divided by its maximum error (usually in 1943). (d) Same as (c), for SST. (e) Area-weighted normalized annual grid box error for SSS and SST.

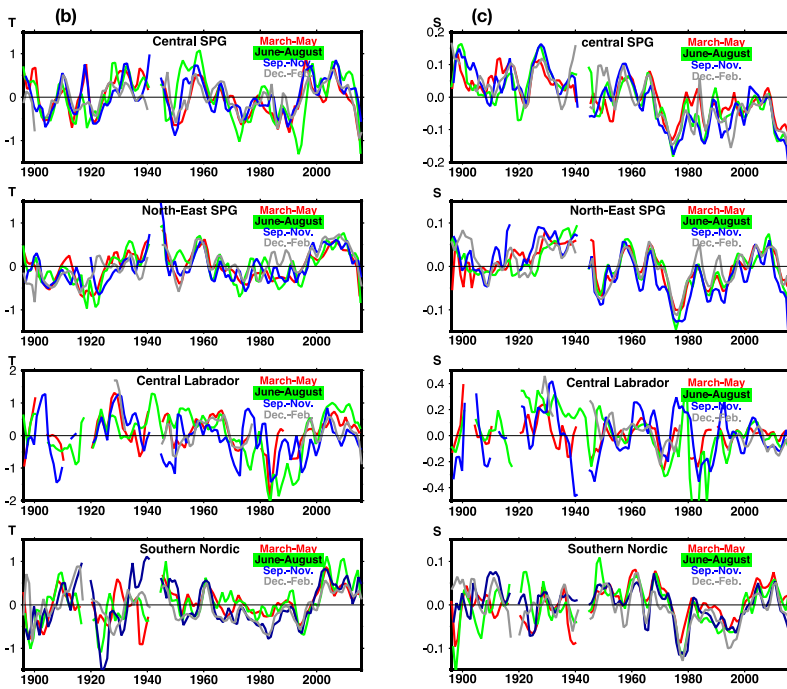
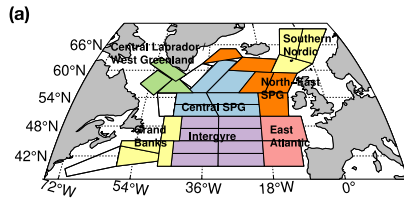


**Figure 3.** (a) Regional domains described in the text. (b-c) Seasonal time series for (b) T (°C) and (c) S (PSS-78) averaged over four domains portrayed in (a): central SPG, north-east SPG, central Labrador Sea / West Greenland, and the southern Nordic Seas.

15  
16  
17  
18  
19  
20  
21  
22  
23  
24  
25  
26  
27  
28  
29  
30  
31  
32  
33  
34  
35  
36  
37  
38  
39  
40  
41  
42  
43  
44  
45  
46  
47  
48  
49  
50  
51  
52  
53  
54  
55  
56  
57  
58  
59  
60  
61  
62  
63  
64  
65

**Table 3.** Seasonal RMS and Pearson correlation coefficient. RMS values are in °C for T, and PSS-78 for S (×1000).  
Corresponding regions are shown on Fig. 3a.

<b>Region</b>	<b>Length</b>		<b>12-2</b>	<b>3-5</b>	<b>6-8</b>	<b>9-11</b>		<b>12-2</b>	<b>3-5</b>	<b>6-8</b>	<b>9-11</b>
Central SPG	112-116 yrs	<b>T RMS</b>	0.304	0.407	0.505	0.404	<b>S RMS</b>	73	60	72	79
		<b>T corr.</b>					<b>S corr.</b>				
		<b>12-2</b>		0.58	0.52	0.57	<b>12-2</b>		0.72	0.77	0.78
		<b>3-5</b>			0.55	0.71	<b>3-5</b>			0.79	0.82
		<b>6-8</b>			0.62	<b>6-8</b>				0.86	
<hr/>											
<b>Region</b>	<b>Length</b>		<b>12-2</b>	<b>3-5</b>	<b>6-8</b>	<b>9-11</b>		<b>12-2</b>	<b>3-5</b>	<b>6-8</b>	<b>9-11</b>
N-E SPG	113-115 yrs	<b>T RMS</b>	0.339	0.338	0.375	0.336	<b>S RMS</b>	42	41	44	55
		<b>T corr.</b>					<b>S corr.</b>				
		<b>12-2</b>		0.65	0.54	0.60	<b>12-2</b>		0.72	0.75	0.73
		<b>3-5</b>			0.76	0.71	<b>3-5</b>			0.81	0.78
		<b>6-8</b>			0.74	<b>6-8</b>				0.80	
<hr/>											
Southern Nordic		<b>T RMS</b>	0.358	0.351	0.425	0.524	<b>S RMS</b>	41	40	47	41
		<b>T corr.</b>					<b>S corr.</b>				
		<b>12-2</b>		0.31	0.40	0.61	<b>12-2</b>		0.50	0.43	0.66
		<b>3-5</b>			0.69	0.41	<b>3-5</b>			0.66	0.52
		<b>6-8</b>			0.57	<b>6-8</b>				0.61	
<hr/>											
Central Labrador/ West Greenland*		<b>T RMS</b>	0.47	0.385	0.482	0.602	<b>S RMS</b>	130	95	131	162
		<b>T corr.</b>					<b>S corr.</b>				
		<b>12-2</b>		0.81	0.20	0.60	<b>12-2</b>		0.37	0.50	0.27
		<b>3-5</b>			0.60	0.78	<b>3-5</b>			0.56	0.50
		<b>6-8</b>			0.52	<b>6-8</b>				0.42	

16  
17  
18  
19  
20  
21  
22  
23  
24  
25  
26  
27  
28  
29  
30  
31  
32  
33  
34  
35  
36  
37  
38  
39  
40  
41  
42  
43  
44  
45  
46  
47  
48  
49  
50  
51  
52  
53  
54  
55  
56  
57  
58  
59  
60  
61  
62  
63  
64  
65

		<u>12-2</u>	<u>3-5</u>	<u>6-8</u>	<u>9-11</u>		<u>12-2</u>	<u>3-5</u>	<u>6-8</u>	<u>9-11</u>
Grand Banks	<b>T RMS</b>	0.95	0.792	0.890	0.990	<b>S RMS</b>	148	156	132	150
	<b>T corr.</b>					<b>S corr.</b>				
	<b>12-2</b>		0.26	0.33	0.29	<b>12-2</b>		0.09	0.24	0.51
	<b>3-5</b>			0.56	0.21	<b>3-5</b>			0.49	0.33
	<b>6-8</b>				0.44	<b>6-8</b>				0.50
<hr/>										
		<u>12-2</u>	<u>3-5</u>	<u>6-8</u>	<u>9-11</u>		<u>12-2</u>	<u>3-5</u>	<u>6-8</u>	<u>9-11</u>
Intergyre	<b>T RMS</b>	0.49	0.42	0.61	0.49	<b>S RMS</b>	87	76	82	100
	<b>T corr.</b>					<b>S corr.</b>				
	<b>12-2</b>		0.56	0.19	0.42	<b>12-2</b>		0.64	0.65	0.73
	<b>3-5</b>			0.44	0.53	<b>3-5</b>			0.51	0.55
	<b>6-8</b>				0.42	<b>6-8</b>				0.59
<hr/>										
		<u>12-2</u>	<u>3-5</u>	<u>6-8</u>	<u>9-11</u>		<u>12-2</u>	<u>3-5</u>	<u>6-8</u>	<u>9-11</u>
East Atlantic	<b>T RMS</b>	0.37	0.37	0.41	0.51	<b>S RMS</b>	53	61	55	54
	<b>T corr.</b>					<b>S corr.</b>				
	<b>12-2</b>		0.59	0.41	0.57	<b>12-2</b>		0.40	0.53	0.56
	<b>3-5</b>			0.57	0.52	<b>3-5</b>			0.59	0.34
	<b>6-8</b>				0.38	<b>6-8</b>				0.51

\* small number of common points, and varying number of boxes; thus not reliable, in particular for S.  
Both for Southern Nordic and Central Labrador, very different number of years in winter and other seasons  
(only on the order of 60 years with winter data in some of the boxes included in the average)

1  
2  
3  
4  
5  
6  
7  
8  
9  
10  
11  
12  
13  
14  
15  
16  
17  
18  
19  
20  
21  
22  
23  
24  
25  
26  
27  
28  
29  
30  
31  
32  
33  
34  
35  
36  
37  
38  
39  
40  
41  
42  
43  
44  
45  
46  
47  
48  
49  
50  
51  
52  
53  
54  
55  
56  
57  
58  
59  
60  
61  
62  
63  
64  
65

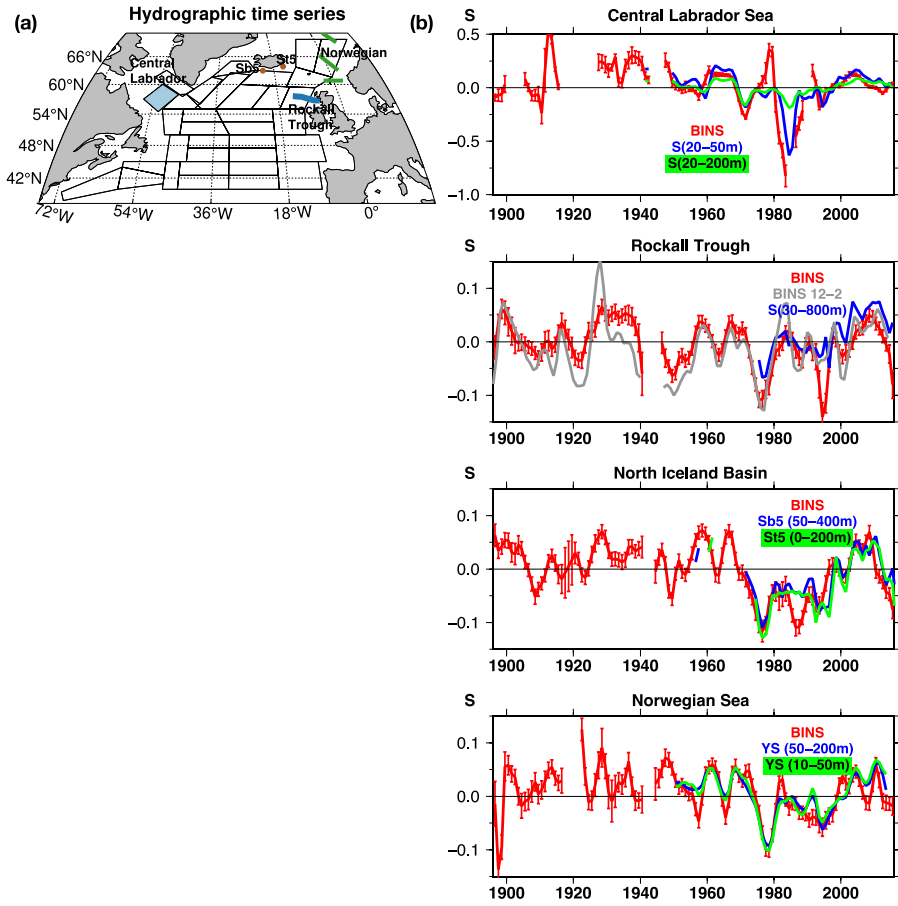


**Figure 4.** (a) Map showing hydrographic time series locations with BINS grid boxes. (b) Comparison for S of BINS (in red) with hydrographic time series low passed 1-2-1 over successive years; Central Labrador Sea (top; green and blue for different layer averages), Rockall Trough (top middle; the green curve is from BINS but for the winter (Dec-Feb.) season; blue is the vertically averaged (30-800m) S time series), North Iceland Basin (lower middle; two vertically averaged station time series are presented); and eastern Norwegian Sea (bottom; the blue and green time series is a compilation of the offshore data (median averaged) in 3 Norwegian Sea sections presented in Yashayaev and Seidov (2015), for two different depth ranges). One standard deviation rms error bars are added on the BINS series.

16  
17  
18  
19  
20  
21  
22  
23  
24  
25  
26  
27  
28  
29  
30  
31  
32  
33  
34  
35  
36  
37  
38  
39  
40  
41  
42  
43  
44  
45  
46  
47  
48  
49  
50  
51  
52  
53  
54  
55  
56  
57  
58  
59  
60  
61  
62  
63  
64  
65

**Table 4a.** Hydrographic sections and BINS: RMS variability for S (PSS-78) and T (°C), and lag-0 correlation coefficient.

Region	Years S	RMS (S)			Years T	RMS (T)		
		section	BINS	corr (S)		section	BINS	corr (T)
S Rockall (30–800m)	37	.040	0.048	0.73	37	0.284	0.350	0.80
S Iceland (50–400m)	47	.050	0.043	0.81	47	0.413	0.391	0.87
Central Labrador (20–50m)	69	.155	0.169	0.76	67	0.715	0.716	0.74
Norwegian Sea (10-50m)	64	.039	0.038	0.82	64	0.31	0.31	0.87

**Table 4b.** Hydrographic section lag correlation with BINS.

Region	Lag	Years (S)	corr. (S)	Years (T)	corr. (T)
South Rockall	-2	35	0.57	35	0.56
(30–800m)	-1	36	0.70	36	0.65
	0	37	0.73	37	0.80
	+1	37	0.77	37	0.80
(BINS leads)	+2	37	0.68	37	0.72

Region	Lag	Years (S)	corr. (S)	Years (T)	corr. (T)
South Iceland	-2	45	0.54	44	0.59
(50–400m)	-1	46	0.68	45	0.74
	0	47	0.81	45	0.87
	+1	47	0.88	45	0.89
(BINS leads)	+2	47	0.83	45	0.81

Region	Lag	Years (S)	corr. (S)	Years (T)	corr. (T)
Eastern Norwegian Sea	-2	64	0.48	64	0.70
(10-50m)	-1	64	0.72	64	0.81
	0	64	0.82	64	0.87
	+1	64	0.74	64	0.83
(BINS leads)	+2	64	0.54	64	0.72

1  
2  
3  
4  
5  
6  
7  
8  
9  
10  
11  
12  
13  
14  
15  
16  
17  
18  
19  
20  
21  
22  
23  
24  
25  
26  
27  
28  
29  
30  
31  
32  
33  
34  
35  
36  
37  
38  
39  
40  
41  
42  
43  
44  
45  
46  
47  
48  
49  
50  
51  
52  
53  
54  
55  
56  
57  
58  
59  
60  
61  
62  
63  
64  
65

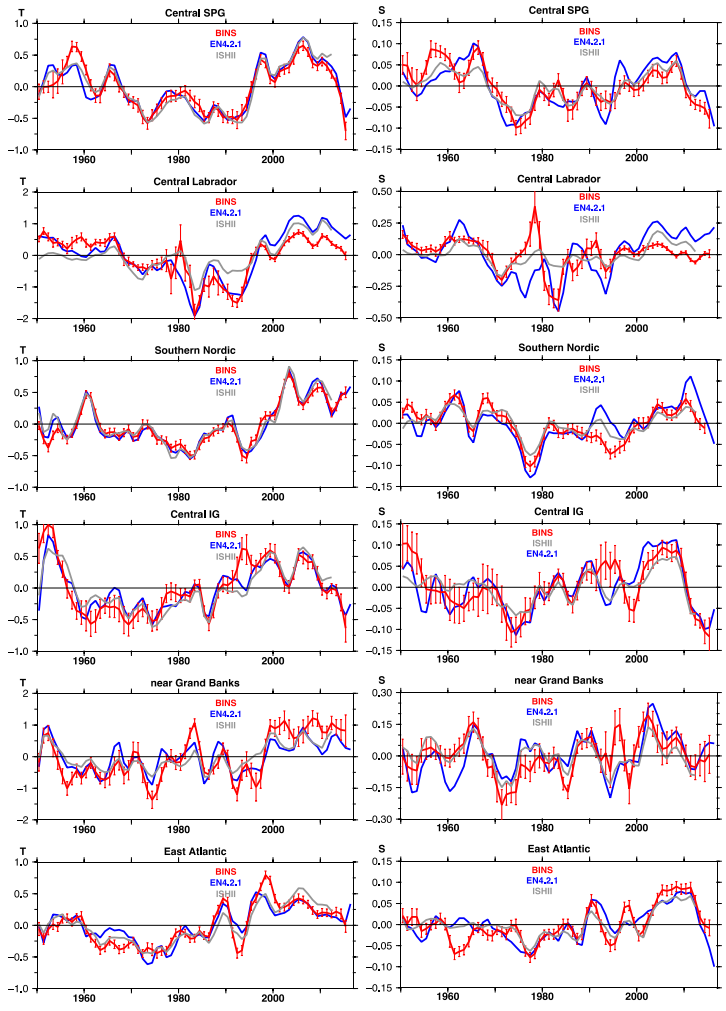


**Figure 5.** Comparison of regional T (left, °C) and S (right, PSS-78) time series from BINS with EN4 (1950-2015) and ISHII (1950-2012) surface products. The regional domains are the ones presented in Fig. 3. Here, the SPG region includes both the central SPG and the north-east SPG (and the south Greenland/southwest Irminger Sea box). One standard deviation rms error bars are added on the BINS series.



16  
17  
18  
19  
20  
21  
22  
23  
24  
25  
26  
27  
28  
29  
30  
31  
32  
33  
34  
35  
36  
37  
38  
39  
40  
41  
42  
43  
44  
45  
46  
47  
48  
49  
50  
51  
52  
53  
54  
55  
56  
57  
58  
59  
60  
61  
62  
63  
64  
65

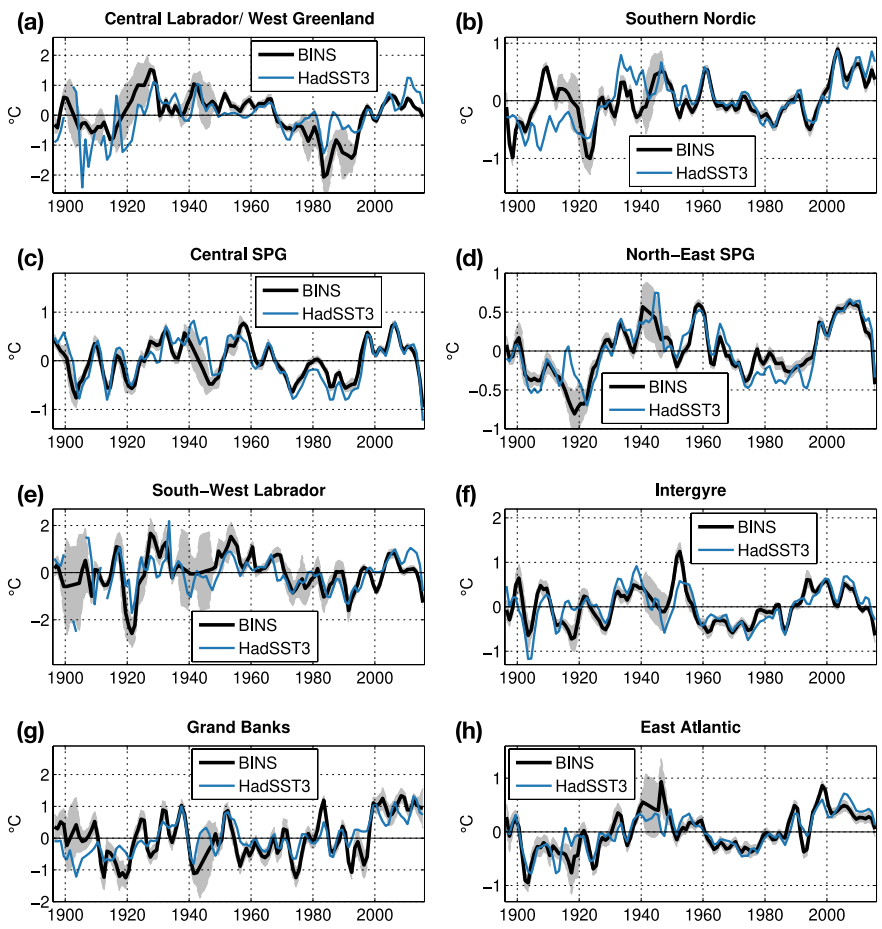
**Table 5.** RMS variability and correlation with BINS: (a) EN4, (b) ISHII.

<b>(a) EN4 / BINS</b>		<b>RMS (S)</b>			<b>corr (S)</b>	<b>RMS (T)</b>		<b>corr (T)</b>
		<b>(PSS-78)</b>			<b>°C</b>			
<b>Region</b>	<b>Time period</b>	<b>EN4</b>	<b>BINS</b>			<b>EN4</b>	<b>BINS</b>	
SPG	1950–2015	0.050	0.046	0.78		0.36	0.34	0.93
Central Labrador/ West Greenland	1950–2015	0.173	0.121	0.49		0.76	0.63	0.87
Central Labrador/ West Greenland	excluding 1976–1979	0.169	0.112	0.67		0.78	0.64	0.87
Southern Nordic S	1950–2015	0.045	0.039	0.75		0.34	0.32	0.96
Intergyre	1950–2012	0.057	0.057	0.78		0.33	0.43	0.85
Grand Banks	1950–2012	0.098	0.114	0.40		0.47	0.69	0.42
East Atlantic	1950–2012	0.037	0.042	0.73		0.26	0.32	0.84

<b>(b) ISHII / BINS</b>		<b>RMS (S)</b>			<b>corr (S)</b>	<b>RMS (T)</b>		<b>corr (T)</b>
		<b>(PSS-78)</b>			<b>°C</b>			
<b>Region</b>	<b>Time period</b>	<b>ISHII</b>	<b>BINS</b>			<b>ISHII</b>	<b>BINS</b>	
SPG	1950–2012	0.034	0.045	0.90		0.38	0.34	0.95
Central Labrador/ West Greenland	1950–2012	0.075	0.124	0.55		0.50	0.64	0.74
Central Labrador/ West Greenland	excluding 1976-79	0.077	0.115	0.61		0.52	0.65	0.75
Southern Nordic	1950–2012	0.028	0.040	0.91		0.35	0.32	0.9
Intergyre	1950–2012	0.034	0.045	0.71		0.34	0.34	0.62
Grand Banks	1950–2012	0.068	0.124	0.45		0.41	0.65	0.42
East Atlantic	1950–2012	0.030	0.040	0.73		0.28	0.32	0.65

1  
2  
3  
4  
5  
6  
7  
8  
9  
10  
11  
12  
13  
14  
15  
16  
17  
18  
19  
20  
21  
22  
23  
24  
25  
26  
27  
28  
29  
30  
31  
32  
33  
34  
35  
36  
37  
38  
39  
40  
41  
42  
43  
44  
45  
46  
47  
48  
49  
50  
51  
52  
53  
54  
55  
56  
57  
58  
59  
60  
61  
62  
63  
64  
65



**Figure 6.** Area-averaged BINS and HadSST3 SST anomalies: (a) central Labrador / West Greenland, (b) southern Nordic, (c) central SPG, (d) north-east SPG, (e) south-west Labrador, (f) intergyre, (g) Grand Banks / Labrador Current, (h) east Atlantic. Shading indicates  $\pm 2$  BINS error terms. The corresponding regions are shown in **Fig. C1**.

1  
2  
3  
4  
5  
6  
7  
8  
9  
10  
11  
12  
13  
14  
15  
16  
17  
18  
19  
20  
21  
22  
23  
24  
25  
26  
27  
28  
29  
30  
31  
32  
33  
34  
35  
36  
37  
38  
39  
40  
41  
42  
43  
44  
45  
46  
47  
48  
49  
50  
51  
52  
53  
54  
55  
56  
57  
58  
59  
60  
61  
62  
63  
64  
65

**Table 6.** HadSST3 correlation with BINS SST

<b>Region</b>	<b>Time period</b>	<b>corr</b>	<b>Time period</b>	<b>corr</b>
Central SPG	1896–2015	0.84	1950–2015	0.95
N-E SPG	1896–2015	0.87	1950–2015	0.93
Central Labrador/ West Greenland	except 1900–01, 1910	0.57	1950–2015	0.72
SW Labrador	except 1900–01, 1904–1905, 1912	0.56	1950–2015	0.71
Southern Nordic	1896–2015	0.65	1950–2015	0.93
Intergyre	1896–2015	0.74	1950–2015	0.84
Grand Banks	1896–2015	0.67	1950–2015	0.82
East Atlantic	1896–2015	0.82	1950–2015	0.89

1  
2  
3  
4  
5  
6  
7  
8  
9  
10  
11  
12  
13  
14  
15  
16  
17  
18  
19  
20  
21  
22  
23  
24  
25  
26  
27  
28  
29  
30  
31  
32  
33  
34  
35  
36  
37  
38  
39  
40  
41  
42  
43  
44  
45  
46  
47  
48  
49  
50  
51  
52  
53  
54  
55  
56  
57  
58  
59  
60  
61  
62  
63  
64  
65

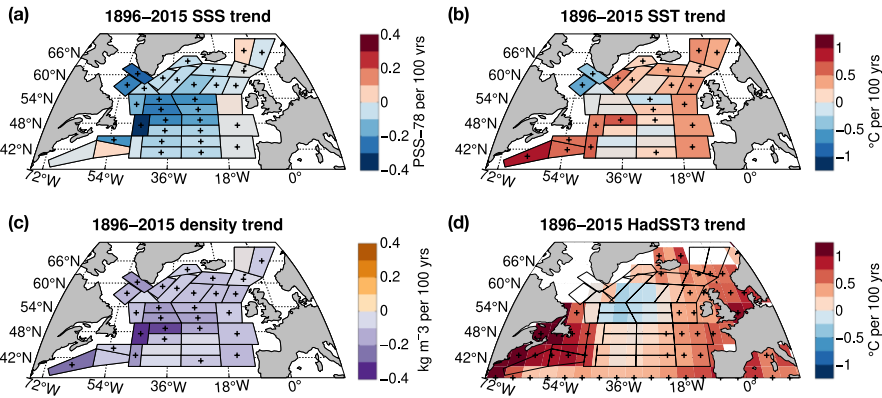


**Figure 7.** Trend over 1896–2015 (a) SSS; (b) SST; and (c) density; per 100 years. Pluses indicate where the slope magnitude is larger than twice the estimated error. (d) HadSST3 trend, per 100 years.

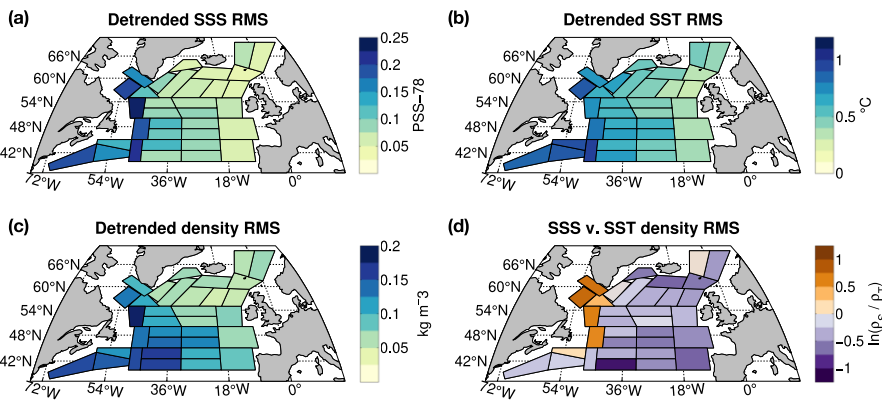


**Figure 8.** Detrended interannual (1-2-1 filtered) RMS variability for (a) SSS, (b) SST, and (c) density ( $\rho$ ). (d) Ratio of the contributions of detrended SSS and SST to density RMS variability (plotted as a logarithm).

1  
2  
3  
4  
5  
6  
7  
8  
9  
10  
11  
12  
13  
14  
15  
16  
17  
18  
19  
20  
21  
22  
23  
24  
25  
26  
27  
28  
29  
30  
31  
32  
33  
34  
35  
36  
37  
38  
39  
40  
41  
42  
43  
44  
45  
46  
47  
48  
49  
50  
51  
52  
53  
54  
55  
56  
57  
58  
59  
60  
61  
62  
63  
64  
65

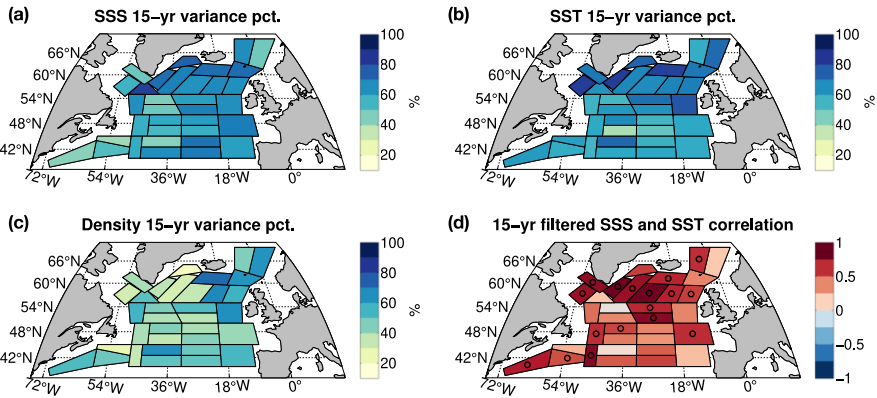


**Figure 9.** Percentage of detrended interannual (1-2-1) variance explained by the 15-year low-pass filtered time series for (a) SSS, (b) SST, and (c) density. (d) Detrended correlation coefficient between the low-pass filtered SSS and SST. Circles indicate where the correlation is significant at  $p < 0.05$ , estimated with a random-phase bootstrap test to account for serial autocorrelation (Ebisuzaki, 1997).

1  
2  
3  
4  
5  
6  
7  
8  
9  
10  
11  
12  
13  
14  
15  
16  
17  
18  
19  
20  
21  
22  
23  
24  
25  
26  
27  
28  
29  
30  
31  
32  
33  
34  
35  
36  
37  
38  
39  
40  
41  
42  
43  
44  
45  
46  
47  
48  
49  
50  
51  
52  
53  
54  
55  
56  
57  
58  
59  
60  
61  
62  
63  
64  
65

### Appendix A. Comparison with Friedman et al. (2017)

The BINS boxes mainly use the same underlying SSS data as the large boxes north of 40°N in Friedman et al. (2017). The datasets cover a similar area (Fig. A1a), though as mentioned previously, the BINS boxes more carefully avoid shelf regions (except for southwest Greenland and the southern part of the Grand Banks). Most of the source data used in the two analyses are the same. Additionally, BINS also incorporates two small datasets from the 1900s and 1910s, plus a few recent transects (and 2014–2015). There are more gaps in the 19 BINS time series than in Friedman et al. (2017): in particular in 1918–1921, and during and just after WWII; these gaps are linearly interpolated in the smaller boxes. Also, when sampling is poor, but varying geographically within the larger boxes, it is possible that some spatial variability is aliased in the temporal variability in the larger boxes.

Fig. A1b compares the NATL index from Friedman et al. (2017), area-averaged SSS from 45°–62°N, with SSS averaged over a similar area in BINS. [NATL from Friedman et al. (2017) is only plotted through 2012, as 2013 was subject to endpoint smoothing]. The two products are very highly correlated ( $r=0.94$ , 1896–2012), and compatible considering the differences in area and error estimates. Greater differences are found for smaller regions in the first half of the record, particularly during the gap years mentioned above (not shown)

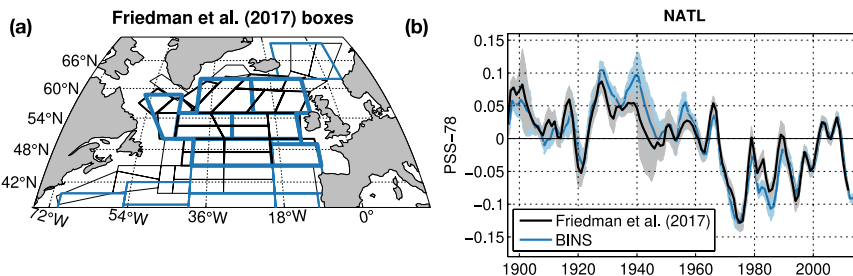


Figure A1. (a) Grid boxes from Friedman et al. (2017) (blue) and BINS (black). Thick lines indicate the NATL region. (c) Comparison of NATL index from Friedman et al. (2017) and BINS grid boxes. Anomalies are from 1896–2012; shading indicates  $\pm 2$  error terms.

1  
2  
3  
4  
5  
6  
7  
8  
9  
10  
11  
12  
13  
14  
15  
16  
17  
18  
19  
20  
21  
22  
23  
24  
25  
26  
27  
28  
29  
30  
31  
32  
33  
34  
35  
36  
37  
38  
39  
40  
41  
42  
43  
44  
45  
46  
47  
48  
49  
50  
51  
52  
53  
54  
55  
56  
57  
58  
59  
60  
61  
62  
63  
64  
65

**Appendix B. Comparison with Reverdin et al. (2018)**

As a check on the BINS time series, we compare the boxes with time series constructed with mostly similar data, monthly binned along two ship routes since mid-1993, intersecting near 59.5°N/32°W: AX02 between Iceland and southern Newfoundland and AX01 between the North Sea and southern Greenland, mostly along 59.5°N (Reverdin et al. 2018), shown in **Fig. B1a**. Time series along AX02 start in July 1993 with few gaps, whereas for AX01 some large data gaps were filled until late 1997. These time series, referred to as B-AX01 and B-AX02, provide increased spatial resolution at seasonal time scales, and portray very coherent variability where they intersect.

We illustrate the comparison of interannual variability of T and S between B-AX01 and BINS for overlapping boxes in the common period 1993-2015 (**Fig. B1b**). For S, the corresponding filtered RMS variability is larger in B-AX01 than in BINS by up to 20%, but with very high correlation coefficients (all larger than 0.95). The smaller RMS amplitudes of salinity in BINS probably result from the larger box sizes and the resulting spatial averaging. RMS variability is more similar for T, but with a slightly smaller correlation in the Iceland Basin (0.80) where gaps in 1993-1997 were the most common in B-AX01. Altogether, the comparisons for the two ship tracks suggest that the method used for BINS in the box averaging to produce interannual variability yields correct results when data coverage is sufficient.

1  
2  
3  
4  
5  
6  
7  
8  
9  
10  
11  
12  
13  
14  
15  
16  
17  
18  
19  
20  
21  
22  
23  
24  
25  
26  
27  
28  
29  
30  
31  
32  
33  
34  
35  
36  
37  
38  
39  
40  
41  
42  
43  
44  
45  
46  
47  
48  
49  
50  
51  
52  
53  
54  
55  
56  
57  
58  
59  
60  
61  
62  
63  
64  
65

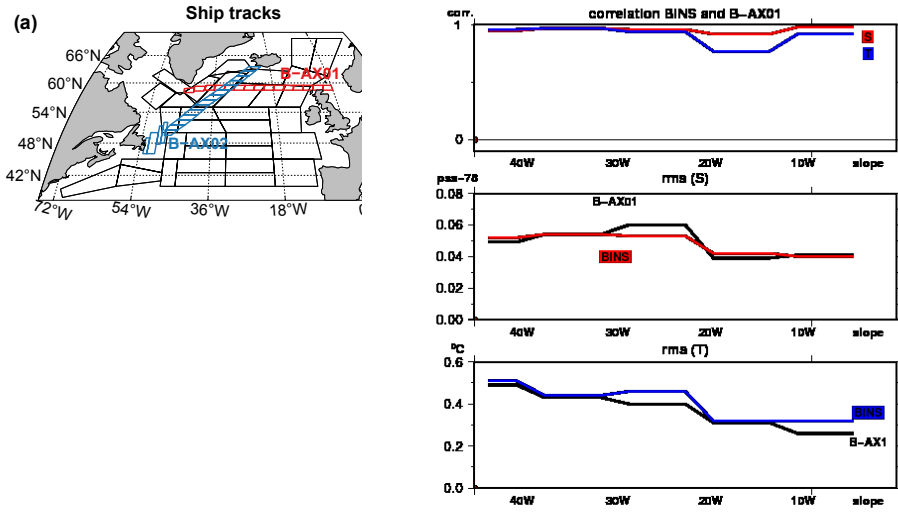


**Figure B1.** (a) AX01 (red) and AX02 (blue), from (Reverdin et al. 2018). (b) Comparison of B-AX01 with BINS, 1993–2015. The monthly time series of B-AX01 have been yearly-averaged (Dec-Nov), low-pass (1-2-1) filtered over successive years, and then averaged over the bins in BINS: correlation coefficient (top) for T (blue) and S (red), and RMS (middle for S and bottom for T) (B-AX01 in black, BINS in blue (T) and red (S)).



1  
2  
3  
4  
5  
6  
7  
1004  
8  
9  
10  
11  
12  
13  
14  
15  
16  
17  
18  
19  
20  
21  
22  
23  
24  
25  
26  
27  
28  
29  
30  
31  
32  
33  
34  
35  
3005  
3006  
3007  
3008  
4009  
4010  
4011  
42  
43  
44  
45  
46  
47  
48  
49  
50  
51  
52  
53  
54  
55  
56  
57  
58  
59  
60  
61  
62  
63  
64  
65

**Appendix C: Locations of BINS and HadSST3 grid boxes.**

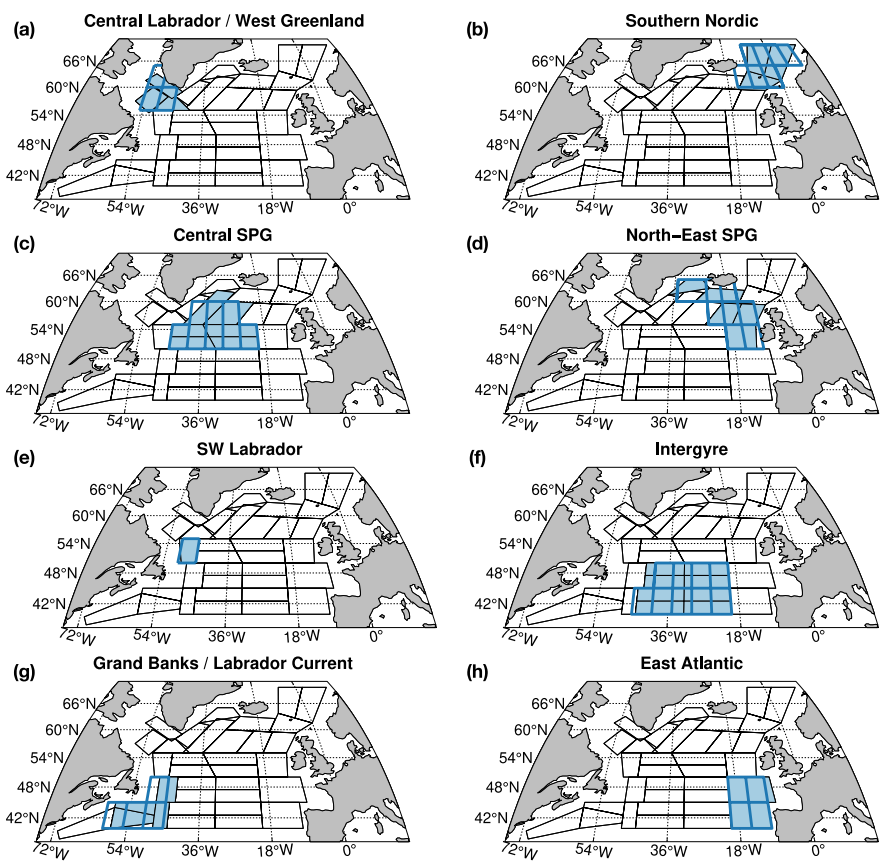


**Figure C1.** Locations of BINS and HadSST3 grid box regions used in the Section 3.3. Thick blue lines show the  $5^{\circ} \times 5^{\circ}$  HadSST3 grid boxes; shading shows the corresponding BINS grid boxes: (a) central Labrador / West Greenland, (b) southern Nordic, (c) central SPG, (d) north-east SPG, (e) south-west Labrador, (f) intergyre, (g) Grand Banks / Labrador Current, (h) east Atlantic.

Dear reviewers, dear Editor,

Thank-you for your thoughtful reviews.

The time series are made available (up to 2018) at LEGOS/OMP ([www.legos.obs-mip.fr/observations/sss/datadelivery/products/tsd-bins-naspg](http://www.legos.obs-mip.fr/observations/sss/datadelivery/products/tsd-bins-naspg)). We are currently discussing with the site managers how they will be referenced on the OMP SEDOO site with a proper doi and this should be available within a week..

We have followed reviewer 1's advice on how to improve figures 4 and 5 (see below). Part of the plot resolution issue is due to conversion in pdf, but that will not be the case in the final, published version.

The response to the different comments is provided below (lines with *Au*).

With best regards, Gilles Reverdin.

Reviewer #1: In this manuscript, the authors present a binned annual product (BINS) of sea surface temperature, salinity, and density for 1896-2015 in the subpolar North Atlantic between 40°N and 70°N. This paper describes the validation of the presented dataset. The methodology for the validation seems reasonable and this is a useful dataset for long-term studies. I recommend accepting this manuscript with minor revisions and look forward to the second part of this study that examines the decadal and multi-decadal variability. My comments are below.

Abstract - Is the water density also a surface-only product? For clarity, I recommend changing likes 27-28 in the abstract from "salinity" to "sea surface salinity" to match the acronym and "water density" to "sea surface density (SSD)"

*Au*: thank-you we agree that the changes proposed would make this clearer. Yes, the density is a sea surface density (SSD)

Line 29 - "space" to "spatial"

*Au*: OK

Line 74-75 - Reword this. Upon first read, it gave the impression that hydrographic data have only been used for decadal or longer-term studies, rather than the authors instead describing the temporal extent of the observations.

*Au*: reworded.

Line 111 - How so? The region presented in this dataset is different than the aforementioned studies.

*Au*: it is the binning approach that is common with the aforementioned studies. We reworded the sentence.

Line 155 - Citation please regarding the size of the bias. Also, what about regions south of 55°N and north of 65°N that are included in this dataset? There, is this bias significant?

*Au*: we have reworded the sentence. 'In other parts of the world, this has been documented due to surface heating and evaporation or precipitation (Boutin et al., 2016). In regions of sustained wind conditions, and away from shelves with surface

freshwater sources (melting sea ice or icebergs, outflows from fjords, river plumes), we expect stratification to be small on the order of or less than 0.01 in practical salinity and 0.1°C in temperature. Sustained wind conditions are commonly met in all seasons near 55-65°N, and probably a little less so in particular in spring/summer further south and north.'

Line 182 - Please elaborate. What were the SD criteria for removal?

*Au:* we did not use  $n \cdot SD$ , but a threshold inspired by sigma that varied spatially between 3°C and 6°C.

Line 217 - For a decadal dataset that possesses inadequate sampling of eddies, have you considered removing the eddy component? Otherwise, this will be an inaccuracy that will have to be corrected in any applied study using this research.

*Au:* This would be very interesting to do, and this can be attempted for recent observations, at least since the 1980s for T, and 1993 for S (or 2010, since SSS products are produced...). Unfortunately, we do not know where eddies were located prior to the satellite data era. Thus, this is unfortunately not feasible over such a long period. Indeed, the binned averages are often undersampling eddy variability, which is a significant component of the error budget in western boxes. Thus, we do not see how we could change that sentence.

Line 228 - Is this a fair assumption? Please cite.

*Au:* This assumption neglects the part of the error in SST and SSS that might be correlated due to insufficient sampling of eddy variability. On the other hand, the net effect of this on the density error estimate will depend on characteristics of eddies, and cannot be estimated off hand. We are more concerned for that on the seasonal variability and on what we estimate as March density. We don't think that this has been addressed in this way in other studies, and we preferred not to expand on it.

Line 254-255 - Why is this?

*Au:* This is an interesting point. We suspect that shallower mixed layer and variable atmospheric forcing might be the reason for summer SST deviating from the other seasons and presenting more variance in the central SPG. Here, we don't want to speculate, and will leave this sentence as written.

Line 269 - Awkward wording. Maybe "This is" to "It is"

*Au:* We changed 'This is for...' by 'For this reason and..., we chose not to...'

Line 282 - Remove "and"

*Au:* Removed.

The description of the datasets in 3.1 should go in the "Data and Methods" section.

*Au:* We thus moved in a section 2.3 titled 'Other products' the presentation of the other datasets and products used in section 3 (first sentences in 3.1, 3.2 and 3.3)

Figure 1 - Does "approximately" refer to the variation in temporal coverage across the selected boxes? If so, please change the climatology to span the same number of years for a more accurate climatology. Are the SST and SSS climatologies over the same years?

*Au:* yes, SST and SSS climatologies are estimated over the same years and encompass the period 1896-2000. On the other hand, years with no data are not always the same in different places, but we agree that it is not necessary to add 'approximately' in the caption. We thus removed 'approximately'

Figures - add error bars to time series.

*Au:* this is a good idea, in particular for BINS averages (we do not have the equivalent values for the curves from other products in figure 4 and 5). On the other hand, we find it difficult to apply, when we overlay different curves for figure 3. We thus only added error bars to the red curves (BINS) for figures 4 and 5.

The authors did well explaining the various sources of bias in all the validated datasets.

Figure 3 - I am confused by panel (a) being on a different page. How will this look in the publication? The text on panels (b) and (c) is hard to read. Also, please make the panels wider to better see the data and reduce white space. The data for "T Central Labrador" and "S Central Labrador" is touching the Y-axis.

*Au:* Figure 3 will be of a higher quality in the final version. We also apologize for panel (a) being on another page, in this version. This is not how it will be in the published paper. We left the same vertical scale for the T-panels (b) as the curves for 'Central Labrador' barely touch the lower axis. We changed the scales for S for central Labrador (-0.5 to 0.5). We also tuned a little the scales for S (second and fourth panels), and for T (first, second and fourth panels) to minimize white space.

Figure 4b - "central" to "Central"

*Au:* Corrected

Figure 4b - again, data is cut off by Y-Axis.

*Au:* We changed 'Central Labrador Sea' scale to avoid the slight cut-off, and we added error bars on BINS curve.

Figure 5 - Font is too small, data is cut off, and there are no error bars/shading

*Au:* Font is too small only because of the issue of conversion in pdf. The font quality is much better in the original. Data cut off (slightly) for Central Labrador Sea corrected by extending slightly the scale. Some of the scales were modified on other panels to minimize white space, and we added error bars on BINS curve.

Figure 6 - This is a much more appealing figure. Please make your other figures like this one.

Figure B1 (b) - Change font and font size for readability

*Au:* This is just an issue of conversion. Font is quite readable in the original eps file.

Reviewer #2: Our ability to look into the past ocean state is restricted by data coverage that greatly reduces back in time. Various efforts have been put forward to homogenize data time series. The authors focus on box averaging approach that has

been proven useful by the team's previous efforts. This paper extends the approach described by Friedman et al. (2017) by including both, SST and SSS anomaly data and by the better shaping of averaging boxes. This approach provides reasonable agreement with alternative compilations on rather large spatial scales and multi-year periods. Given sparse historical data coverage, especially for salinity, the box averaging of anomalies is a practical approach among a few. To some extent, it has been explored before (say in Grodsky et al., 2006), but only in terms of significantly shorter, regional (tropical Atlantic box) study.

The paper mostly focuses on data description. But, to my surprise, there is no link to the dataset described in the paper.

*Au:* thank-you very much for your 'positive' appreciation of the paper. We decided to place the dataset on the same site that we used for the time series of Friedman et al (2017). For the convenience of the users, we decided to slightly extend in time the time series of the paper to 2018 (which implies that the 1-2-1 running-averaged time series is really updated to 2017). However, we decided to introduce a small inconsistency in our criteria in the western part of the Atlantic to allow larger 'outliers' (as we are quite confident for these recent years that there are not 'errors' in the data). This results in larger error estimates in years 2015-2018 in this region.

Although geophysical interpretations are set aside for a coming paper, this data descriptive part is important. The paper is carefully written with great attention to details and includes an accurate description of data handling procedures. I believe this paper worth publishing. Because it is mostly data descriptive, my evaluation includes only a few minor points.

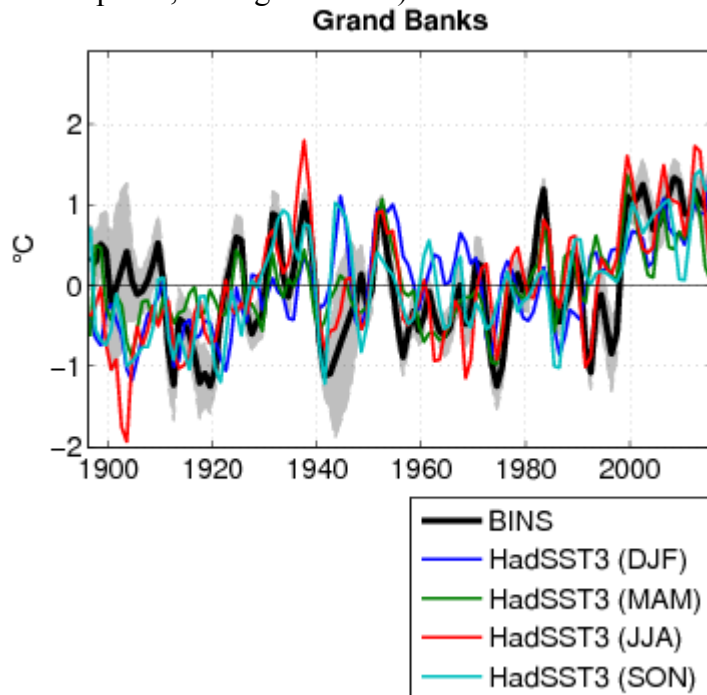
Minor:

The Abstract states that BINS resolves space scales of the order of 200 to 500 km. I don't see a confirmation of this statement in the main text. Are these scales dictated by characteristic size of a bin? Which zonal and meridional scales are resolved? Some of the Figures are only episodically discussed. For an example, rather strong SST anomalies are present in Grand Banks box. Particularly strong warming change of ~2C is present in the BINS in the late 1990s. This change is almost twice as strong as in the HadSST3. Could this particular episode be validated/explained? Normally, salinity contribution to water density increases at cold temperatures. But, Fig.8d depicts mostly zonal dependency rather than meridional dependency consistent with cooler SST in the north. Could you please come up with more explanation of this result?

*Au:* The scale of 200 to 500 km is dictated by the number of data available and thus by the bin size necessary to reduce the sampling error. The scales resolved thus correspond to the typical size of the boxes. This is variable but hovers around 200-500 km. Typically, thus we could resolve spatial wavelengths on the order of 3 box size (~1000 km) (thus box size ~scale). Some boxes are distorted zonally, while other are in a different direction, based on considerations on ocean structures (thus by the orientation of oceanic fronts or the direction of currents). Thus, we have changed the sentence in the introduction.

*Au:* We agree that some features require further discussion. We thank the reviewer for having pointed out the differences for the Grand Banks box time series. We are rather

confident in our time series, but have no explanation on why the SST variability portrayed there is different than in HadSST3 (or in EN4, to some extent) since the mid-1990s. We checked data distribution, which is certainly not ideal in particular over the southern Grand Banks bin for that period. There should not be major issues with seasonal sea ice, and the fact that most of the boxes in BINS that are included do not include the fall season is not the major reason for the discrepancies with HADSST3 (in HadSST3, the different seasons have the same timing for the different recent peaks, see figure below).



We also agree that the spatial distribution in Figure 8d is indeed worth further comments, which we have now introduced. Indeed, the mostly zonal structure in this ratio does not follow the expectation of having a pattern closer to the one in SST (thus with an increase in the north). This is because of the decrease in  $\text{rms}(\text{SSS})/\text{rms}(\text{SST})$  (compare 8 a to 8b) towards the north that compensates the effect of decreasing temperature.

Edits:

Line 343 but that exclude(s) Nansen

Line 356 For SSS, the large positive peak in BINS originate(s)

Line 450 boxes with 5 or less (replace 'less' by 'fewer') years

Line 485 density tends to be positively correlated to (replace 'to' by 'with') SSS

Lines 506-7 Indeed, the low-pass filtered correlation of SSS and SST (Fig. 8d) is positive in most grid boxes. Should it be Fig.9d?

Line 550 Possibly, (the) insufficient accuracy of [remove the] binned time series and the change in

Line 577 We base our evaluation (smth is missing there) that they provide reasonable

Grodsky, S. A., J. A. Carton, and F. M. Bingham (2006), Low frequency variation of sea surface salinity in the tropical Atlantic, *Geophys. Res. Lett.*, 33, L14604, doi:10.1029/2006GL026426

*Au* : Thank-you very much for the 'Edits' proposed that we have incorporated.